2012

Multi-wavelength, multi-beam, photonic based sensor for object discrimination and positioning

Kavitha Venkataraayan
Edith Cowan University

Edith Cowan University

Copyright Warning

MULTI-WAVELENGTH, MULTI-BEAM, PHOTONIC BASED SENSOR FOR OBJECT DISCRIMINATION AND POSITIONING

By

Kavitha Venkataraayan

This thesis is presented in fulfilment of the requirements for the degree of

Doctor of Philosophy (Engineering)

at

Electron Science Research Institute

Faculty of Computing, Health and Science
Edith Cowan University

AUGUST
2012

USE OF THESIS

The Use of Thesis statement is not included in this version of the thesis.

DECLARATION

I certify that this thesis does not, to the best of my knowledge and belief:

(i) *incorporate without acknowledgment any material previously submitted for a degree or diploma in any institution of higher education.*

(ii) *contain any material previously published or written by another person except where due reference is made in the text; or*

(iii) *contain any defamatory material.*

I also grant permission for the Library at Edith Cowan University to make duplicate copies of my thesis as required.

Signature: …kavitha venkataraayan…

Date: …..…8/8/2012…

ACKNOWLEDGEMENTS

First, I would like to thank my principal supervisor, Professor Kamal Alameh, for his excellent supervision and continued support throughout the entire course of my PhD. I also like to thank my co-supervisors, Dr. Sreten Askraba and Professor Clifton Smith, for their wisdom and guidance, as well as their motivation and encouragement for creative ideas within the optics and security field. I am grateful for the times they had dedicated for discussions during various stages of the project.

I am indebted to all my colleagues and friends who have helped me in many ways. My sincere thanks to Mrs. Linda Arthur, Mrs. Tiella Turkovic & Mr. Paul Roach for all their administrative support and help rendered to me. I would like to thank the ECU Graduate Research School for giving me an opportunity to commence my PHD and support during my tenure.

I warmly thank my parents, in-laws and my sister for their love, encouragement and continued support throughout my studies.

I lovingly thank my husband, Jay and our kids Darin & Iniyaa for being a constant source of support with patience, understanding and encouragement for the past three years.

PUBLICATIONS

Journal publications

1. **KAVITHA VENKATARAAYAN**, SRETEN ASKRABA, KAMAL E. ALAMEH & CLIFTON L. SMITH (2010) Photonic-based multi-wavelength sensor for object identification. *Optics Express,* 18**,** 3774-3783.

2. **KAVITHA VENKATARAAYAN**, SRETEN ASKRABA, KAMAL E. ALAMEH & CLIFTON L. SMITH (2011) Optical-Cavity-Based Multiwavelength Sensor for Spectral Discrimination and Object Position Detection. *JOURNAL OF LIGHTWAVE TECHNOLOGY,* 29**,** 2365 - 2371.

3. **KAVITHA VENKATARAAYAN**, SRETEN ASKRABA, KAMAL E. ALAMEH & CLIFTON L. SMITH (2012) Multi-wavelength laser sensor for intruder detection and discrimination. *Optics and Lasers in Engineering,* 50**,** 176-181.

Conference proceeding publications

1. **KAVITHA VENKATARAAYAN**, SRETEN ASKRABA, KAMAL E. ALAMEH & CLIFTON L. SMITH (2010) Multi-wavelength laser scanning architecture for object discrimination *7th international symposium on- high capacity optical networks and enabling technologies.* Cairo, Egypt.

2. **KAVITHA VENKATARAAYAN**, SRETEN ASKRABA, KAMAL E. ALAMEH & CLIFTON L. SMITH (2010) Object Discrimination Using a Multi-Wavelength Photonic Sensor. *International Cyber Resilience conference.* Perth, WA, School of Computer and Information Science, Security Research Centre, Edith Cowan University, Perth, Western Australia.

ABSTRACT

Over the last decade, substantial research efforts have been dedicated towards the development of advanced laser scanning systems for discrimination in perimeter security, defence, agriculture, transportation, surveying and geosciences. Military forces, in particular, have already started employing laser scanning technologies for projectile guidance, surveillance, satellite and missile tracking; and target discrimination and recognition. However, laser scanning is relatively a new security technology. It has previously been utilized for a wide variety of civil and military applications. Terrestrial laser scanning has found new use as an active optical sensor for indoors and outdoors perimeter security. A laser scanning technique with moving parts was tested in the British Home Office - Police Scientific Development Branch (PSDB) in 2004. It was found that laser scanning has the capability to detect humans in 30m range and vehicles in 80m range with low false alarm rates. However, laser scanning with moving parts is much more sensitive to vibrations than a multi-beam stationary optic approach. Mirror device scanners are slow, bulky and expensive and being inherently mechanical they wear out as a result of acceleration, cause deflection errors and require regular calibration.

Multi-wavelength laser scanning represent a potential evolution from object detection to object identification and classification, where detailed features of objects and materials are discriminated by measuring their reflectance characteristics at specific wavelengths and matching them with their spectral reflectance curves. With the recent advances in the development of high-speed sensors and high-speed data processors, the implementation of multi-wavelength laser scanners for object identification has now become feasible.

A two-wavelength photonic-based sensor for object discrimination has recently been reported, based on the use of an optical cavity for generating a laser spot array and maintaining adequate overlapping between tapped collimated laser beams of different wavelengths over a long optical path. While this approach is capable of discriminating between objects of different colours, its main drawback is the limited number of security-related objects that can be discriminated.

This thesis proposes and demonstrates the concept of a novel photonic based multi-wavelength sensor for object identification and position finding. The sensor employs a

laser combination module for input wavelength signal multiplexing and beam overlapping, a custom-made curved optical cavity for multi-beam spot generation through internal beam reflection and transmission and a high-speed imager for scattered reflectance spectral measurements. Experimental results show that five different laser wavelengths, namely 473nm, 532nm, 635nm, 670nm and 785nm, are necessary for discriminating various intruding objects of interest through spectral reflectance and slope measurements. Various objects were selected to demonstrate the proof of concept.

We also demonstrate that the object position (coordinates) is determined using the triangulation method, which is based on the projection of laser spots along determined angles onto intruding objects and the measurement of their reflectance spectra using an image sensor. Experimental results demonstrate the ability of the multi-wavelength spectral reflectance sensor to simultaneously discriminate between different objects and predict their positions over a 6m range with an accuracy exceeding 92%.

A novel optical design is used to provide additional transverse laser beam scanning for the identification of camouflage materials. A camouflage material is chosen to illustrate the discrimination capability of the sensor, which has complex patterns within a single sample, and is successfully detected and discriminated from other objects over a 6m range by scanning the laser beam spots along the transverse direction.

By using more wavelengths at optimised points in the spectrum where different objects show different optical characteristics, better discrimination can be accomplished.

TABLE OF CONTENTS

LIST OF ACRONYMS

AMCW:	Amplitude Modulated Continues Wave
ASIC:	Application-Specific Integrated Circuits
CCD:	Charged Coupled Device
CIP:	Critical Infrastructure Protection
CMOS:	Complementary Metal-Oxide Semiconductor
CW:	Continuous Wave
DN:	Digital Number
EM:	Electro Magnetic
FAR:	False Alarm Rate
FMCW:	Frequency Modulated Continues Wave
FOV:	Field of View
FWHM:	Full Width Half Maximum
IDS:	Intrusion Detection System
IFOV:	Instantaneous Field Of View
IPS:	Integrated Physical Security
IR:	Infra-Red
ITC:	International Training Courses
LADAR:	Laser Detection and Ranging
Lidar:	Light Detection and Ranging
LPAS:	Laser Perimeter Awareness System

NCPC:	National Crime Prevention Centre
PIDS:	Perimeter Intruder Detection Systems
PMT:	Photo Multiplier Tube
PPS:	Physical Protection System
PSDB:	Police Scientific Development Branch
RADAR:	RAdio Detection And Ranging
SNR:	Signal to Noise Ratio
TC-SPC:	Time Correlated Single Photon Counting
TDC:	Time-to-Digital Converter
TLS:	Terrestrial Laser Scanning
TOF:	Time –Of –Flight

LIST OF SYMBOLS

$\boldsymbol{R}$	Distance from the transmitter's aperture to the target
$\boldsymbol{C}$	Speed of light
$\boldsymbol{\tau}$	Round trip time of the laser pulse
$\boldsymbol{R_{max}}$	maximum measurable range
$\boldsymbol{\tau_{max}}$	maximum measurable time
$\boldsymbol{T_r}$	laser pulse rise time
$\boldsymbol{\delta_{r\text{-}p}}$	Uncertainty in range estimation pulse system
$\boldsymbol{P_{thr}}$	Threshold level
$\boldsymbol{P_{peak}}$	Peak level
$\boldsymbol{z}$	Range for an FMCW laser
$\mathbf{B}$	Beat frequency
$\boldsymbol{T_r}$	Period of frequency sweep
$\boldsymbol{\Delta f}$	Change in swept frequency
Δt_{dead}	Dead time
$\boldsymbol{\Delta\phi}$	Phase difference
$\mathbf{P_r}$	Received signal power (watts)
$\mathbf{P_t}$	Transmitted signal power (watts)
$\mathbf{D_r}$	Diameter of receiver aperture (metres)
$\boldsymbol{\beta}$	Laser beamwidth (radians)

η_{sys}	System transmission factor
η_{atm}	Atmospheric transmission factor
σ	Target cross section
$\bar{F}_p$	Time-average radiant flux (W)
α	Fraction of reflected radiant flux passing through the interference filter to the photomultiplier tube
A_R	Capture area of the receiver
$\bar{F}_T$	Time-average transmitted radiant flux
ρ	Measurement of the diffuse reflectance of the target surface
η	Quantum efficiency of the photocathode
h	Planck's constant
P_m and P_b	Slope and z-intercept of a projected ray
L_m and L_b	Slope and *z*-intercept the lens line
f	Effective position of laser spot sensor
D	Baseline
fn	Receiving lens f-number
λ□	Laser wavelength
δ_p	Pixel position accuracy
$\bar{I}_d$	Time-average radiant intensity, in watts per steradian
p_d	Diffuse reflectance
S_{beam}	Beam spacing
C_{width}	Width of the cavity

$\boldsymbol{\theta_r}$	Angle of refraction
$\boldsymbol{P_1 - P_n}$	Intensities of the outgoing laser beam
$\boldsymbol{z_R}$	Rayleigh range,
$\boldsymbol{W_0}$	laser beam radius
$\mathbf{n_{ac}}$ **and** $\mathbf{n_{ca}}$	Refractive index ratios
h, d **and** ***g***	Distances travelled by the optical beam from the laser aperture to quasi-cavity's entrance window
$\boldsymbol{R_1}$ **and** $\boldsymbol{R_2}$	Inner and outer cavity interfaces
$\mathbf{S_1}$**,** $\mathbf{S_2}$**,** $\mathbf{S_3}$ **and** $\mathbf{S_4}$	Slope values
a, b **and** $\boldsymbol{\sigma}$	Maximum value, maximum position and standard deviation of the fitting Gaussian beam

LIST OF FIGURES

CHAPTER 1

INTRODUCTION

1.1 BACKGROUND OF THE STUDY

Security systems have become increasingly important for reducing crime and terrorism worldwide. Terrorist attacks around the world have raised some significant issues for the management of the critical infrastructures of nations. Protecting the critical infrastructures from terrorism presents a massive challenge because these infrastructures are complex, interdependent and sensitive to disruptions that can lead to cascading failures with serious consequences. As nation's critical infrastructures are usually a subset of the potential targets of terrorist acts, a national infrastructure protection plan balancing the efforts of government and private institutions not only increases security over the long term but also appropriately addresses the vulnerability and criticality of all targets. According to the United States National Strategy of Homeland Security, strategic objectives for security are (i) to prevent terrorist attacks within the United States; (ii) to reduce America's vulnerability to terrorism; and (iii) to minimize the damage and recover from attacks that do occur (Office Of Homeland Security, 2002).

People are dependent on physical networks and virtual networks. Physical networks can include power and transportation systems, whereas virtual networks are based on electronic and communication systems. Any small network problem due to criminal activities would disrupt entire system and cause significant damage to the Nation. So it is important to safeguard every part of the networks to protect the critical infrastructure. There are specific organisations in most of the countries to reduce the criminal activities and protect the assets, for example; the UK Home Office and Canada`s National Crime Prevention Centre (NCPC) are in charge to prevent the United Kingdom and Canada from crime and terrorism. These organisations have taken steps to introduce a cost effective analysis in their nations (Dossetor, 2011).

Another way to reduce the crime and threat of terrorism on buildings containing natural assets is through Physical Security. There are Physical Security systems such as Integrated Physical Security (IPS) and the Physical Protection System (PPS). These systems are designed to assimilate people, events and tools to protect the natural assets from attack by terrorism. These systems have been built on the concepts of Deterrence, Detect, Delay, Response, Recovery and Re-assessment to secure the facilities and protect the assets of people, information and material (Einstein, 2011, Garcia, 2008). High-quality physical security uses the concept of layered defence in appropriate combinations to deter and delay intrusions which are passive defence; and detect and respond to intrusions which are active defence. The detection, delay and response functions are significant functions when designing successful PPS. The delay system could be ultimately penetrated, without detection, in that case the response function cannot be alerted (Rodriguez et al., 1991). The physical protection system was developed by the United States Sandia National Laboratories in the early 1970`s; and from 1978 to 1996 it was taught through 12 International Training Courses (ITC) with attendees from 58 countries (Soo Hoo and Chapek, 1996).

Intrusion detection is designed to detect a person or vehicle attempting to gain unauthorized entry in to the area under surveillance and it is also a part of PPS. There are two types of intrusion detection sensors: (i) exterior intrusion detection sensors are those used in outdoor environments and (ii) interior intrusion detection sensors are those used inside the building. But unlike interior intrusion detection sensors, which are limited only for indoor applications, exterior intrusion detection sensors can certainly be used indoors. Basically sensors can be classified into several groups with classifications as passive or active sensors, covert or visible sensors and volumetric or line detection sensors. The sensors are grouped by mode of application in the physical detection space, which could be (i) a buried line, in which the sensors are along a line buried in the ground, (ii) a fence-associated space, in which the sensors are either mounted on the fence or form a sensor fence or (iii) a freestanding space, i.e. being neither buried nor associated with a fence, but mounted on a support in free space. The applications for interior sensors are; boundary penetrating sensors detect penetration of the boundary to an interior area. The interior motion sensors detect the motion of an intruder within a confined interior area, and proximity sensors can detect an intruder in the area immediately adjacent to an object in an interior area (Garcia, 2008).

Over the last decade, terrestrial laser scanning (TLS) has increasingly played an advanced role in exterior and interior intrusion sensing as a part of Critical Infrastructure Protection (CIP), specifically Perimeter Intruder Detection Systems (PIDS) (Hosmer, 2004). Defence and Security organisations have adopted laser scanning technologies for projectile guidance, surveillance, satellite and missile tracking and target discrimination and recognition. Terrestrial laser scanning was an evolution from Lidar - which stands for Light Detection and Ranging. Lidar is an optical remote sensing technology that can measure the distance to, or other properties of a target by illuminating the target with light, often using pulses from a laser. Lidar systems are also used in applications that require measuring thermal, structural, and dynamical properties of the atmosphere, threshold detection of biologically harmful gases, and spectral signatures of specific targets. These abilities of a Lidar system have enabled many industrial applications.

Laser scanners also use the same technology as Lidar for detection, but laser scanning technologies provide non-contact measurement systems that scan their surroundings in two-dimensions. These technologies have been used for industrial and commercial applications, where the shape, size and other physical properties of target materials or objects have to be analysed. One of the emerging application areas of laser scanners is security intrusion detection. Substantial research efforts have been devoted towards the development of advanced techniques for remote intrusion sensing, especially the laser scanning technique. An early laser scanning system has been tested in the British Home Office – Police Scientific Development Branch (PSDB) in 2004. It was found that laser scanning has particularly the capability to detect humans within a 30m range and vehicles within a 80m range with low false alarm rates (Hosmer, 2004).

In the context of security systems, laser scanning sensors (discussed in Chapter 3-Section 3.2) based on beam deflection for security are much more sensitive to vibration than sensors based on multi-beam and stationary optics (Taylor et al., 1998). Also mirror-based scanners are slow, bulky and expensive. Moreover beam deflection components can also cause deflection errors due to electro-mechanical moving parts, acceleration, wobble, jitter and wear out. In addition, a beam defection unit usually requires a regular calibration (Schnadt and Katzenbeißer, 2004). There are different types of self calibration methods for different applications, but such methods also cause some errors (Lichti et al., 2011).

There are other methods for illuminating entire scenes without mechanical scanning, based on the use of a pulsed laser source in conjunction with time –of –flight (TOF) measurements (Elkhalili et al., 2004). In this method the (round-trip) distance from the transmitter to the target is measured by determining the time delay between the emitted and received laser pulses. The scene of interest is flood illuminated and imaged onto the focal plane of an image sensor, so that each pixel measures the round-trip time of the transmitted photons that are scattered off the target, thus, a 3D image can be obtained with a single pulse (Aull, 2005). This method is known as time correlated single photon counting (TC-SPC), which has been used for the specific purpose of detecting photons that pass through mesh textured obstruction such as foliage and reflect back to the detector unit. Scannerless Laser Detection and Ranging (LADAR) have also been developed, where ranging is based on flood illumination and phase-shift or TOF sensitive pixels of the detector array. However, this method is inefficient because it requires a high-optical-power laser source to illuminate the desired scene.

The purpose of this thesis is to explore novel intrusion detection architectures based on static laser scanning over a wide angle of view. Criteria for an ideal optical scanner include a wide scanning range, no moving parts, high resolution, high speed and low power consumption. Generally, mechanical light-beam deflectors produce large deflection angles with relatively low speeds, whereas non-mechanical deflectors tend to produce smaller angles of deflection at high speeds. Therefore a challenge currently exists to produce a laser scanning architecture capable of achieving a large angular range of light transmission with high speed and high light intensity of each propagated beam with few or no moving parts.

A multi-wavelength laser scanning architecture that can generate multiple laser spots with no moving parts is proposed and experimentally demonstrated. This architecture eliminates many movement-related issues inherent in mirror driven scanners. Methods for target material analysis include target material identification and discrimination; and identifying the location of target material are explored. This thesis also contributes to the advancement of laser based remote sensing methods for the protection of critical infrastructure and assets. Therefore, the demonstration of the proposed architecture will enable the development of application-specific scanning architectures where sensor size, scanning time and power efficiency are critical factors.

1.2 SIGNIFICANCE OF THE STUDY

The thesis addresses two research questions, namely (i) intrusion detection and object location based on static laser scanning and (ii) object identification and discrimination based on multi-wavelength laser scanning.

1.2.1 Static laser scanning architecture

The investigation discusses the significance of developing static laser scanning architectures featuring wide scanning range, no moving parts, high resolution, high speed and low power consumption. Generally, mechanical light-beam deflectors produce large deflection angles with relatively low speeds, whereas non-mechanical deflectors tend to produce smaller angles of deflection at high speeds. Therefore, currently the R&D challenge is to produce a scanning architecture capable of achieving a large angular range of light transmission with high speed and high light intensity of each propagated beam with no moving parts.

The performance of a laser beam scanning unit is limited by manufacture tolerances, ecological factors, the mechanical movement of the mirror, ball bearings and motor. So, the development of a static scanning system without any moving parts is a significant achievement because the inherent scanning errors and problems caused by the movement of the mirror and servo motor are difficult to compute and correct. According to Stutz (Stutz, 2005), problems associated with rotational scanners are (i) synchronization with other time-dependent elements in the system is rather difficult, (ii) motor stability and durability at higher rotation speeds (there is an upper limit to the rotation speed due to the tensile strength of the mirror material and the mirror must not disintegrate at the maximum rotational speed). The significance of this static scanning system is that it eliminates the movement related problems and errors and has the capability to produce multiple laser beams to scan the entire scene.

1.2.2 Multi-wavelength laser scanning for target discrimination

The detection and analysis of light reflected off a target object or material in free space is one of the key advantages of remote sensing, which is utilized in a large variety of industrial applications such as security, defence, disaster and emergency situations, agriculture, mining, surveying, transportation, navigation and traffic control. Multi-wavelength laser scanning is a natural progression from target detection to target

identification and classification, where specific features of target objects and materials are discriminated by measuring their reflectance characteristics at specific wavelengths and matching them with their spectral reflectance curves. With the advances in the development of high-speed sensors and high-speed data processors, the implementation of multi-wavelength laser scanners for object identification has now become feasible.

While holographic gratings can be used to generate multiple single-wavelength laser spots for intruder detection, the same cannot be implemented for multi-wavelength laser scanning. The reason being laser beams of different wavelengths will be diffracted from a holographic grating at different angles, hence making this technique impractical for maintaining a high-degree of overlapping between beams of different wavelengths projected at a particular spot. A two-wavelength photonic-based sensor for target object discrimination has recently been reported (Klančnik S, 2007), where an optical cavity is used for generating a laser spot array and maintaining adequate overlapping between collimated laser beams of different wavelengths over a long optical path (Sahba et al., 2007a) However, the main drawback of this approach is the limitations in the number of objects that can be discriminated (Klančnik S, 2007). By increasing the number of wavelengths at which target objects exhibit different optical characteristics, the number of objects and materials that can be identified and discriminated increases significantly, especially if an efficient computer algorithm is developed to predict the position of the target.

1.3 AIM OF THE STUDY

The aim of this study is to design and develop a proof-of-concept motionless wide-angle multiwavelength laser scanner demonstrator for intruder detection applications.

The objectives of this thesis are:

(1) To design and develop an intruder detection sensor demonstrator using multi-wavelength laser diodes, in conjunction with a uniquely shaped beam-splitting optical cavity and high speed photo-detector array to scan the field of interest without using any moving parts.

(2) To design and develop a multi-wavelength laser combination module with five lasers of different wavelength and four beam combiners to obtain more detailed optical signatures of the intruding objects.

(3) To experimentally demonstrate material identification and discrimination through multi-wavelength laser intruder detection sensors over a long distance (exceeding 5m) from the laser transmitter.

(4) To experimentally demonstrate the capability of the intruder detection system to discriminate complex materials like camouflage materials.

(5) To develop a computer algorithm for the laser scanning system that detects the position of an object within a large Field of View (FOV).

In general, the objectives listed above address the problems associated with mechanically controlled mirror-based laser scanners.

1.4 ORGANISATION OF THE THESIS

This thesis is organised as follows:

Chapters 2 and 3 present a comprehensive review on laser RADAR, problems with LADAR, laser ranging methods, surface reflection and laser scanning for security system, which includes laser scanning fundamentals and examples of intruder detection system and also laser scanner placements.

Chapter 4 introduces the optical cavity, which is also known as the multi beam generator. The working principle of the optical cavity is discussed in detail. Beam propagation through optical cavity is explained with some examples. Optimization of the thin-film broadband coating and theoretical calculations for beam transmission are thoroughly discussed. Also, the advantages of curved optical cavity over rectangular cavity are discussed.

Chapters 5 and 6 describe and demonstrate the concept of object discrimination and object positioning through photonic based multi-wavelength intruder detection sensors. The combination of multi-wavelength lasers using beam splitters is explained in detail. Discrimination and identification of various objects is demonstrated experimentally over a range of up to 6m form the optical cavity. Modification to the initial experiment is discussed to provide transverse scanning thus discriminating complex materials such as camouflage materials. Object positioning through laser triangulation is also described and demonstrated.

Finally, a comprehensive conclusion and recommendation for future work is presented in Chapter 7.

CHAPTER 2

LASER RADAR AND RANGING METHODS

2.1 INTRODUCTION

Laser RADAR (LADAR), also known as light detection and ranging (Lidar) uses the same principle as RADAR (Radio Detection And Ranging) to derive information about an object from a distance. While both techniques use the transmittance of EM radiation towards a target or scene of interest and detect scattered radiation, RADAR uses wavelengths within the radio band of the EM spectrum whereas LADAR uses laser light in the ultraviolet, visible and infrared wavebands. Apart from analysing the properties of solid mass objects, this form of remote sensing is also useful for the detection of non-solid atmospheric variants such as temperature, wind velocity, as well as aerosol and cloud properties. The basic difference is that the radar uses the wavelength which is within the radio band whereas the LADAR uses wavelengths in UV, visible, near infrared or infrared lights. Laser scanning is the direct extension of conventional radar techniques to optical (very short) wavelengths (Wagner et al., 2004).

This chapter will begin with the introduction of the laser ranging methods such as Pulsed Time Of Flight (TOF), Frequency Modulated Continues Wave (FMCW) and Amplitude Modulated Continues Wave (AMCW). Introduction of Laser RADAR is followed by laser ranging methods. The problems associated with Laser RADAR is discussed in Section 2.4, which includes mixed pixels, range-reflectance crosstalk, temporal mixing, photon noise, intensity and range drift. Triangulation method for range measurements are concisely discussed in section 2.5. Later in Section 2.6, surface reflectance, which includes specular and diffuse reflection, is briefly discussed.

2.2 LASER RANGING METHODS

Many modern range finding techniques involve the projection of a laser beam on a target, while an imaging device measures the relative position of the projected pattern (Baribeau and Rioux, 1991). There are three significant methods for measuring the time taken for the laser beam to strike the target and return back to the imaging device; they are pulsed time of flight, frequency modulated continues wave, amplitude modulated continues wave and triangulation (Bosch and Lecure, 1995). Ranging methods can also be divided in to monocular or multiple method (Jarvis, 1983, Moring et al., 1989, Ailisto et al., 2002). Figure 2.1 shows the classification of optical range finding (Ailisto et al., 2002).

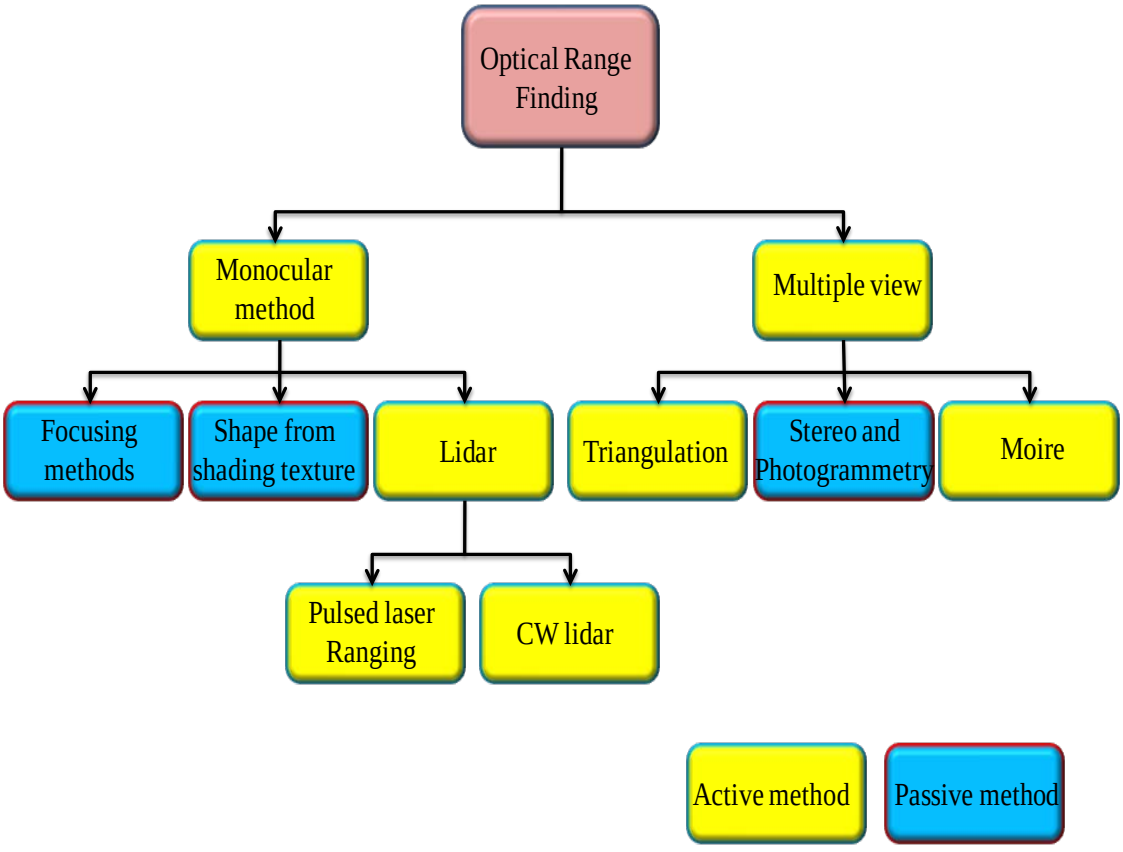

Figure 2.1: Classification of optical range finding techniques (Ailisto et al., 2002)

The 3D reconstruction profile of the target through laser scanning for on-site surveillance employs one of the three most significant ranging methods (Gonçalves et al., 2001). The range and accuracy of ranging methods are given in the table 2.1. The table shows the maximum range for the triangulation method to be 10m, but Wu et al. (Wu et al., 2006) have developed and demonstrated a triangulation-based range of up to 45m.

Table 2.1. Classification of laser scanners (Schulz and Ingensand, 2004)

Range finding method	Range(m)	Accuracy(m)	Manufacturer Examples
Pulsed ToF	~1000	>10	Mensi, Riegl, Cyra, Callidus, SICK, LaserOptronix
CW phase difference	<100	<10	Zoller+Froehlich, IQSun
Triangulation	<10	<1	Minolta, Leica

2.2.1 Pulsed Time of Flight

TIME-OF-FLIGHT (TOF) laser rangefinders are used in industrial measurement applications such as the measurement of levels in silos and containers, profiling and scanning, in traffic safety applications such as collision avoidance, speed measurement and traffic control, and in other applications such as positioning, surveying, docking, 3D mapping (Palojarvi et al., 2002) (Poppinga et al., 2010). TOF involves measuring the round trip time of a laser pulse, that is the time taken for a laser pulse to travel from the laser aperture to the target and reflect back to the receiver section of the rage finder (Boehler, 1999). The distance of the target can be calculated, since the light travels at a constant and finite velocity (Beraldin et al., 2003),

$$R = c \cdot \frac{\tau}{2}, \qquad \text{Eqn. (2.1)}$$

where R is the distance from the transmitter's aperture to the target, c is the speed of light and τ is the round trip time of the laser pulse.

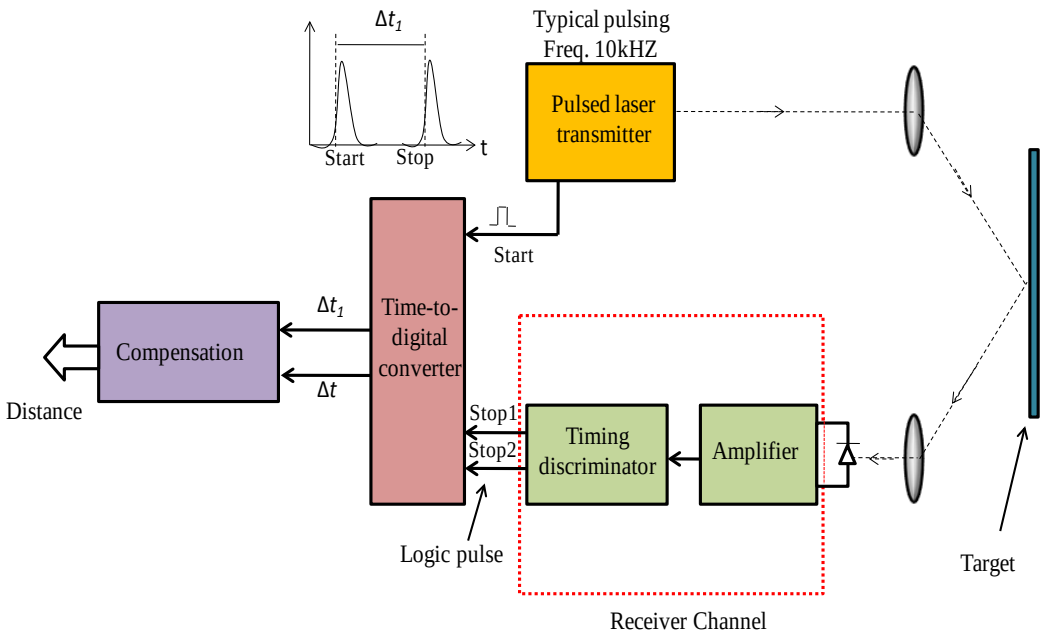

Figure 2.2: A typical block diagram of a pulsed TOF laser rangefinder system (Kurtti and Kostamovaara, 2010).

A laser rangefinder device typically consists of pulsed laser transmitter, the necessary optics, a receiver channel and a Time-to-Digital Converter (TDC), as shown in Figure 2.2. The laser pulse transmitter produces an optical pulse after triggering. The trigger signal in the laser radar device is optical, thus reducing the interference between the laser pulse transmitter and the other electronics. The generated short laser pulse typically has a full width half maximum (FWHM) of around 3ns and is usually guided to illuminate and detect an optically visible target (Kurtti and Kostamovaara, 2010).

Palojarvi, et al. (2002) designed a special receiver channel in which the receiver channel converts the optical pulse to an accurately timed, logic-level voltage signal. The receiver channel circuitry comprises external avalanche photodiodes for the start and stop receiver channels, and a full custom Application-Specific Integrated Circuits (ASIC), which includes both the start and stop receiver channels. The receiver channels typically produce differential logic-level timing signals for the Time to Digital Converter (TDC).

The TDC converts the time interval between the logic-level start and stop signals to a digital word. The TDC operates by digitizing the time interval roughly using an 8-bit counter clocked by a 100 MHz external oscillator. This oscillator allows a large measurement range (Palojarvi et al., 2002), where the resolution of range is directly proportional to the time resolution and is given by (Wehr and Lohr, 1999).

$$\Delta R = c \cdot \frac{\Delta \tau}{2}. \qquad \text{Eqn. (2.2)}$$

The maximum measurable range, R_{max}, is directly proportional to maximum measurable time (Wehr and Lohr, 1999), τ_{max}, i.e.

$$R_{\max} = c \cdot \frac{\tau_{\max}}{2} \qquad \text{Eqn. (2.3)}$$

The uncertainty in the range estimation pulse system was derived by (Beraldin, 2004) and given by

$$\delta_{r-p} \approx \frac{c}{2} \cdot \frac{T_r}{\sqrt{SNR}}, \qquad \text{Eqn. (2.4)}$$

where T_r is the laser pulse rise time, $\delta_{r\text{-}p}$ is uncertainty in range estimation pulse system and SNR is the signal-to-noise ratio. By averaging over N measurements, $\delta_{r\text{-}p}$ can be reduced by a factor proportional to the square root of N.

According to Thiel and Wehr (Thiel and Wehr, 2004), for any transmitted laser pulse, several return signals can be generated due to either the surface reflectivity of target objects or the topology of the scene or due to fogs or dusts. Thiel and Wehr (2004) used, for the first time, threshold detection, whereby once the received signal exceeded a fixed threshold, the time counter was reset, and a transmit pulse was generated. In case of weak received signals, the threshold level was not defined, leading to inaccurate return time and long slant range. To compensate for this intensity dependent threshold setting, the following equation for calculating the measurement time, t_k, was used

$$t_k = \frac{P_{thr} \cdot t_r}{P_{peak}} \qquad \text{Eqn. (2.5)}$$

where P_{thr} is the threshold level, P_{peak} is the peak level, and t_r is the rise time.

2.2.2 Frequency modulated continues wave (FMCW)

Another method for laser range finding is the frequency modulated continues wave (FMCW) technique. The emitted light wave can be modulated by a sine wave at varying frequency and then mixed with the reflected signal. The frequency of the sine wave can

be linearly modulated directly at the laser diode using an acousto-optic modulator (Dandridge and Goldberg, 1982). By applying triangular or saw-tooth wave modulation, as shown in Figure 2.3, a chirp waveform is produced. With triangular frequency modulation, the distance to the target is proportional to the maximum beat frequency, known as the absolute difference in frequency between the returning signal and emitted signal.

For the FMCW method, the range to the target is calculated using the following formula:

$$z = \frac{c\Delta t}{2} = \frac{cBT_r}{4\Delta f} \qquad \text{Eqn. (2.6)}$$

where,

z is the range for an FMCW laser.

c is the speed of light.

B is the beat frequency.

T_r is the period of frequency sweep.

Δf is the change in swept frequency.

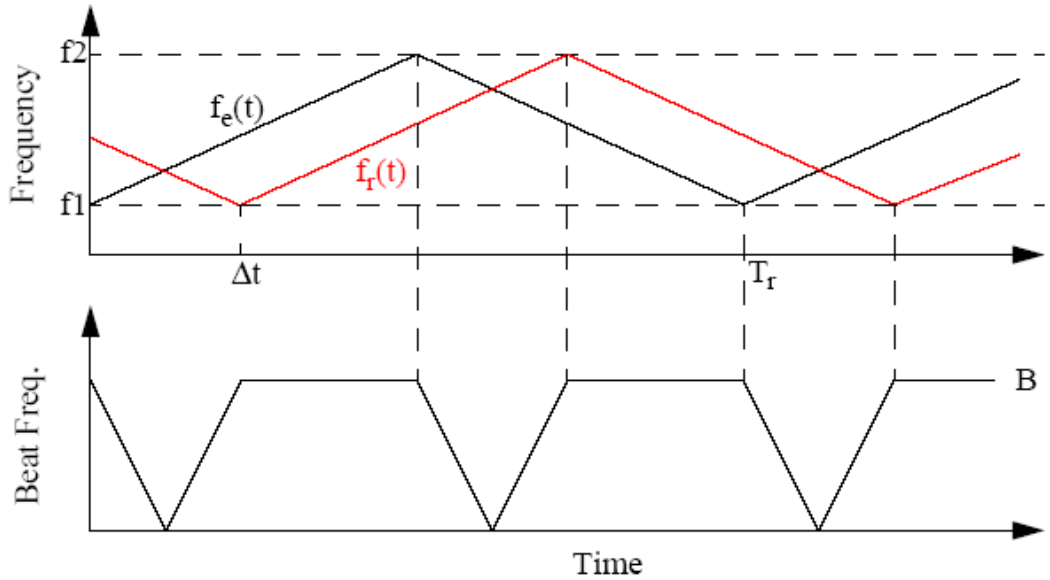

Figure 2.3: Beat frequency that results from a modulated transmitted signal and its corresponding reflected signal (Hancock, 1999)

Hancock (1999) stated that many factors have to be considered while choosing the FMCW parameters, and that the beat frequency, B, cannot be measured at all the time period. The time interval over which the beat frequency cannot be measured is called the dead time (Δt_{dead}), and is given by

$$\Delta t_{dead} = \frac{2\Delta t}{T_r} \qquad \text{Eqn. (2.7)}$$

So for a longer T_r, less noise can occur, because the sampling time has to be increased to measure B. However, a shorter period of frequency sweep increases the data rate of the sensor.

According to Hancock (1999), the maximum measurable distance is given by

$$z_{\max} = \frac{cT_r}{4} \qquad \text{Eqn. (2.8)}$$

Thus, the minimum measurable distance depends on the sampling time taken to sample the beat frequency B.

2.2.3 Amplitude Modulated Continuous Wave (AMCW)

The amplitude modulated continuous wave (AMCW) method is based on modulating the power of the emitted light with a sine wave of a given frequency. The reflected energy is delayed by a travel time Δt and it is relatively shifted in phase with respect to the emitted energy. By applying the AMCW to two relatively different signals a better range resolution is achieved (Hancock, 1999).

The distance R to an object is proportional to the phase difference, $\Delta\phi$, up to an ambiguity of a 2π phase difference (Hebert and Krotkov, 1991).

$$R = \frac{\lambda}{4\pi}\Delta\varphi \qquad \text{Eqn. (2.9)}$$

According to Beraldin (Beraldin 2004), the range uncertainty is approximately:

$$\delta \approx \frac{1}{4\pi}\frac{\lambda}{\sqrt{\text{SNR}}} \qquad \text{Eqn. (2.10)}$$

Hebert and Krotkov (1991) provided another prediction of the maximum ambiguity interval, given by

$$R_{ambig} = \frac{c}{2f} = \frac{\lambda}{2} \qquad \text{Eqn. (2.11)}$$

Amplitude modulated continuous wave range sensors would approach perfection if they emit a zero-width laser beam and observe the returned signal through an infinitely small receiver. Every point of the target cross section with the laser beam is usually referred to as the footprint of the beam (Hebert and Krotkov, 1991).

2.3 LASER RADAR (LADAR)

The basic components of the LADAR system consist of the transmitter, the receiver and the detector unit. LADAR system designs have either a bistatic or a monostatic configuration. In a monostatic system, the transmitter and receiver are located together, while in a bistatic design the two components are separate. Another design consideration is to employ either a biaxial or coaxial sensor arrangement. In a biaxial arrangement, the axes of the transmitter and receiver have different orientations. Backscattered light can be detected by the receiver only when the subject is beyond a certain distance. The axes of the transmitter and receiver are the same in a coaxial arrangement.

The transmitter unit uses either a continuous wave (CW) or pulsed laser to launch light into the atmosphere. A beam expander is usually used to minimize divergence of the laser beam. The relationship between beam divergence and the size of the field of view of the detector are proportional and a smaller detector field of view reduces the detection of any background radiation, which can be caused by either natural or artificial light sources.

A LADAR receiver is comprised of optical components to collect scattered light and direct it onto the detector. The first, or primary, optical component can range in diameter from 10 cm up to a few metres depending on the range of detection. The simplest and most common form of processing of the scattered light is spectral filtering using a band pass filter which enables selective transmittance of light depending on the wavelength of the incoming photons.

The purpose of a LADAR detector is essentially to generate an electrical current through the photodetection of an optical signal, making a permanent record of the measured intensity. Photomultiplier tubes (PMTs) convert incident photons within the visible and ultraviolet wavelength bands into an electrical current pulse which is detected by electronics. The photons can be counted individually using time correlated single photon counting (TC-SPC), or an average current from the PMT output pulses can be measured and recorded. While TC-SPC is a far more precise method of detection, it is conventionally difficult to accomplish when the PMT output pulses become close to or greater than the average pulse width. However, recent advances in fast detector technologies employing CMOS timing circuitry have enabled 3D images to be obtained from a single laser pulse (Elkhalili et al., 2004, Hauge, 2003). Recently, a LADAR system has been able to measure the structure of forest canopies and obtain accurate information on individual tree and stand level forest structure (Van Leeuwen et al., 2011).

The radar equation is the fundamental model for describing the measurement process in terms of sensor and target characteristics (Wagner et al., 2004). The intensity of the received laser pulse can be determined from the following range equation:

$$P_r = \frac{P_t D_r^4}{4\pi R^4 \beta_t^2} \cdot \eta_{sys} \cdot \eta_{atm} \cdot \sigma \qquad \text{Eqn. (2.12)}$$

where ,

P_r is the received signal power (watts)

P_t is the transmitted signal power (watts)

D_r is the diameter of receiver aperture (metres)

R is the range from sensor to target (metres)

β is the laser beamwidth (radians)

η_{sys} is the system transmission factor

η_{atm} is the atmospheric transmission factor

σ is the target cross section

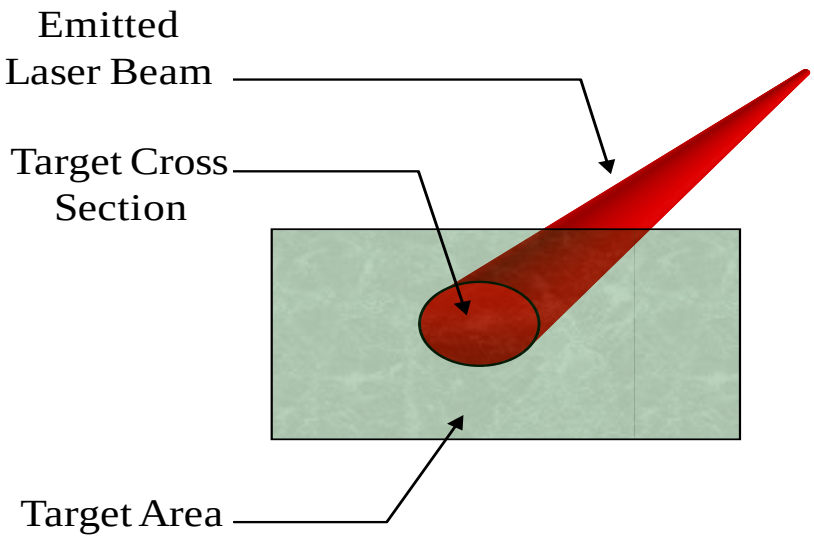

Figure 2.4: Illustration of backscattering cross section.

The radar equation shows that the received power is a function of transmitter power, laser beamwidth and aperture size of the receiver, system losses, and atmospheric transmission. The properties of the target are described by a single quantity, the backscattering cross section (Wagner et al., 2004).

The cross section is also called the footprint of the beam shown in Figure 2.4. (Hebert and Krotkov, 1991).The instantaneous field of view(IFOV) is defined as the angular field of view of the optical system (Campbell, 1996).

2.4 PROBLEMS WITH LADAR

The most common problems associated with laser range measurements, namely, the "mixed pixels", range reflectance crosstalk and temporal mixing, photon noise and intensity and range drift, will be discussed in the following sub-sections.

2.4.1 Mixed Pixels

Mixed pixels are those that receive reflected energy from two surfaces separated by a large distance. Mixed pixels can result in reported ranges that are on neither surface, but somewhere between the two ranges, or even worse, either behind or in front of both surfaces. This is a common problem with AMCW-based laser radars and cannot be completely eliminated (Hancock et al., 1998). The problem of mixed pixels is also known as mixed measurements.

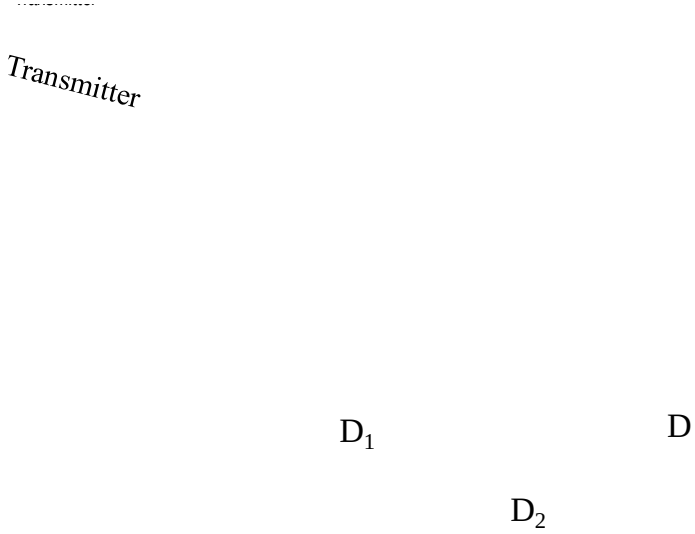

Figure 2.5: Side view of surface 1 occluding surface 2 (Hebert and Krotkov, 1991).

Figure 2.5 shows the geometry of the measurement at an occluding edge, two objects at distances D_1 and D_2 from the sensor ($D_1 < D_2$) and separated by a distance D. The "Mixed pixels" problem introduces offsets to the ranges measured to the object edges. Because of the laser beam divergence, when the laser beam falls on the object edge, one part of it is reflected off the object surface, and another – from the object surface behind it (sometimes at a large distance away) or not at all (if there is no object behind within the scanner operating range). If the distance between the two object surfaces is less than half the pulse width (expressed in metres), then the receiver cannot distinguish between the pulses returned from both surfaces. The range is therefore estimated by averaging the ranges to the points on both surfaces. Evidently, the problem of "mixed pixels" cannot be completely eliminated. However, a laser scanner with a small beam divergence can partially overcome the mixed pixels problem (Hebert and Krotkov, 1991).

From the experiments reported by Tuley et al. (Tuley et al., 2005), mixed pixels or mixed measurements can occur due to several reasons:

1) overlap of the laser beam onto two objects at the edge of an object.
2) target structures are thinner than the beam.
3) non-ideal characteristics of the SICK LMS-291-SO5 laser.
4) ground interaction.

2.4.2 Range-reflectance cross talk and temporal mixing

Reflectance crosstalk refers to the effect the intensity of reflected light from an object has on the range measurement accuracy. Crosstalk is a phenomenon in which reflectance or intensity values affect the measured range. To some degree, intensity always affects the range values. According to Hancock (Hancock, 1999), lower intensity values decrease the signal-to-noise ratio, and therefore, increase the variance in measured range, although this should not affect the average range.

Crosstalk is caused by the nature of AMCW measurements which relies on the reflectance of the target as shown in the following equation given by Hebert and Krotkov (Hebert and Krotkov, 1991):

$$\overline{F}_p = \left(\frac{\alpha A_R \overline{F}_T}{\pi} \cdot \frac{\rho \cos \alpha}{r^2} \right) \qquad \text{Eqn. (2.13)}$$

where,

$\overline{F}_p$ is the time-average radiant flux (W).

α is the fraction of reflected radiant flux passing through passing through the interference filter to the photomultiplier tube

A_R is the capture area of the receiver

$\overline{F}_T$ is the time-average transmitted radiant flux.

ρ is a measurement of the diffuse reflectance of the target surface, calculated as a ratio between the incident and reflected flux. This would vary between 0 for a perfectly black surface and 1 for a perfectly white surface.

Temporal mixing occurs when, within a single sample, the laser moves from one surface to another. This is especially noticeable at edges between darker and lighter surfaces. As a laser moves from a dark surface to a light surface, the amplitude of the return signal varies. This can lead to large errors in phase estimation and thus produces large range errors.

2.4.3 Photon Noise

Photon noise is the most dominant noise source amongst other sources such as laser noise, ambient noise, dark-current noise, secondary emission noise and subsequent emission noise (Hebert and Krotkov, 1991) (Nitzan et al., 1977).

According to the assumption reported by Nitzan et. al (Nitzan et al., 1977), photoemission is a Poisson process and the signal to noise ratio (SNR) based on photon noise is given by:

$$SNR = \left(\frac{\alpha \eta \lambda A_R \bar{F}_T}{\pi h c} \cdot \frac{\rho \cos \alpha}{r^2} \right)^{\frac{1}{2}} \qquad \text{Eqn. (2.14)}$$

where 'η' is the quantum efficiency of the photocathode used in the scanning system and 'h' is Planck's constant.

Generally, a lower intensity implies a higher noise in the range measurement, and the reflectance property of the observed scene in outdoor environment is susceptible to crosstalk.

2.4.4 Intensity and Range Drift

Over a period of time a drift in measured intensity can occur due to change in the temperature of laser source. Due to a change in temperature, there is a change in length of the laser cavity, which in turn changes the laser frequency (or wavelength). This change in frequency can generate a subsequent change in phase, thus, resulting in a continuous offset in AMCW range measurements, which depends on the change in temperature.

2.5 TRIANGULATION

Active triangulation is one of the first range imaging approaches used in robotics, displacement sensing and obstacle detection systems (Hebert, 2000, Pears, 1992) (Zeng.L et al., 1999) (Klančnik S, 2007). Triangulation is a trigonometric technique to calculate the range and position to the target based on the length and angle parameters between a laser emitter, a target and a detector (Rioux, 1984). The basic geometry principle of active laser triangulation is illustrated in Figure 2.6.

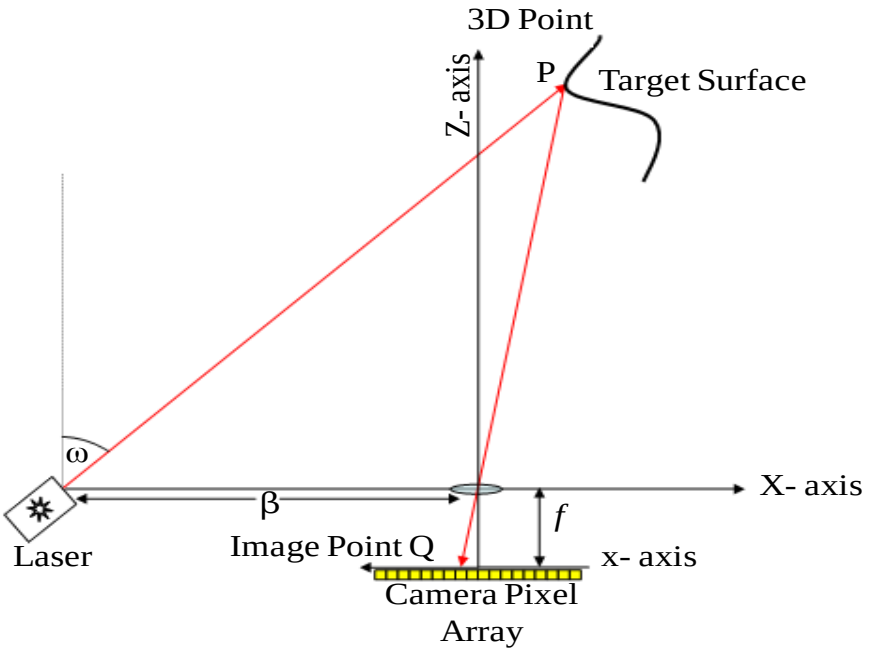

Figure 2.6: Basic principle of active laser triangulation (Sahba et al., 2008).

An imaging device of focal length *f* is positioned in line with the *Z*-axis and has the *X*-axis running through its lens centre. To the left of the lens, at a baseline distance *β*, a laser source launches a light beam at a variable angle *w*, as illustrated in Figure 2.6. The image point lying on the *x*-axis, together with *β*, *w* and *f* determine the *X* and *Z* coordinates of the illuminated target point *P* (Hartrumpf and Munser, 1997). The distance *Z*, from the projected laser spot to the lens centre is calculated using Equation (2.17) below.

The basic equation for deriving X and Z, from image formation and hence locating the object in the (*X*, *Z*) plane is given by the following equations (Hartrumpf and Munser, 1997):

$$X = \frac{xZ}{f} - x \quad \text{and} \quad Z = \frac{X + b}{\tan(\theta)} \qquad \text{Eqn. (2.15)}$$

$$X = x\left(\frac{f\tan(\theta) - b}{x - f\tan(\theta)}\right) \qquad \text{Eqn. (2.16)}$$

$$Z = f\left(\frac{x - b}{x - f\tan(\theta)}\right) \qquad \text{Eqn. (2.17)}$$

The baseline distance b, can be calculated as shown in equation (2.18) (Sahba et al., 2008):

$$b = \sqrt{\left(\left(\frac{L_b - P_b}{P_m + L_m}\right) - L(x)\right)^2 + \left(\left(\frac{(P_m.L_b) - (L_m.P_b)}{P_m.L_m}\right) - L(z)\right)^2} \qquad \text{Eqn. (2.18)}$$

where P_m and P_b are the slope and z-intercept of a projected ray, respectively. L_m and L_b are the slope and z-intercept the lens line, respectively.

Figure 2.7 illustrates the triangulation technique with the laser source and the image sensor (Beraldin, 2004). The dimensions of the triangle can be determined with both the angles $\propto$ and β relative to its baseline D. The range measurement accuracy is mainly dependent on the pixel position accuracy, which is limited by sub pixel speckle noise in the case of laser beam projection (Baribeau and Rioux, 1991).

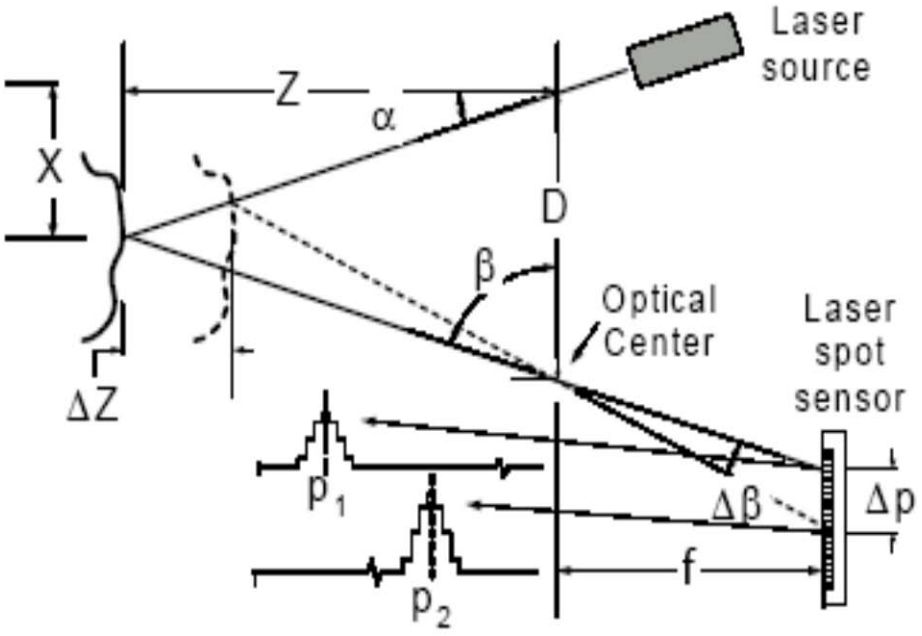

Figure 2.7: Laser based single spot optical triangulation (Beraldin, 2004).

The range measurement accuracy δ_z is given by

$$\delta_z \approx \frac{Z^2}{f \cdot D}\delta_p \qquad \text{Eqn. (2.19)}$$

where, f is the effective position of laser spot sensor, D is the baseline, δ_p is the uncertainty in laser spot position and Z is the distance to object.

δ_p is the pixel position accuracy given by:

$$\delta_p = \frac{1}{\sqrt{2\pi}} \cdot \lambda \cdot fn \qquad \text{Eqn. (2.20)}$$

where, fn is the receiving lens f-number and λ is the laser wavelength.

Though the laser triangulation method has many advantages, still it has some limitations. When a laser beam strikes a sun-illuminated object or a material, due to the brightness of the sunlight, the scattered laser beam will be combined with the background light making it difficult for the imager to resolve the laser beam power. A solution to such problem is to reduce the size of the lens aperture to narrow the laser beam to reduce the scattering effect. To suppress the background colour contrast or noise, a narrowband filter can be placed in front of the imager so that only a narrow band of wavelengths is detected by the imager thus reducing the total background noise and preventing the photodetectors from getting saturated by the unwanted sunlight.

The resolution of the triangulation system is directly related to its baseline distance (Hebert, 2000). However, a frequently encountered problem in the laser triangulation method is the occlusion problem, where a large baseline distance can block the laser spot from imager's field of view, as shown in Figure 2.8 (Bradshaw, 1999).

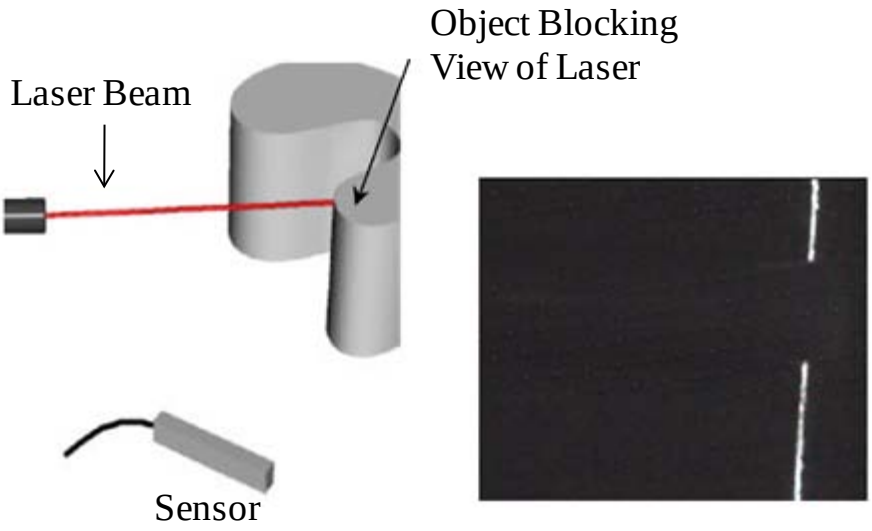

Figure 2.8: Occlusion of a laser spot with respect to the image sensor (Bradshaw, 1999).

The occlusion problem can, however, be solved by using a synchronous scanning system, where the separation between the laser and imager is widened and a narrow line width laser is used in conjunction with a very small field of view receiver that is synchronously scanned (Rioux, 1984). Generally, the projected laser light is synchronised with its detection at the sensor, through the use of three scanning mirrors. A typical model of dual- view triangulation is shown in Figure 2.9. (Blais, 2006).

The ray geometry of the synchronous scanning system shown in Figure 2.10 has a rotating pyramidical mirror which could also be replaced with a two sided horizontal scanning mirror (Besl, 1988). The laser beam is first deflected by the rotating pyramidical mirror to the mirror M_1. From M_1 the laser beam is made to intrude into a vertical nodding mirror, M_3, and then the beam strikes the target surface.

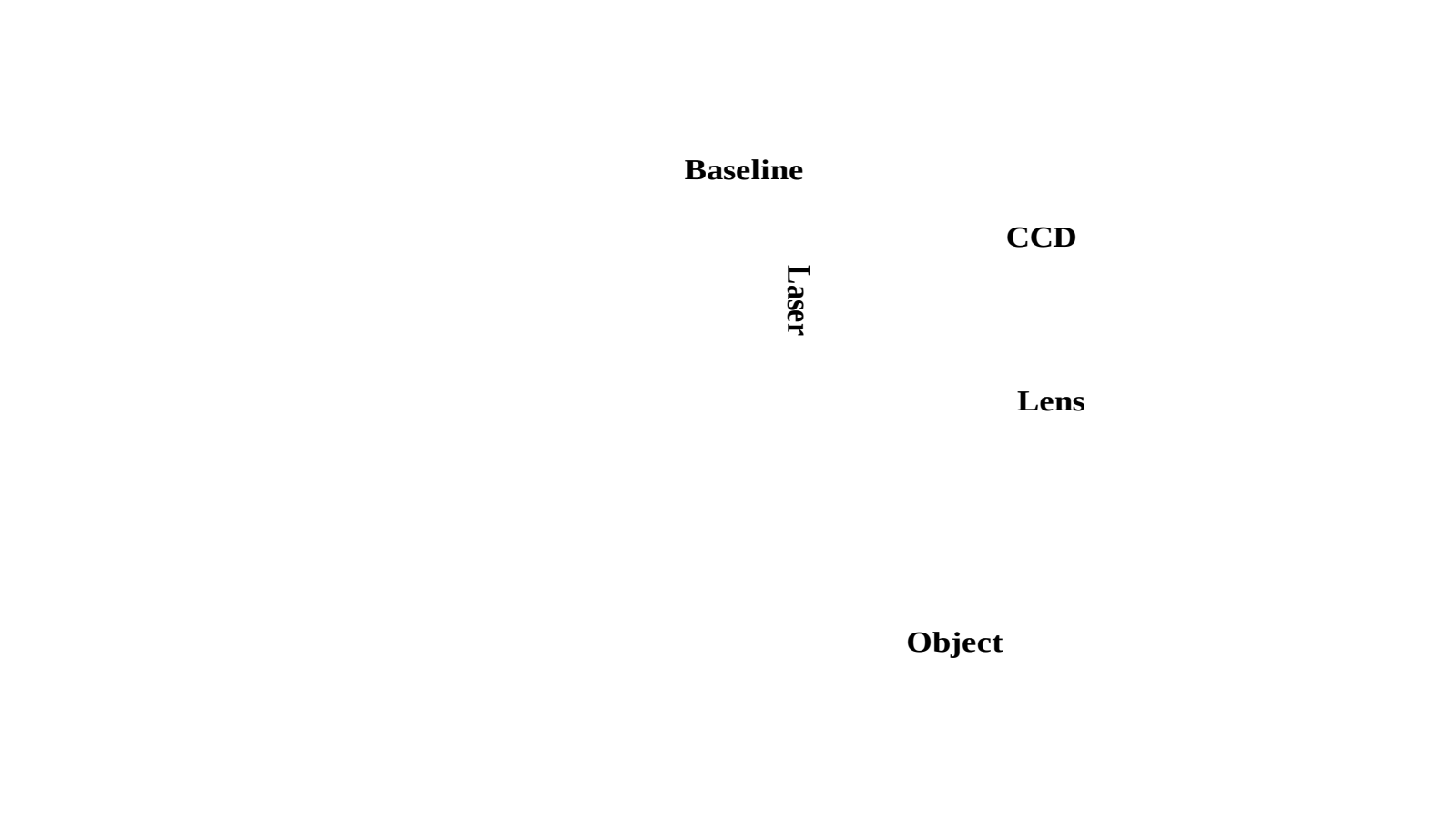

Figure 2.9: Dual-view laser triangulation (Blais, 2006).

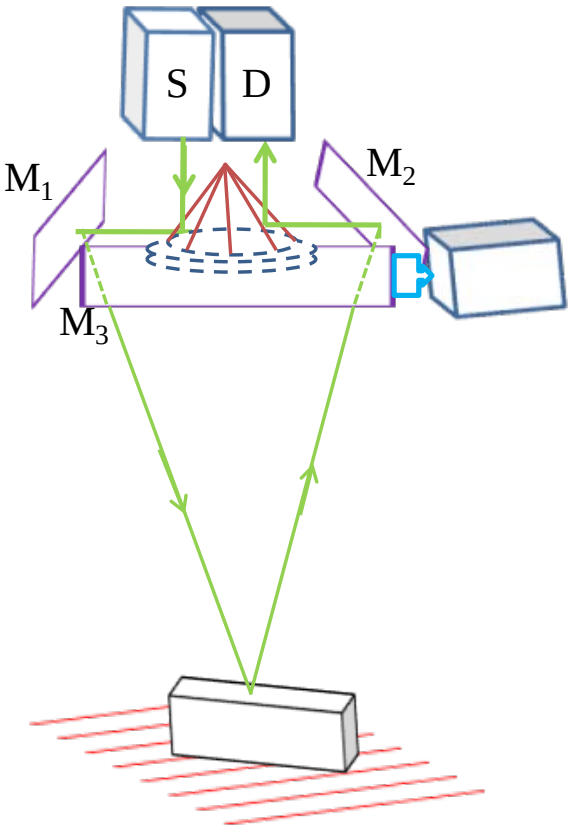

Figure 2.10: Ray geometry of the synchronized scanning system (Rioux, 1984).

The laser beam is reflected from the target and strikes the fixed mirror M_2, which directs the laser beam to the opposite face of the pyramidical mirror and then deflected towards the detector. This type of ray geometry provides longer focus on the projected laser beams and also provides higher range resolution with a short baseline.

Edge curl is another problem encountered in laser triangulation, whereby the laser beam strikes the edge of the object or target, preventing the whole laser beam from being imaged by the imager. According to Bradshaw (Bradshaw, 1999), the intensity of the captured image can be processed to reduce the effect of the edge curl.

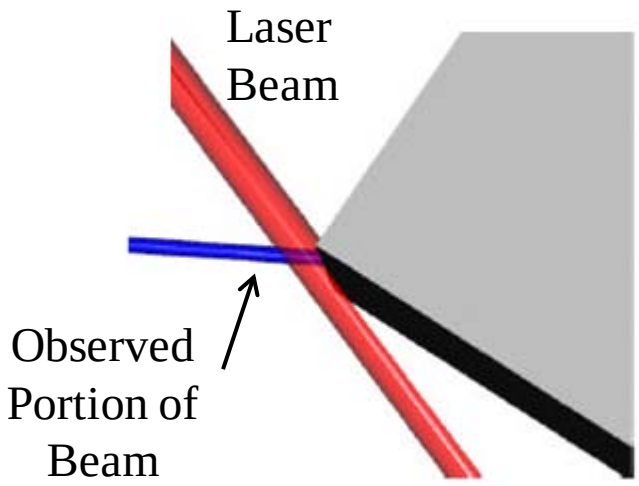

Figure 2.11: Illustration of the edge curl problem (Bradshaw, 1999).

Note that, the edge curl effect can also occur for a target material texture having dark and light areas, when the laser beam strikes in between two different areas, the reflected intensity of the laser beam will be different for each area, producing an asymmetrical laser spot image.

2.6 SURFACE REFLECTANCE

Reflection occurs when light changes the direction as it strikes a surface, such as a mirror. There are two types of reflection, illustrated in Fig. 2.12, namely, specular reflection (incoming light from a single incoming direction (a ray) is reflected into a single outgoing direction, and the angle of incidence equals the angle of reflection) and diffuse reflection (incoming light is reflected, or diffused, in a broad range of angles). Reflection is determined by the surface characteristics and it also depends on the wavelength of light striking the surface (Campbell, 1996).

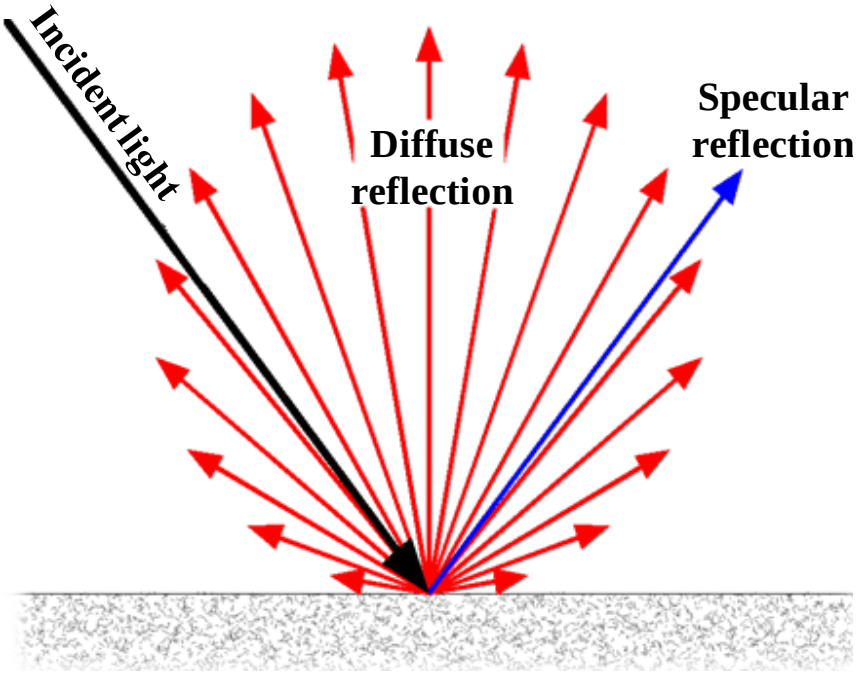

Figure 2.12: Illustration of specular and diffuse reflection types.

Figure 2.13 illustrates the surface reflectance for a collimated laser beam striking a surface. The reflected light has both specular and diffuse components, however, it is always possible to adjust the laser incidence angle and the imager field of view in such as way that the specular beam is routed outside the field of view of the imager and only the diffuse component is imaged, as reported by Nitzan (Nitzan et al., 1977).

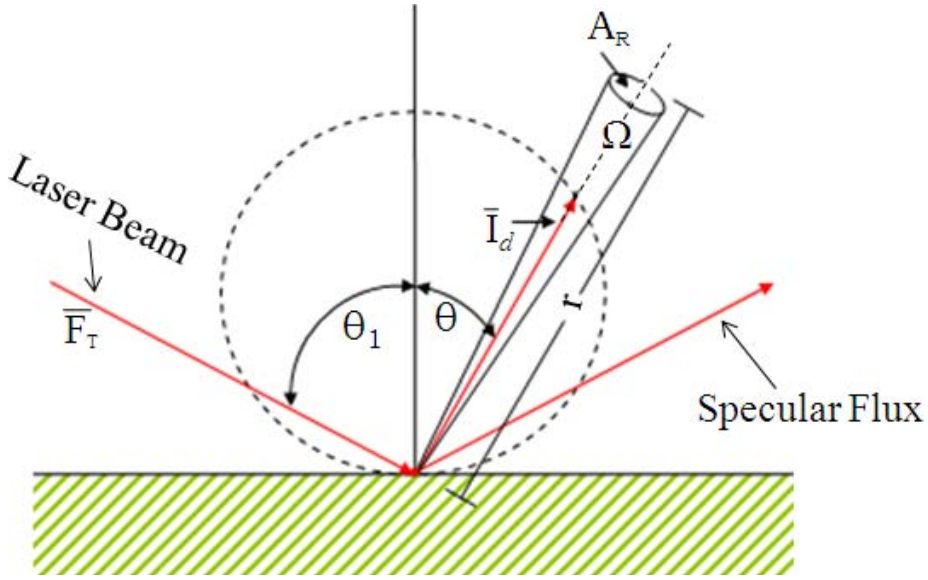

Figure 2.13: Specular and diffuse reflection component of an incident laser beam (Nitzan et al., 1977)

The diffuse component is calculated using Lambert's cosine law (Nitzan et al., 1977)

$$\bar{I}_d = \frac{\overline{F}_T}{\pi} \rho_d \cos\theta \qquad \text{Eqn. (2.21)}$$

where $\bar{I}_d$ is the time-average radiant intensity, in watts per steradian, of the reflected light for an incidence angle θ, p_d is the diffuse reflectance, and $\overline{F}_T$ is the incident radiant flux.

Reflection off objects exhibiting physical and chemical properties has recently been investigated by Nishino (Nishino et al., 2011). Figure 2.14 shows the reflection versus incident angle for smooth metals, which are electrical conductors, and dielectric media, which are insulators. Most of the metal surfaces exhibit over 50% of reflection whereas the reflectance of a wide range of dielectric surfaces is below 20%.

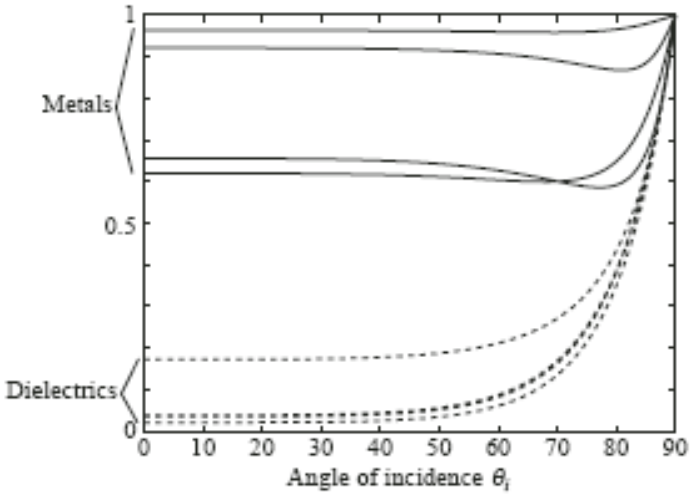

Figure 2.14: Fresnel reflectance for smooth metal and dielectric surfaces (Westin et al., 2004).

Examples of typical reflectivity's for some coloured materials are (Marbs, 2007):

- White dull spray paint, reflectivity 90%
- Gray dull spray paint, reflectivity 40%
- Black dull spray paint, reflectivity 8%
- Denim, reflectivity 10% - 20%, matt black clothing is even lesser than denim (Hosmer, 2004).

2.7 CHAPTER SUMMARY

In this chapter, the fundamentals of laser RADAR (Radio Detection and Ranging) and the difference between laser RADAR and LADAR (Light Detection and Ranging) have been described. Active and passive methods of optical range finding have been classified and discussed in detail. Also, the optical ranging methods, namely the Time Of Flight (TOF) and active triangulation methods have been reviewed. Furthermore, range resolution and range uncertainty for pulsed TOF, amplitude modulated continuous wave and frequency modulated continues wave approaches have been discussed.

Problems associated with laser ranging have also been discussed, including (i) mixed pixels, also known as mixed measurements, (ii) reflectance crosstalk, which affects the accuracy of the range measurements and (iii) temporal mixing that affects the range measurements by producing large phase errors when the laser moves from a dark surface to a light surface. The impact of photon noise, which is created by ambient light in outdoor environments, has been described, as well as the impact of temperature on intensity and range drift. Most of the conventional ranging problems have also been discussed. Two types of surface reflections were investigated and typical reflectivity's of metals, dielectric and few materials were reviewed.

Since this thesis focuses on laser-based intrusion detection for security systems, the next Chapter will investigate laser scanning methods for perimeter security, mechanical beam deflectors and the various problems associated with them.

CHAPTER 3

OVERVIEW OF LASER SCANNING

3.1 INTRODUCTION

This chapter contains the fundamental theories of laser scanning techniques and discusses the issues associated with them. Basic knowledge of the laser scanning unit, various laser scanning directions and different laser scanning methods are presented. The operation principles of polygonal mirror, holographic and galvanometric scanners are discussed, along with the problems associated with their beam deflection unit in Section 3.3. Laser scanning methods for intrusion detection and discrimination are discussed in Section 3.4. This includes the core of physical perimeter security, exterior and interior detection sensors, laser scanning for perimeter security and the benefits and limitations of laser scanning.

3.2 LASER SCANNING ARCHITECTURE

A laser scanning system provides accurate geometric information about a target, such as distance, position, attitude and co-ordinates, by recording the time of flight of the laser signal with high precision. The resolution of a laser scanning system depends on the scanning mechanism used to deflect the laser beam from the laser source to the desired target surface. Conventional laser scanning systems are based on two- or three-dimensional opto-mechanical laser scanning. This type of laser scanning can be used for various types of applications, such as airborne topographic mapping, surveying of buildings and plants and model generation for animation purposes (Thiel and Wehr, 2004).

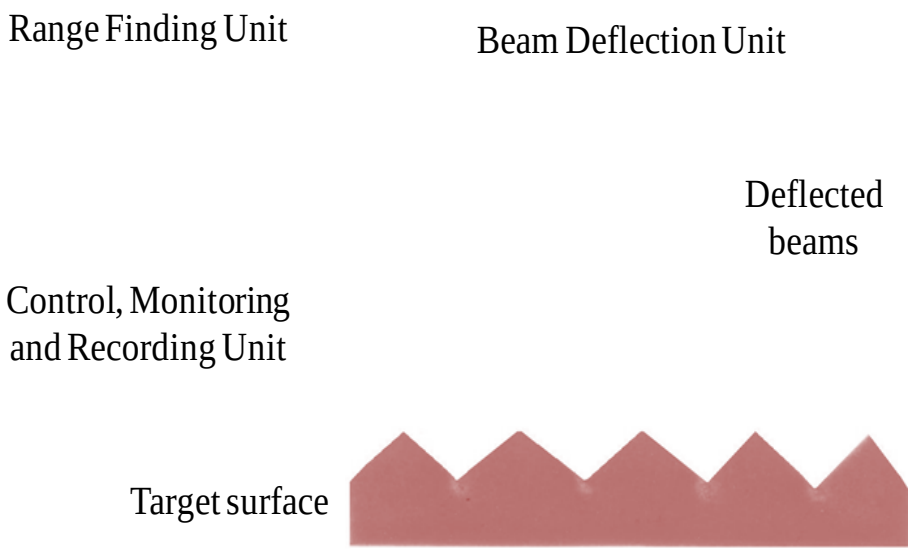

Figure 3.1: A basic laser scanner setup. (Thiel and Wehr, 2004).

A typical laser scanner consists of the key components shown in Figure 3.1. The performance of a laser scanner is determined by the ranging accuracy, the precision of the laser beam deflection mechanism, the opto-mechanical scanning technique and the measurement rate.

Laser-beam-scanning systems can be divided into the following two categories:

(1) Space-angular-scanning systems and

(2) Surface-scanning systems.

According to Li and Katz (Li and Katz, 1995) the space-angular-scanning system (e.g. a Lidar) is suitable for detecting events in an active or passive way along a given direction, whereas the surface-scanning system is suitable for detecting information from a given surface or inducing a physical effect such as photoconductivity or photo magnetism on the surface during the scan.

A beam deflection unit, illustrated in Figure 3.1, can typically deflect a laser beam through electro-mechanical scanning. Figure 3.2 illustrates the motion of a laser scanner in the nodding and panning directions using 3D Cartesian space, as reported by Hebert and Krotkov (Hebert and Krotkov, 1991).

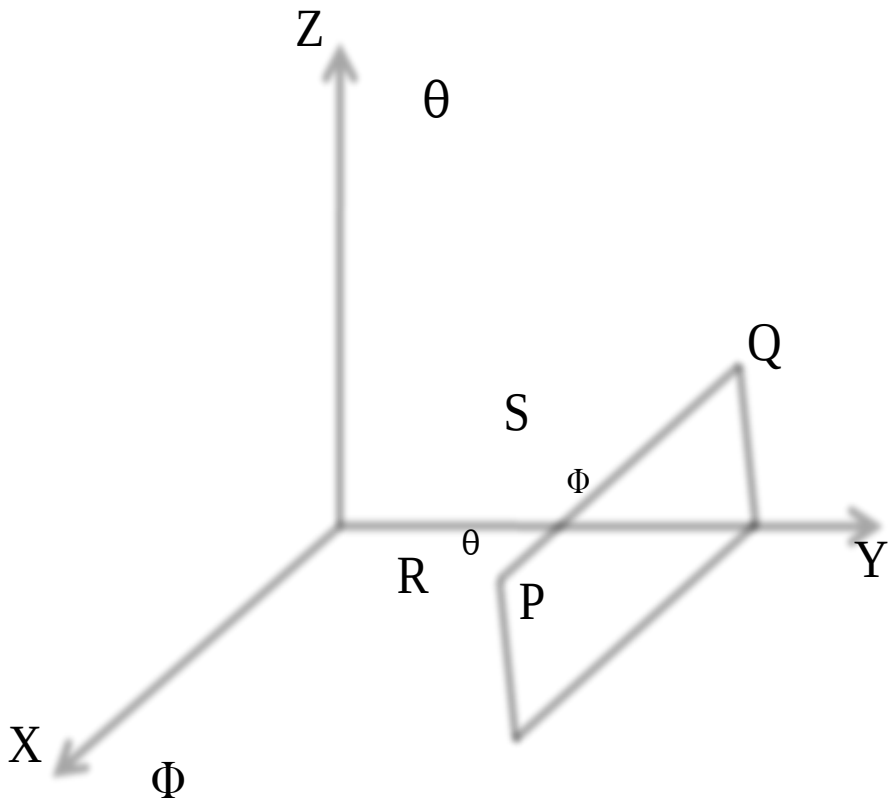

Figure 3.2: Illustration of azimuth (θ around the z axis) and elevation (ϕ around the x axis) laser scanning (Hebert and Krotkov, 1991).

The principal ray is launched along the y-axis. Points P and Q indicate the corners of the reference frame. R and S are the ranges from the innermost point of the scanner to P and Q respectively. Range S requires only an elevation as Q lies in the same degree of the azimuth of the innermost point, whereas R requires an elevation as well as a pan to reach P.

A 2D laser scanner with a 180° scanning range and a servo drive results in several possible combinations of scan planes and rotation axes to realise a 3D scan. Four of these combinations are shown in Figure 3.3, and named as pitching scan, rolling scan, yawing scan and yawing scan top, respectively (Wulf and Wagner, 2003).

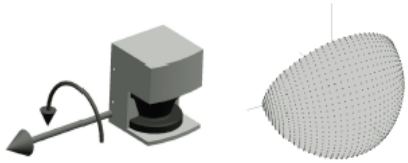

(a) Pitching Scan.

(b) Rolling Scan.

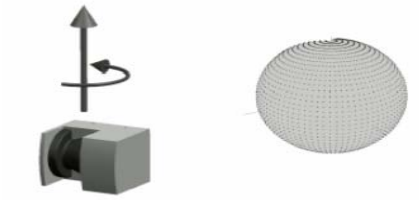

(c) Yawing Scan

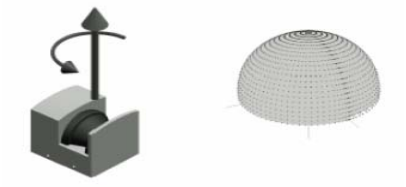

(d) Yawing Scan top.

Figure 3.3: Scanning motion directions - (a) pitching scan, (b) rolling scan, (c) yawing scan, (d) yawing scan top (Wulf and Wagner, 2003).

The pitching scan shown in Figure 3.3a is based on horizontal plane scanning thus pitching up and down. For the rolling scan shown in Figure 3.3b, the mirror rotates around the centre of the scanner. Both the yawing and yawing top scans shown in Figure 3.3(c and d) are based on vertical plane scanning where the mirrors are rotating around the upright z-axis.

Two of the most important factors used to measure a scanner's performance are the angular range of deflection and scanning speed. According to Taylor et al., (Taylor et al., 1998) conventional laser scanning takes a long time to create an image because the beam deflection mirror does not move fast enough to scan a target at a sufficient speed. Laser scanning is much more sensitive to vibrations than a multi-beam stationary-optics approach. Schnadt and Katzenbeißer (Schnadt and Katzenbeißer, 2004) stated that "the mirror-device scanners are slow, bulky and expensive". Moreover, according to Elkhalili, et al. (Elkhalili et al., 2004), mirror driven scanners can also cause deflection errors due to mechanics, acceleration and wear out, and additionally, they require regular calibration.

3.3 MECHANICAL LASER BEAM DEFLECTORS

A mechanical laser beam deflector functions on the basis of projecting a beam of light to a mirror component, which deflects the light at an angle equal to the angle of incidence. Then the mirror is rotated vertically or horizontally to deflect the laser beam to another position that depends on the panning or nodding shift made. Rotating prisms can also be used as mirrors for laser beam deflection.

3.3.1 Galvanometer laser scanner

Figure 3.4 shows a typical single point scanner employing a galvanometer. Galvanometer-based scanners can be classified as two types, namely, board band and resonant galvanometers.

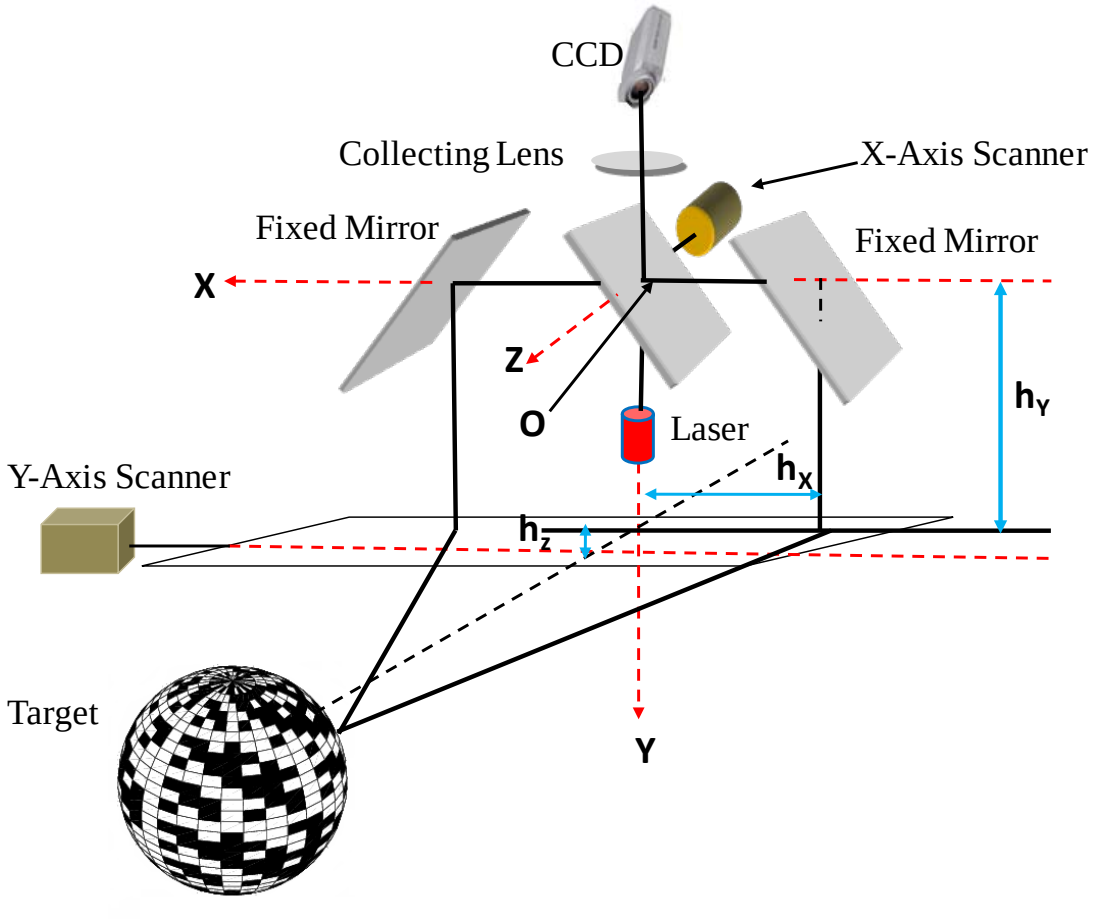

Figure 3.4: An example of a single point scanner using galvanometers (Blais, 2004).

According to Blais (Blais, 2004), a broadband galvanometer can be rotated to any arbitrary position as required as it can execute a linear ramp or hold a fixed position.

This is an important feature as one can obtain any angular position by applying the correct corresponding current pulse, and attain deflection angles that are in the order of 10 degrees, thus achieving thousands of resolvable spots.

The resonant galvanometer is a static system that operates with a constant scanning frequency. It is ideal for repetitive scans, where relevant parameters are fixed. However, it can only operate at a scanning frequency much higher than a broadband galvanometer.

Stutz (Stutz, 2005) has indicated that the limitation in the use of galvanometer laser scanners because of the physical dimensions of the revolving mirrors directly affects the scanning speed, weight and bulk as well as the number of resolvable spots. Scanning a large number of resolvable spots requires a sufficiently large mirror, which reduces the angular spread of the laser beam set by diffraction at the mirror. Also, a larger mirror requires higher power to drive, has a lower maximum scanning speed and takes a much longer time to accelerate to its constant scanning speed.

3.3.2 Polygonal and holographic laser scanner

The polygonal scanning architecture shown in Figure 3.5 consists of a uni-directional rotating device (i.e. a polygonal mirror), a drive system and a bearing system. Polygonal mirrors are usually fabricated using diamond-turned aluminium; however, glass and beryllium are also used, in some specific applications.

Rotating polygon mirrors are also used as mechanical deflectors for terrestrial LADAR scanners. A polygon-shaped component with mirror-polished sides mounted on a rotating shaft results in a rotating mirror deflector that can scan a surface profile. The laser is pointed at a side of the polygon and deflected according to the position of the polygon at the point in time during its rotation. A new scan is started every time a new side of the polygon intersects the beam.

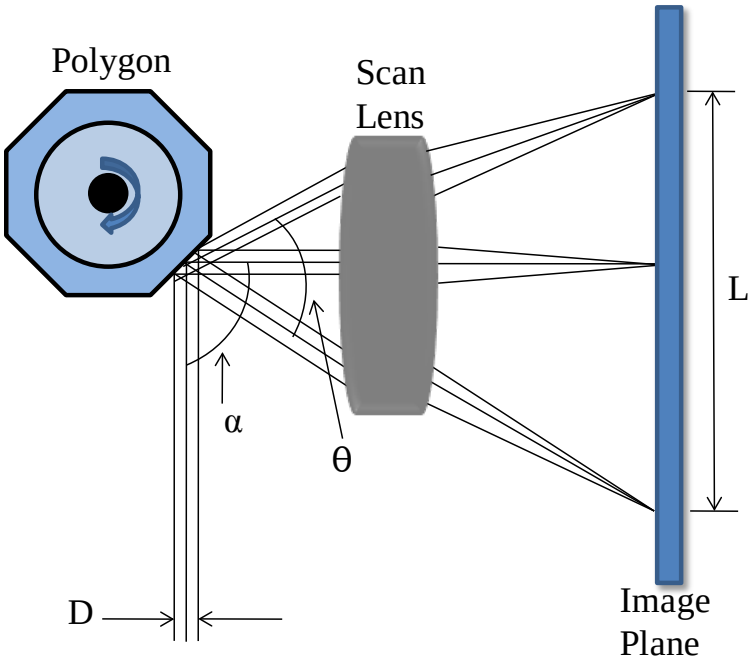

Figure 3.5: Rotating polygon scanner – top view. D is the incident beam diameter, α is the beam-feed angle, θ is the active scan angle and L is the scan length (Stutz, 2005)

According to Stutz (Stutz, 2005), features affecting the polygonal laser scanners include:

- Duty cycle – defined as the ratio of the active scan time to the total scan time
- Operating speed
- Active scan angle
- Beam-feed angle
- Image plane scan length
- Scan lens focal length
- Laser beam spot size
- Laser beam wavelength
- Pixel placement accuracies

The same rotating mechanism of polygon scanners is used in holographic laser scanners, where the light is deflected off through a face of a disk, instead of being mirrored: composed of holographic diffraction gratings in a photo-emulsion on glass substrate that disperses the input beam. The holograms can be either transmissive or reflective.

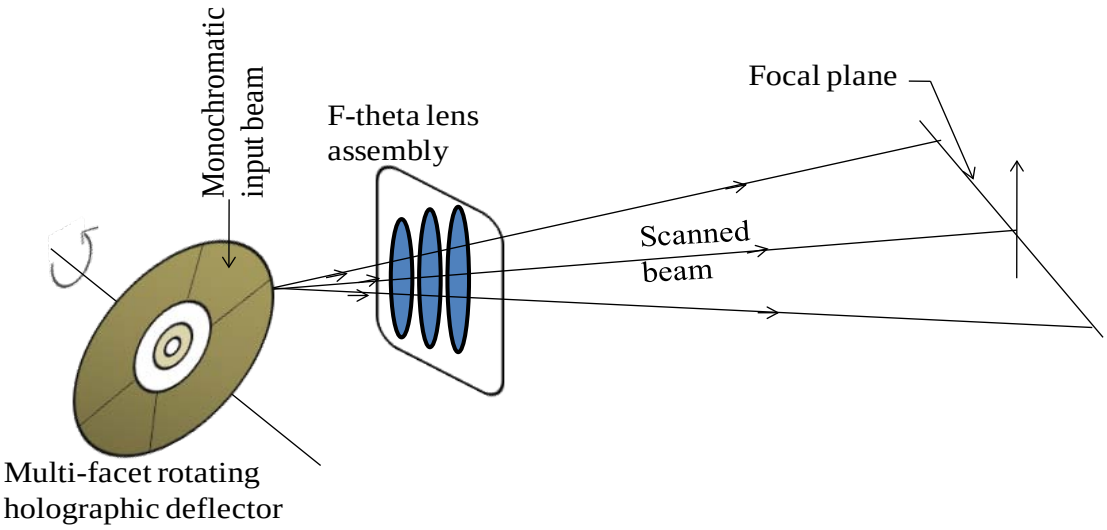

Figure 3.6: Typical holographic scanner setup (Rowe, 1997).

One common form of a holographic scanner setup is shown in Figure 3.6, where a transmission hologram encoded on the rotating disk diffracts the input light beam and a series of lenses optimally shape the diffracted beam to obtain an aberration-free point image. As the hologram rotates, the point image is scanned along a circle in the image plane.

The advantages of holographic scanners hold over typical mirrored polygon scanners as follows (Rowe, 1997, LEOT, 2001):

1. Reduced sensitivity to motor shaft wobbles.
2. Reduced scanner windage due to the aerodynamic nature of the scan disc, allowing higher scan rates.
3. Reduced sensitivity to motor scan jitter due to the transmissive nature of the deflector. This particular feature allows the use of a ball-bearing motor instead of an air-bearing motor.

In general, mechanical light-beam deflectors produce large deflection angles with relatively low speeds, whereas non-mechanical deflectors tend to produce smaller angles of deflection at high speeds. It is very difficult to avoid a trade-off between the angle of deflection and the speed. Balance of the laser scanner package is also crucial, especially at high rotational speeds.

3.4 LASER SCANNING FOR SECURITY SYSTEMS

3.4.1 Physical Protection System

The design and evaluation process of a Physical Protection System (PPS) is shown in Figure 3.7 (Garcia, 2001). The three main functions of PPS or Intrusion Detection System (IDS) are: detect, delay and respond.

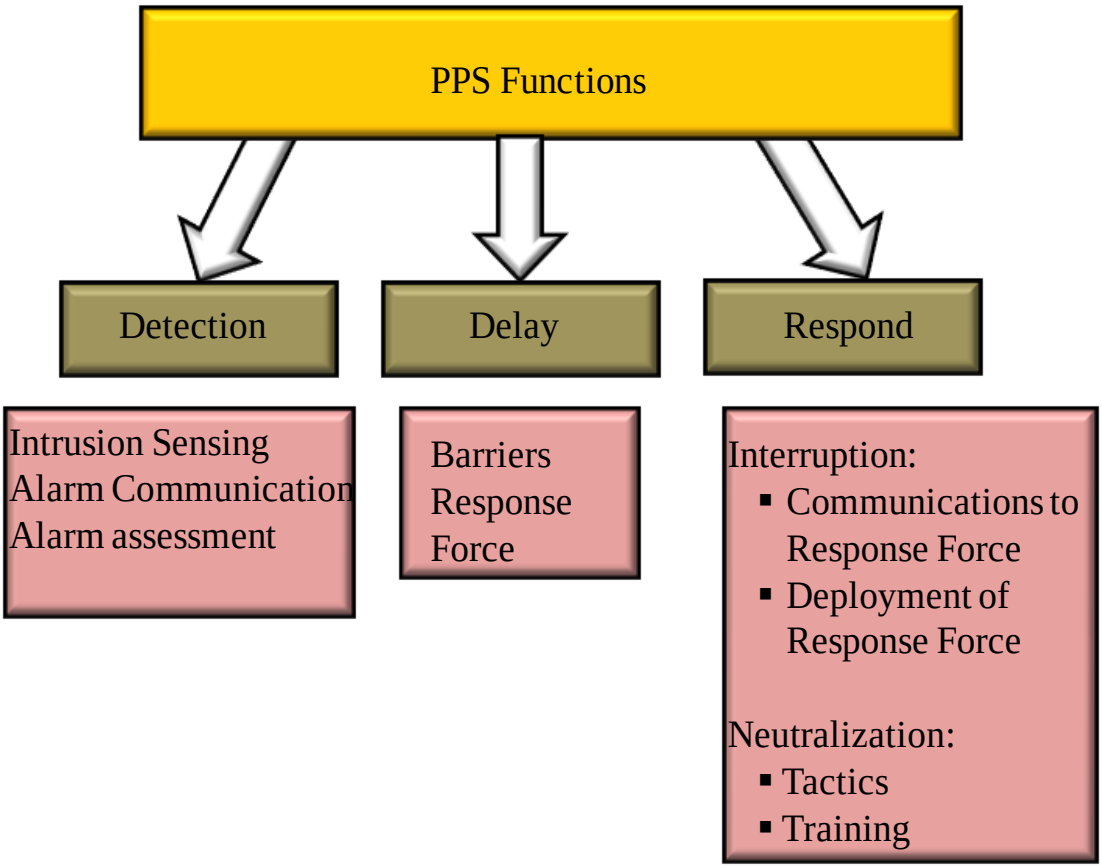

Figure 3.7: The design and evaluation process of a PPS (Garcia, 2006).

Detect: Detection is the discovery of an advisory action. There are three steps to discover an advisory action:

(1) A sensor reacts to a stimulus and initiates an alarm,

(2) Information from the sensor and assessment subsystems is reported and displayed,

(3) A person assesses information and judges the alarm to be valid or invalid (Garcia, 2006). Figure 3.8 illustrates the process of detection in PPS.

Figure 3.8: Detection function in a PPS (Garcia, 2006) (Garcia, 2008).

Delay: Delay is the second function of the PPS. The important task of this function is to increase the advisory task time. Delay can be enforced through pre-existing barriers such as locks, safes, security guards and so many. Delay before detection is primarily a deterrent. Figure 3.9 illustrates the purpose of the delay function in the PPS.

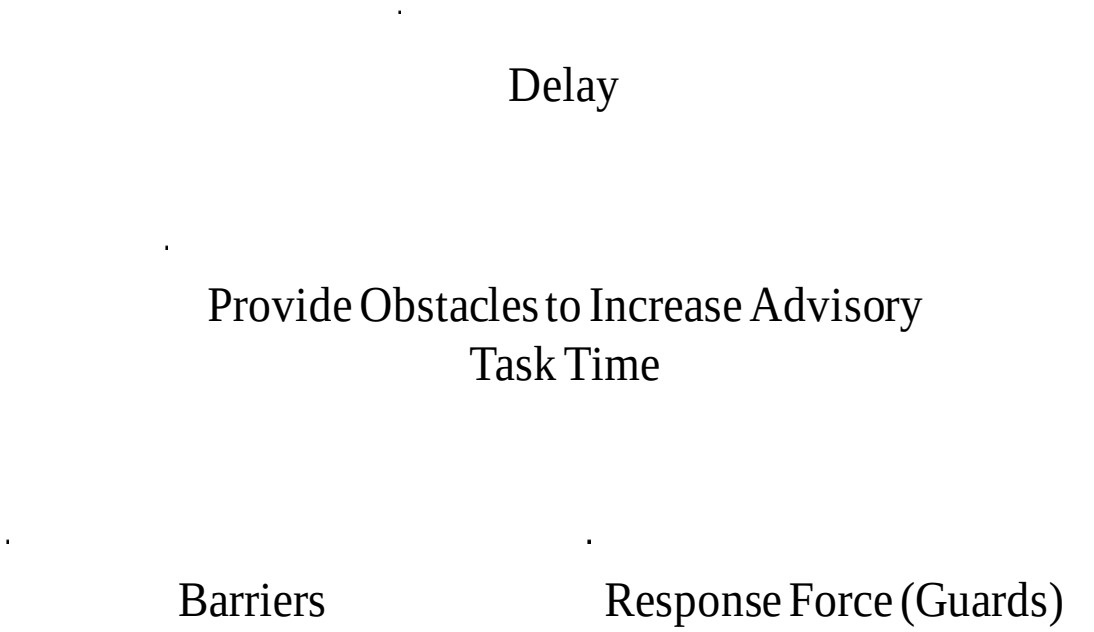

Figure 3.9: Delay function in PPS (Garcia, 2008) (Garcia, 2006).

Respond: The third and the last function of the PPS is to communicate to the response force and prevent the advisory task and take action.

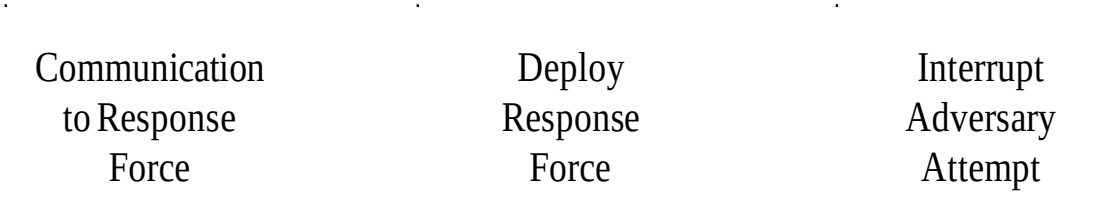

Figure 3.10: Response function in a PPS (Garcia, 2006) (Garcia, 2008).

Figure 3.10 shows the important factors of the response function. The communications to the response force, the time taken to complete the response force deployment and prolong and interrupt the adversary attempt is the major last function of the PPS.

3.4.2 Exterior and Interior Intrusion detection

Exterior intrusion detection sensor are used in an outdoor environment to detect intrusions while interior intrusion detection sensors are typically designed for detection in indoor areas only because (i) they are not designed as weather-proof devices that can survive outdoor conditions and (ii) they are very susceptible to false alarms. When designing an exterior detector, the outdoor environment must be taken into consideration, and in addition to surviving the rigorous outdoor conditions, the exterior detector should be designed for detecting intrusions accurately under rigorous conditions (EPA, 2011, Barnard, 1988).

Various sensor technologies for exterior and interior intrusion detection are displayed in Figures 3.11 and 3.12 (NISE, 1997).

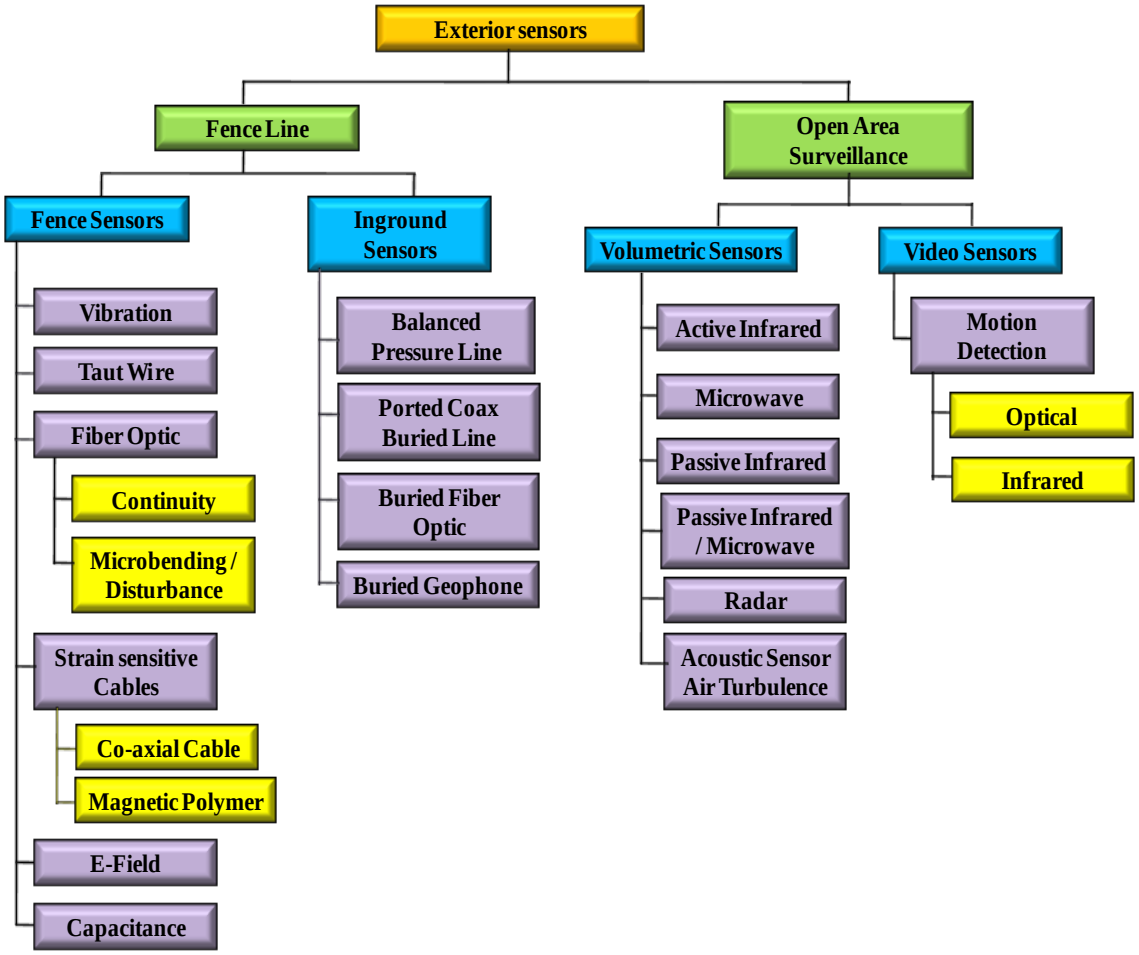

Figure 3.11: Classification of exterior intrusion detection sensors.

Exterior intrusion sensors have a lower possibility of detecting intruders and a higher false alarm rate due to uncontrollable factors such as: wind, rain, ice, stagnant water, blowing debris, random animals and human activity, also due to some electronic interference. These factors often require the use of two or more sensors to ensure an effective intrusion detection screen. (NISE, 1997).

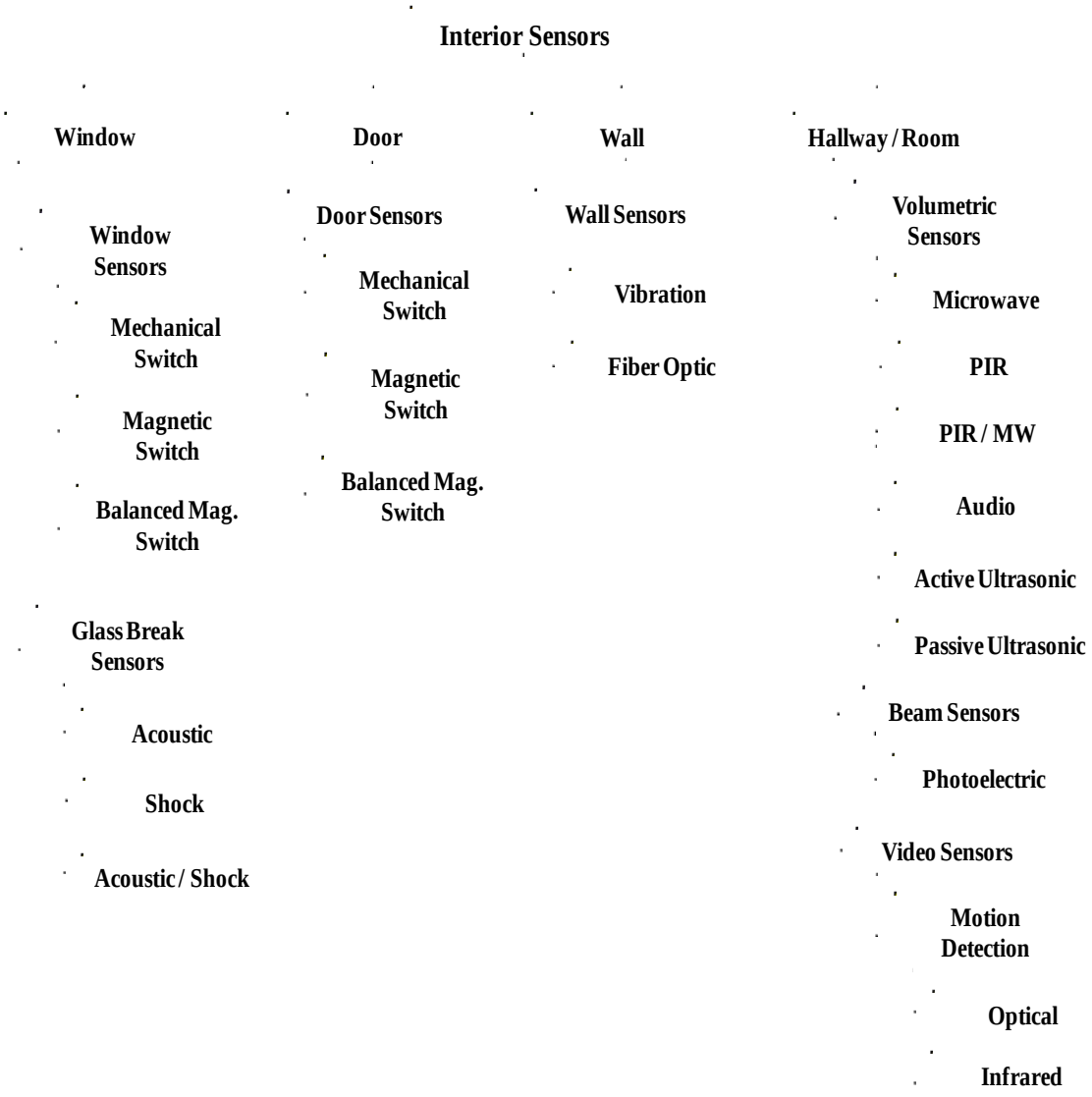

Figure 3.12: Classification of interior intrusion detection sensors.

Interior sensors perform the function through detection of an intruder moving within a secured area, such as a room or hallway and detection of an intruder moving, lifting, or touching a particular object. Interior sensors are also vulnerable to false alarms, however, not to the extent of exterior intrusion sensors, and this is due to the more controlled environment in which the sensors are deployed (NISE, 1997).

3.4.3 Laser Scanning for Perimeter Security

Laser scanning has been used in a large variety of applications, ranging from photo and document scanners to airborne topographic mapping, surveying of buildings and plants and model generation for animation purposes as well as commercial applications (Rioux, 1984). Laser scanning methods can be adapted for deployment in physical security, including perimeter intruder detection.

According to tests conducted to determine the feasibility of using laser scanning for perimeter protection, it has been confirmed that laser scanning is capable of detecting humans and vehicles with a maximum range of 25m and 80m, respectively (Hosmer, 2004). The testing demonstrated large area coverage, the ability to determine intruder size, the definition of multiple detection zones, a good detection range (25m for humans and 80m for vehicles) and low false alarm rate (FAR). It has also been claimed that camouflage and other methods for masking an object can deceive near infrared (IR) devices, but it is impossible to mask a physical volume moving through space, thereby implying that by scanning a plane at high speed and resolution, any object moving through this plane will be detected (Hancock et al., 1998). Riza, et al. (2003) proposed certain criteria for an ideal optical scanner including a wide scanning range, no moving parts, high resolution, high speed and low power consumption (Riza and Muzammil, 2003).

The company SICK produces laser scanners specifically for monitoring a perimeter. A SICK LMS 221 laser scanner was used to conduct that test. This particular laser scanner operates using pulsed TOF (discussed earlier) with beam deflection using a rotating mirror. A scanning angle of 190° degrees was achieved with a maximum radius of 80m. The angular resolution of the pulses can be set between 0.25 - 1°. Depending on the angular resolution, a single scan can take between 10 – 50 milliseconds.

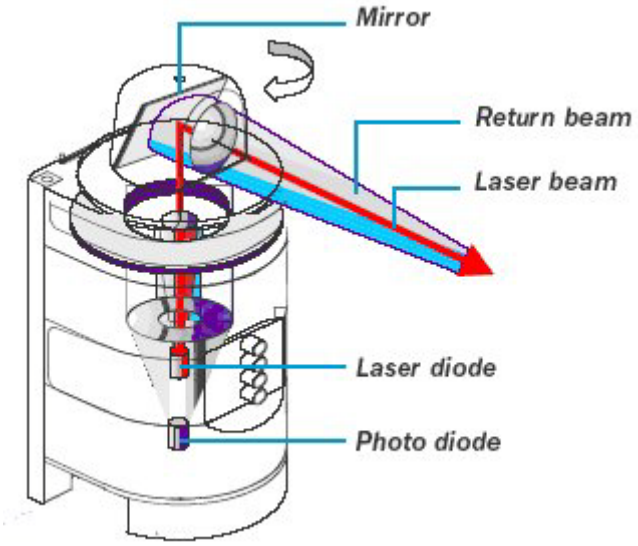

Figure 3.13: The rotating mirror concept for a SICK scanner, showing the Laser Distance Performance and Detection Scanner (LD DPS) model (SICK, 2006).

The principle of operation is depicted in Figure 3.13. The tilted mirror is mounted on a circular plate that is rotated by a motor. The LMS 221 employs an electro-mechanically driven rotating mirror to deflect the pulsed IR laser beam over a 180° field of coverage.

Detection is based on monitoring the contour of the surroundings recorded by the scanner and recognizing changes in its shape due to perturbing objects. Figure 3.14 shows a screenshot of the software user interface used for monitoring the scanned contour.

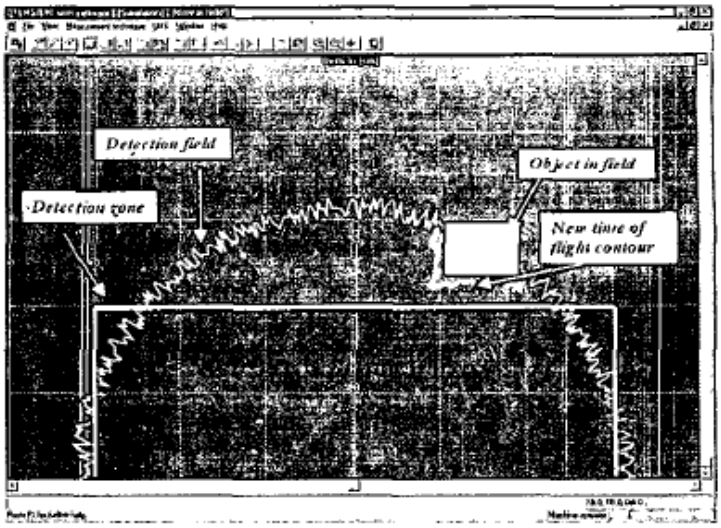

Figure 3.14: A typical screenshot of the SICK software user interface used for monitoring scanned contours in real time (Hosmer, 2004).

Pre-defined criteria can be used to identify targets based on properties such as size and location within the FOV. For this system, the object must be wide enough to intersect two neighbouring beams for detection to occur. By adjusting the angular resolution, the minimum object width required to break two consecutive pulsed beams can be configured, so that filtering out the detection of small objects such as birds flying through the detection field can be achieved. Detection based on the amount of time spent intersecting a series of beams can also be configured so that fast moving objects; for example birds flying through a detection field will not cause an alarm (Hosmer, 2004).

Goodrich Laser Perimeter Awareness System (LPAS) is one of the advanced laser scanning system for perimeter security (Ray et al., 2005, Jamieson and Ray, 2006). This scanner has three modules, namely: the laser module, the scanning head module and the electro-optical module. Figure 3.15 shows the LPAS product and the detailed operation principle of the scan head.

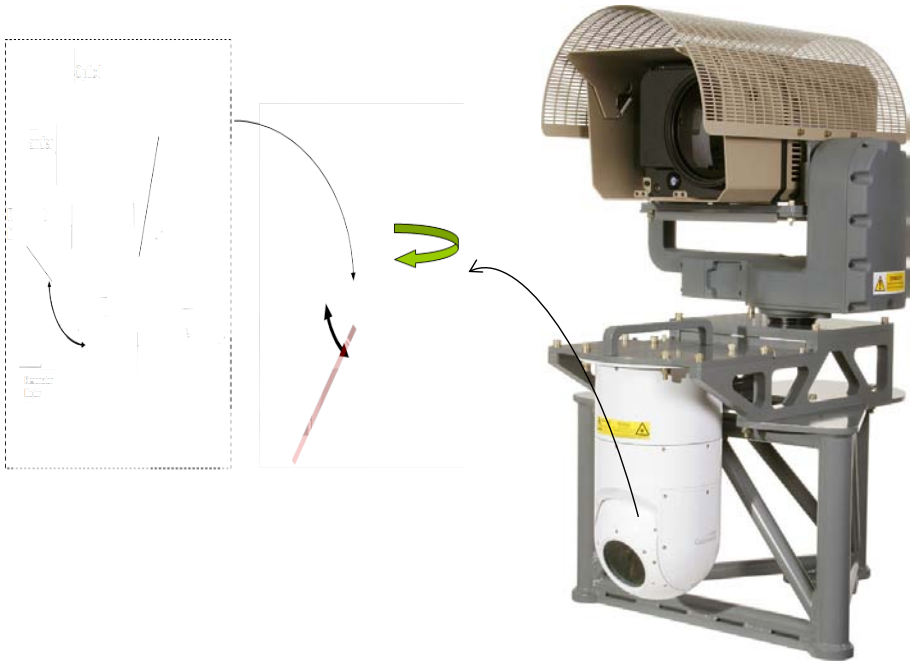

Figure 3.15: (a) Laser Perimeter Awareness System (LPAS) illustrating the deflection motion of the mirror in the scan head (b) Commercial LPAS product with T-2000 thermal camera (Jamieson and Ray, 2006).

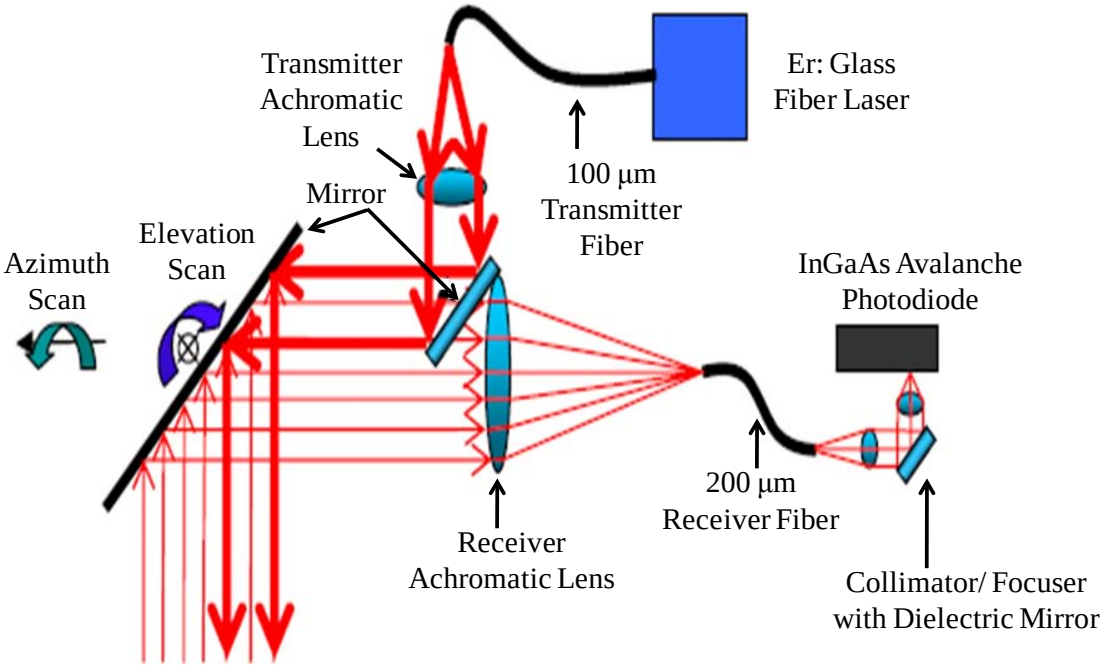

Figure 3.16: Schematic diagram of a LPAS (Ray et al., 2005).

Figure 3.16 shows the schematic diagram of LPAS. It comprises an Erbium doped fibre laser, an achromatic lens that expands the laser beam and transmits it to the oscillating mirror. The resonant motor oscillates the mirror at a frequency in the order of 100 Hz. The resonant scanner assembly and mirror move concurrently, as one unit, in azimuth and elevation producing a two-dimensional angular scan pattern. The unit can cover an area of 20˚ in elevation and 40˚ in azimuth in half a second.

The LPAS locates an intruder and actives the thermal imager, which triggers alert signals. LAPS is based on TOF ranging with a 1.55μm, 10kW Erbium-doped fibre laser. A human intruder at 250m range subtends an angle less than 0.5° in elevation. LPAS is capable of detecting and tracking intruders at ranges of 20m to greater than one kilometre with a high degree of spatial resolution, depending on the size and reflectance of the intruder.

The current-generation sensors for intruder detection and classification for perimeter security was developed at Texas A&M University. These sensors are based on the use of fibre-optic sensing elements in conjunction with advanced signal processing to reduce laser frequency drifts. The sensors can also be used in nuclear power plants and fuel storage facilities as well as at national borders. (Madsen et al., 2007).

Figure 3.17 shows typical placement of security laser scanners for object or intruder detection, reported by the laser scanning sensor companies SICK and Laser Optronix.

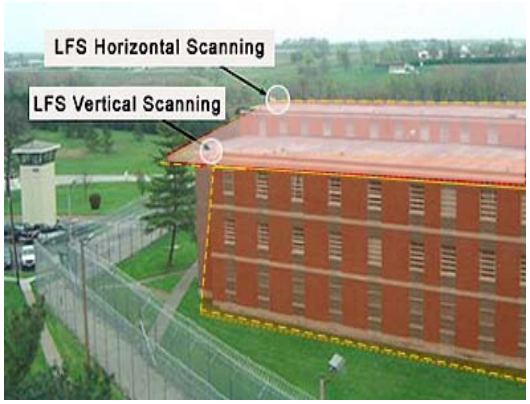

(a) Laser scanning for a perimeter, fence or wall of a building

(b) Laser scanning to protect the facades of a building

(c) Laser scanning across a perimeter

(d) Laser scanning for a fence

(e) Laser scanning for a high level roof protection against intrusion

(f) Laser scanning for indoor area to protect the assets

Figure 3.17: Examples of laser scanning applications for perimeter security (SICK, 2011, SmartSecSystems, n.d, LaserOptronix, n.d).

3.4.4 Laser scanning benefits and limitations

A typical laser scanning system has a transmitter and a receiver, which are coaxially located, so, as terrain sensors, they do not require line of site arrangement. Laser scanners can produce a laser beams along 3 dimensions, and they can also be tunnelled underground. According to Hancock et al. (Hancock et al., 1998) camouflage and other methods for masking an object can deceive near infrared devices, but it is impossible to mask a physical volume moving through the space, thereby implying that by scanning a plane at high speed and high resolution, any object moving through this plane will be detected.

Multiple detection zones can be devised for laser scanning, meaning that a laser scanner can be placed in such a way that its detection field covers an area to be monitored for intrusion. The angular resolution between any two laser beams can be adjusted to ignore unimportant intrusion in the area under control, thus reducing the false alarm rate significantly. A laser scanner can also be devised to ignore the intersection of laser beams for a small period of time, such as the intersection of a flying bird.

The major advantage of laser scanning in comparison with RADAR is the very high resolution of laser beams in comparison to RADAR beams. A typical RADAR pencil beam has a divergence angle of 3 (Gagnon, 2006), whereas a laser has as divergence angle of 2 mrads or 0.114° (Ray et al., 2005).

Laser scanning system performance can be validated by the intrusion detection capability, and this performance depends on the detection probability of the external or internal laser scanners (Lichti and Gordon, 2004). Laser scanners with moving mirrors, such as polygonal mirrors and galvanometric mirror and stepper motors, produce wobble, jitter, wear and tear develop errors in the beam deflection unit. Also, such mirror-driven scanners are bulky, expensive, very slow and require regular calibration (Elkhalili et al., 2004, Schnadt and Katzenbeißer, 2004).

The surface reflectivity of objects has also to be seriously considered, because the detection capability of laser scanners depends on the reflection of the laser beam. For example, if the absorption of laser light is more in the target object, then the received reflected light will be affected by the amount of absorption, which in turn will affect the scanners detection ability. For a few materials, the reflectivity is very low, e.g. black dull spray paint has a reflectivity of 8% (Marbs, 2007), a Denim has a reflectivity that

ranges from 10% - 20% (Hosmer, 2004) while matt black clothes have even less reflectivity than denim materials.

3.5 SUMMARY

The fundamentals of laser scanning (along azimuth and elevation directions) have been overviewed. Mechanical beam deflectors encountered in galvanometer, polygonal and holographic scanners, and the problems associated with their beam deflection units have also been discussed.

Since this thesis focuses on security systems, the core functions of Physical Perimeter Systems (PPS), such as Detect, Delay and Respond have been discussed. In addition, the classification of exterior and interior detection systems has been presented along with the key factors affecting the performance of such systems.

Furthermore, some applications of laser scanning for perimeter security have been discussed, and examples of laser scanner placement have been presented. Finally, the benefits and limitations of laser scanning methods have been discussed.

In Chapter 4, we address the problems associated with electro- mechanical beam deflection, such as wobble, jitter, windage and wear & tear, thereby proposing and demonstrating the concept of a novel photonic approach based on the use of an optical cavity in conjunction with a multiple laser sources of different wavelengths to realise a motionless laser scanner for perimeter security.

CHAPTER 4

DESIGN AND DEVELOPMENT OF A CURVED OPTICAL CAVITY FOR MULTI-BEAM GENERATION

4.1 INTRODUCTION

As discussed in Chapter 3, electro-mechanical beam deflection methods for intrusion sensing have fundamental problems associated with moving parts, which affect the laser scanning performance. The common problems inherent to mechanical scanners, such as wobble, jitter, windage and wear & tear are encountered in all laser scanners employing moving parts, such as rotary mirrors and motorised turning optical heads. To avoid such problems, we propose and demonstrate the principle of a novel motionless laser scanning system for perimeter security based on the use of an optical cavity in conjunction with multiple laser sources of different wavelengths. This optical cavity has many advantages when deployed for intrusion detection, namely, (i) a lower mean time between failure due to a less breakdown probability, (ii) a better probability of detection due to negligible deflected laser beam deviations from the desired optical path and (iii) lower false alarm rate, which usually results from poor system design, inadequate maintenance or component failure (Garcia, 2008).

In this chapter, we describe a novel curved optical cavity consisting of two concentric and cylindrical interfaces with unique optical thin-film coating properties that enable static projection of a laser spot array over a wide angle without any moving parts. The curved optical cavity generates multiple laser spots through internal beam reflections, and the transmitted laser rays cover a wide angle. Later in the chapter, comparison between a rectangular optical cavity and the curved optical cavity is discussed in detail.

In Sections 4.2 and 4.3 the operation principle of the optical cavity and the beam propagation through the optical cavity is discussed in detail alongside with beam spacing calculation and design. Furthermore, the generation of multiple laser beams using a single laser source and the optical power measurements for the transmitted laser beams is also explained.

The optimization of the thin-film coatings at the front and back sides of the optical cavity are discussed in Section 4.4. In section 4.5, the advantages of curved optical cavity over a rectangular optical cavity are discussed. Furthermore, the limitations of the curved optical cavity and the theoretical analysis that predicts the laser spot sizes is also derived.

4.2 OPTICAL CAVITY – OPERATION PRINCIPLE

The picture of the fabricated quasi optical cavity is shown in Figure 4.1. The front and rear side of the optical cavity is coated with unique thin-film properties, but the entrance and the exit windows are un-coated. The laser beam emerging from the laser source is injected in to the entrance window of the optical cavity. An incident laser beam propagates through the optical cavity to produce, through multiple internal reflection and partial transmission, an array of laser spots. The major advantage of using an optical cavity is that it produces multiple laser beams that are spatially separated.

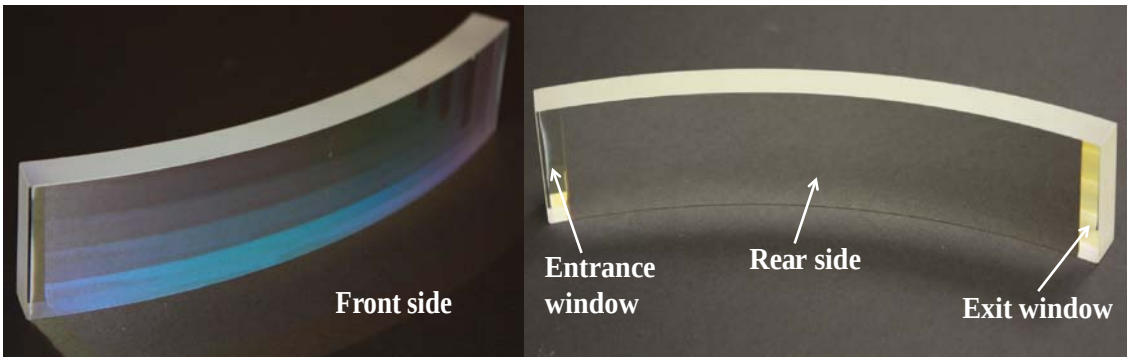

Figure 4.1: Photograph of the fabricated novel optical quasi-cavity.

Figure 4.2 shows a cross sectional schematic of the optical cavity. The incident laser beam, of power *P*, at the entrance window exhibits an optical reflection of 4% at the un-coated entrance window of the cavity, leading to a reflected laser beam, of power *P'*.

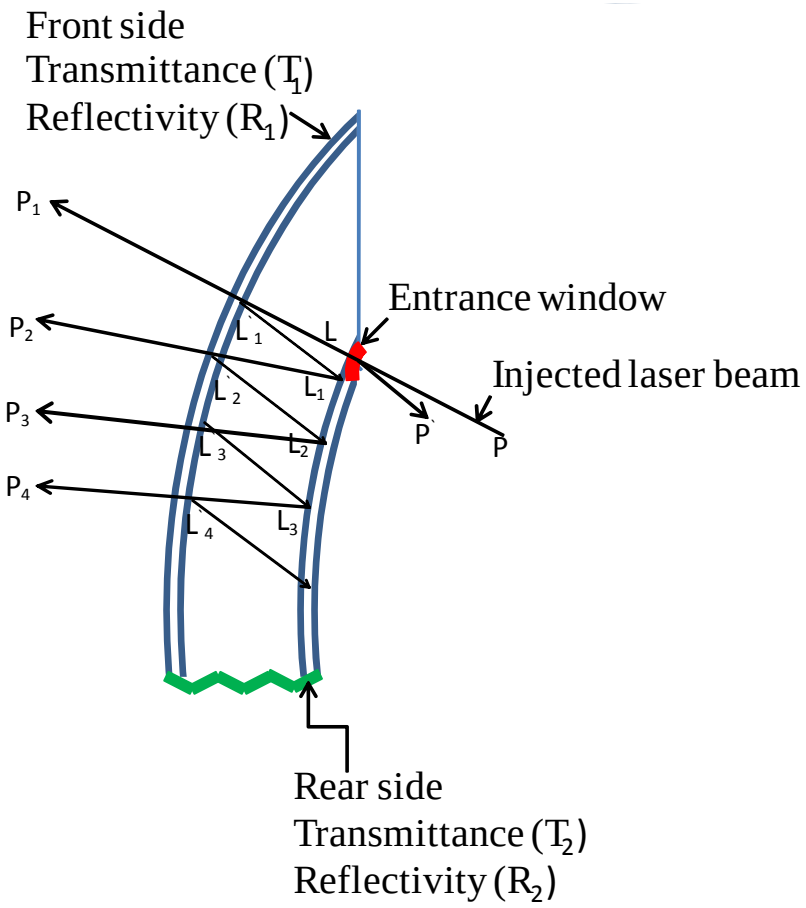

Figure 4.2: A cross sectional schematic of the curved optical cavity.

The front surface of the cavity is coated with a proper thin-film so that a small fraction of the laser light (~13%) is transmitted through the front side of the optical cavity. The optical power levels of the emerged beams are denoted *(P_n)*. The high reflection (>99%) rear surface of the optical cavity almost reflects all the light beams back in to the cavity leading to negligible multiple internal reflection to produce *(P'_n)*. The angle of incident laser beam determines the number of outgoing beams from the cavity.

The internally reflected beams from the front surface are referred as L'_n and L_n. The transmittance and reflectance properties of optical cavity depend on the thin-film coating on both sides of the optical cavity. These properties may vary depending on manufacturer specifications.

The beam spacing, S_{beam} can be calculated using the following equation:

$$S_{beam} = \frac{2 \cdot C_{width}}{\tan \theta_r} \qquad \text{Eqn. (4.1)}$$

where, C_{width} is the width of the cavity and θ_r is the angle of refraction.

According to Snell's law θ_r is given by

$$\theta_r = \sin^{-1}\left(\frac{\sin\theta_i}{n_{cavity}}\right) \quad \text{Eqn. (4.2)}$$

where n_{cavity} is the refractive index of the glass. The optical cavity at the front side is coated for 13% transmission and 99% reflection at the rear side. For each internal reflection, 13% of the power is transmitted and the remaining power is reflected back through the cavity for subsequent beam generation. The spacing between the beams can also be calculated through equation (4.1).

4.3 BEAM PROPOGATION THROUGH OPTICAL CAVITY

Given the optical power *P* and the transmittance and reflection values at both sides of the optical cavity, the intensities of the outgoing laser beam, $P_1 - P_n$, and the values of *L*, *L`*, *P`* can be calculated through the iterative sequence of the following basic equations:

$$L=P-(P*0.04) \quad \text{Eqn. (4.3a)}$$

$$P`=0.04*P \quad \text{Eqn. (4.3b)}$$

$$P_1=(L*T_1)/100 \quad \text{Eqn. (4.3c)}$$

$$L'_1=L-P_1 \quad \text{Eqn. (4.3d)}$$

$$L_1=L'_1*R_2 \quad \text{Eqn. (4.3e)}$$

$$P'_1=L'_1-L_1 \quad \text{Eqn. (4.3f)}$$

For example if the incident laser power *P* is *6mW* and $T_1=13\%$, then

$$L=6-(6*0.04)=5.76\ mW \quad \text{Eqn. (4.4a)}$$

$$P`=0.04*6=0.24\ mW \quad \text{Eqn. (4.4b)}$$

$$P_1=(5.76*13)/100=0.748\ mW \quad \text{Eqn. (4.4c)}$$

$$L'_1=5.76-0.748=5.012\ mW \quad \text{Eqn. (4.4d)}$$

$$L_1 = 5.012 * 0.99 = 4.98\ mW \qquad \text{Eqn. (4.4e)}$$

$$P'_1 = 5.012 - 4.98 = 0.032\ mW \qquad \text{Eqn. (4.4f)}$$

Similarly, through iteration, the values of $\{L_n`, P_n`\}$ can be calculated using equations (4.3a – 4.3f).

The output laser power for each beam was measured using a free-space optical power meter as shown in Figure 4.3 and the results were compared with the theoretical calculation described in equations 4.3(a-f). The diameter of each output collimated beam was 4mm. The active area of the photo-detector had a diameter of 5 mm, which easily accommodated the output beam size. This power meter was mounted onto a linear optical stage, which enabled precise alignment of the laser beams to the centre of the detector's active area, thus accurately measuring the intensities of all laser beams.

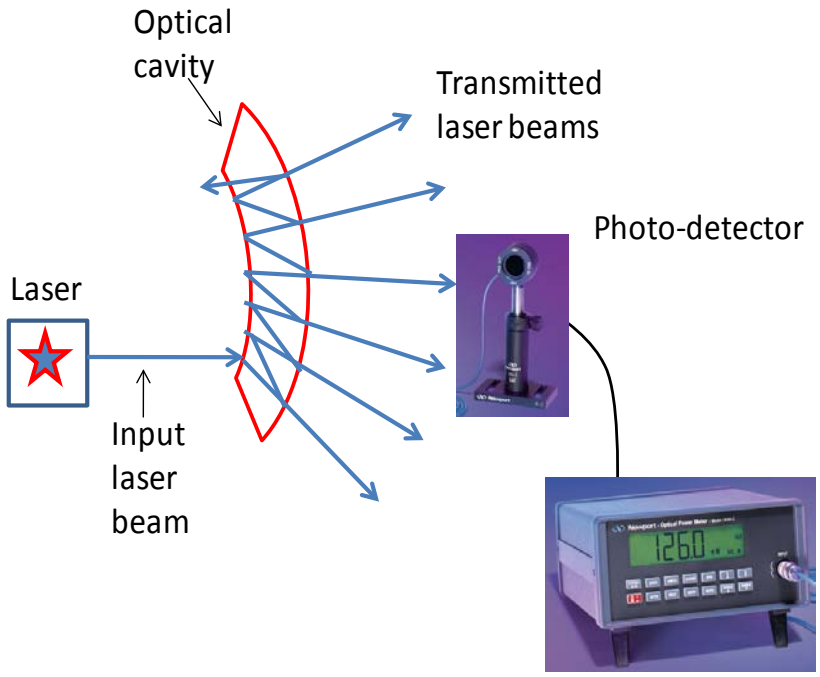

Figure 4.3: Schematic diagram of beam power measurements using a free-space power meter.

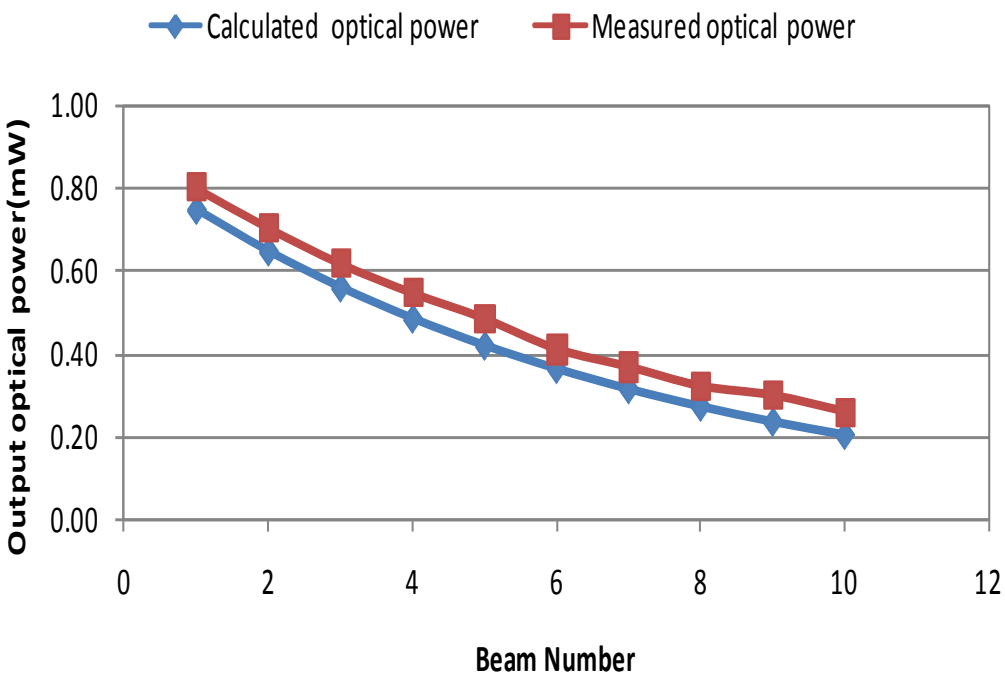

Figure 4.4: Measured and calculated output optical power for an input laser power P = 6mW.

Figure 4.4 shows the output optical power for 10 laser beams generated through the optical cavity and the calculated output power. Equations 4.3(a-f) were iteratively used to predict the output beam intensities P_1 … $P_{10.}$ Figure 4.4 demonstrates excellent agreement between the measured and the calculated output beam intensities.

4.4 OPTIMISATION OF OPTICAL CAVITY'S THIN FILM COATING

As discussed in Section 4.2, the incident laser beam undergoes multiple internal reflections to generate an array of laser spots. As a result, the optical output power profile of the outgoing beams, and hence, the Signal to Noise Ratio (SNR), decreases every time a new beam emerges from the optical cavity. To maintain a constant SNR for all outgoing beams, non-uniform coating can be applied across the front side of the optical cavity.

For example, let us assume the input laser power launched into the optical cavity is *6mW* and the desired output optical power from all the laser beams is *500μW*.

To generate output optical beams of equal intensities, the transmittance values at the various outgoing beam positions can be calculated as follows:

$L=P-(P*0.04) = 5.76mW$ (because the loss due to reflection from the entrance window of the cavity is *4%)*

$$P`=0.04*P = 0.24\ mW$$

$$P_1= L\ T_1 =500\mu W=0.5mW$$

$$T_1 = P_1/L*100 = 8.6\% \qquad \text{Eqn. (4.5a)}$$

$$L_2= L- L\ T_1 = 0.94$$

$$T_2 = P_2/L_2*100 = P_1/L_2*100 = 9.5\% \qquad \text{Eqn. (4.5b)}$$

Similarly, all T_n can be calculated iteratively.

Graphical representation of the above calculation for T_1 till T_{10} is shown in Figure 4.5.

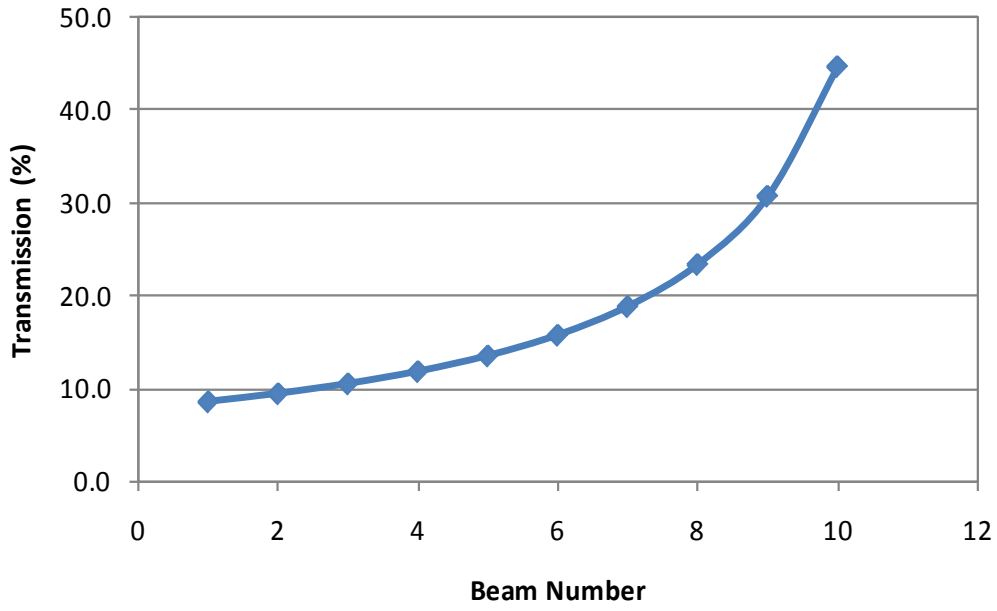

Figure 4.5: Calculated percentage of transmission necessary to generate equal optical output intensities for all laser beams.

For practical embodiments, it is important to ensure that the SNR for each beam is above an adequate value. Figure 4.6 shows a schematic representation of a curved optical cavity employing four different transmittance values, thus producing 15 laser beams with adequate SNR values.

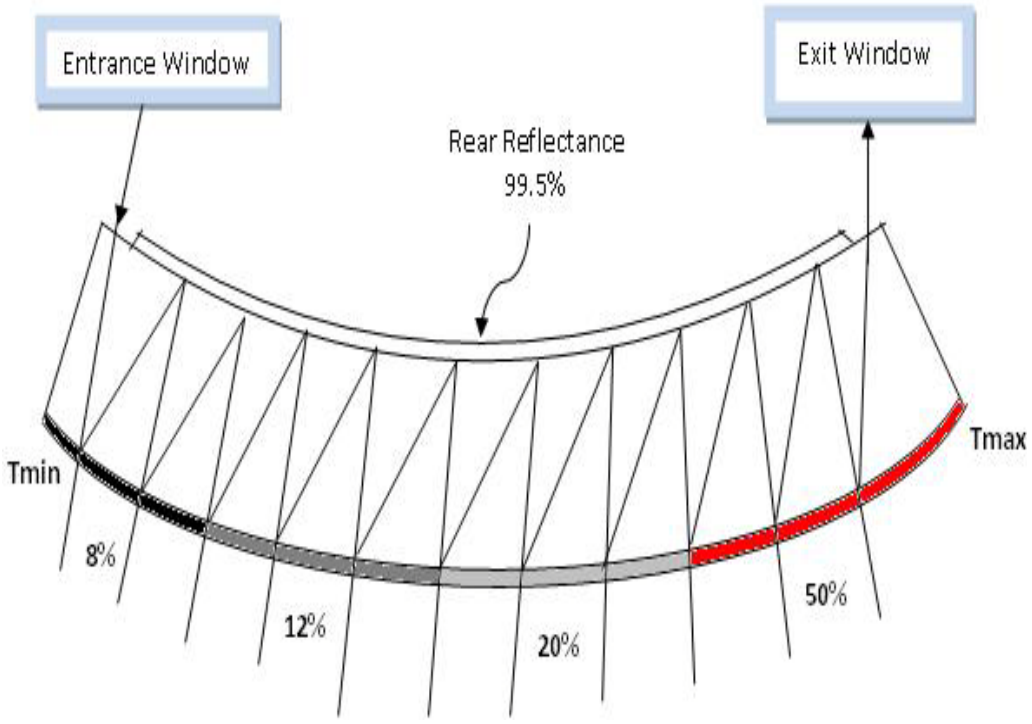

Figure 4.6: Schematic diagram of the optical cavity with four different transmittance values.

The average transmission for first five beams was 8% and 12% for the next four beams, 20% for beams 10 to 13 and 50% for the last two beams as shown in Figure 4.6.

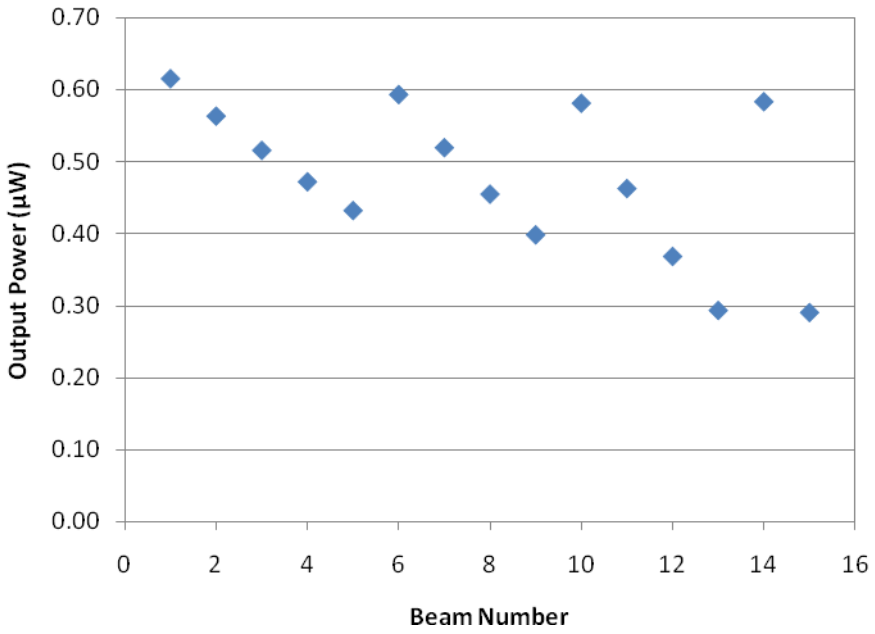

Figure 4.7: Calculated output optical power for four different transmittance coatings applied at the front surface of the optical cavity.

Figure 4.7 shows the output optical beam power calculated using the optimised transmittance values. From Figure 4.7, it is evident that all the incident optical power was transformed to the outgoing beams, and only very few milli-watts (mW) escape from the exit window of the cavity.

4.5 ADVANTAGES OF CURVED OPTICAL CAVITY

An optical cavity was mainly designed to generate an array of laser beams that illuminate the intrusion around a perimeter. The designed optical cavity must spread the laser beams to cover a 180° field of view. Inherently, a rectangular shape optical cavity cannot spread the outgoing beams over a 180° field of view; therefore, multiple rectangular cavities must be joined to monitor a wider field of view around a perimeter, as shown in Figure 4.8.

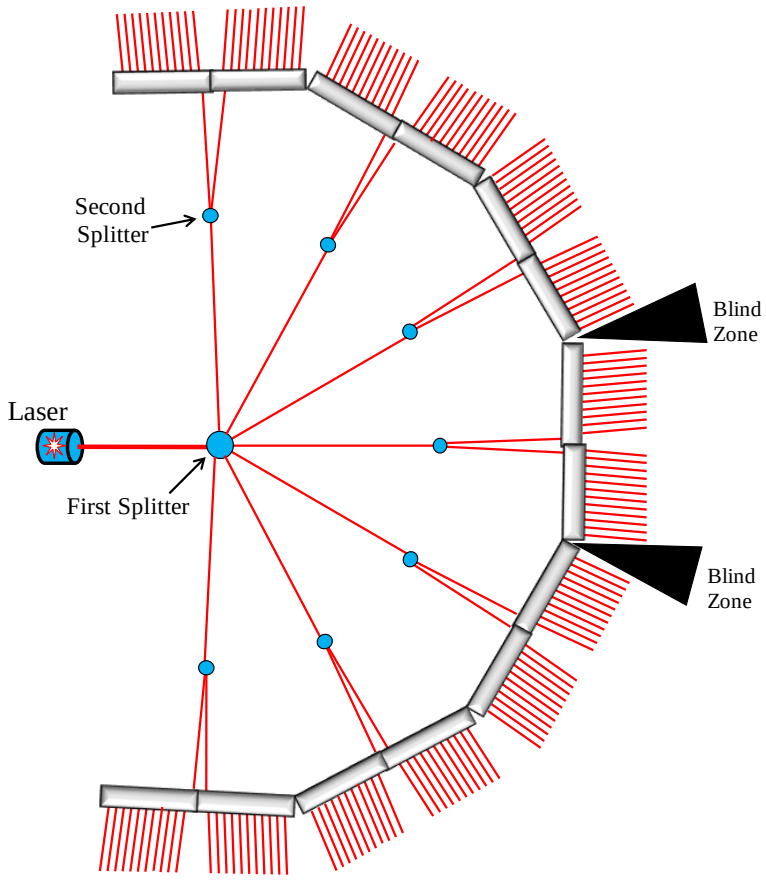

Figure 4.8: Arrangement of rectangular cavities to cover a 180° field of view.

When rectangular cavities are joined together, they create a blind zone, which cannot be illuminated and this is a major drawback of such an approach. The area of the blind zones increases as the target range increases. Therefore, to overcome this issue, the

shape of the optical cavity needs to be modified. The modification of the cavity shape from rectangular to cylindrical provides a potential solution that overcomes the issue of blind zones.

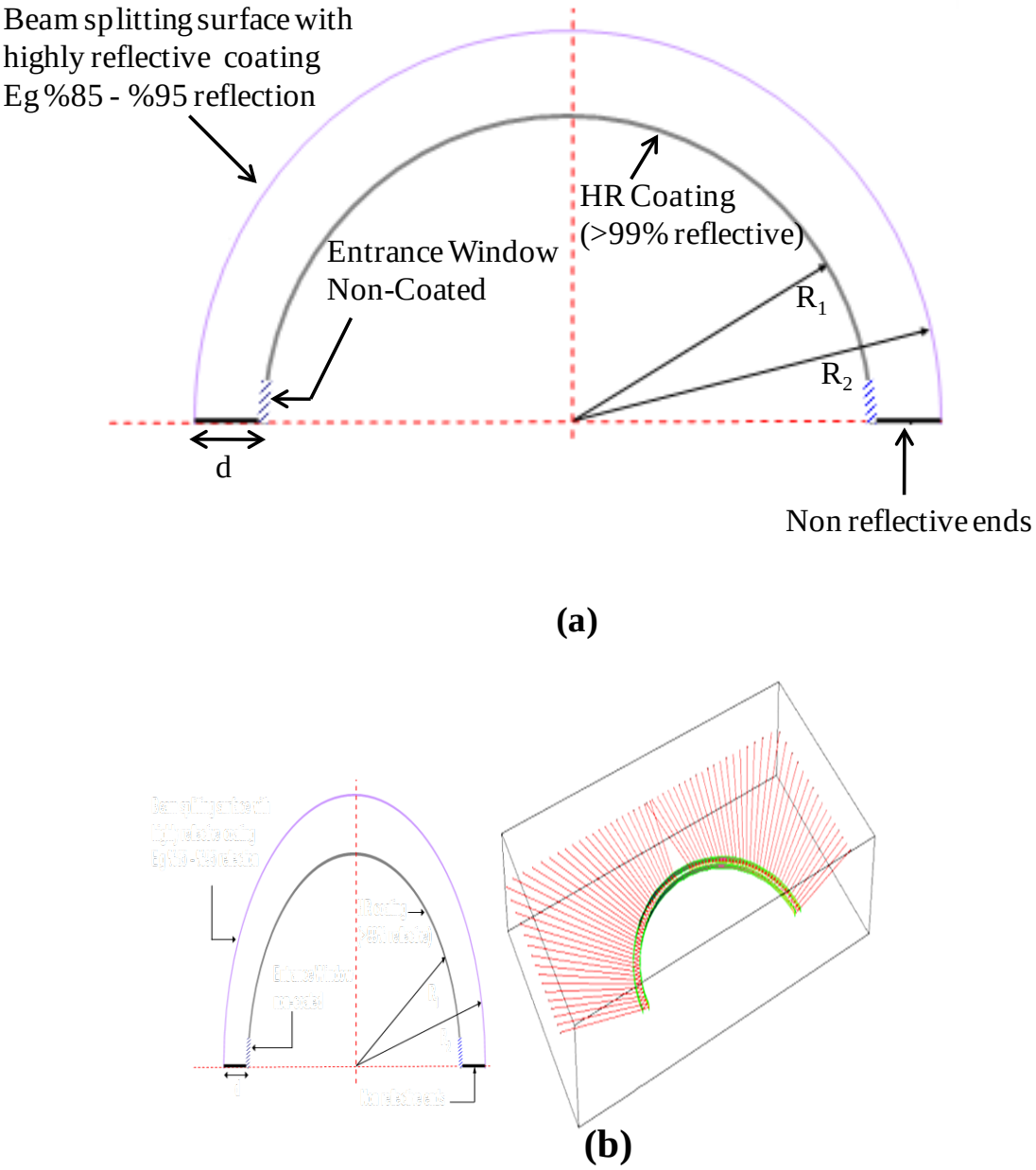

Figure 4.9: Arrangement of curved cavities to cover 180◦ field of view (Sahba et al., 2006a).

The prime advantage to use a curved optical cavity is that it spreads the laser beams over a 180◦ field of view with uniform resolution. Figure 4.9a shows an optical cavity design achieving a 180◦ field of view. Also shown in Figure 4.9b are the simulated outgoing laser beams illuminating a security perimeter.

4.5.1 Limitations of the curved optical cavity

The number of outgoing beams depends upon the angle of incidence of the laser beam onto the entrance window of the cavity.

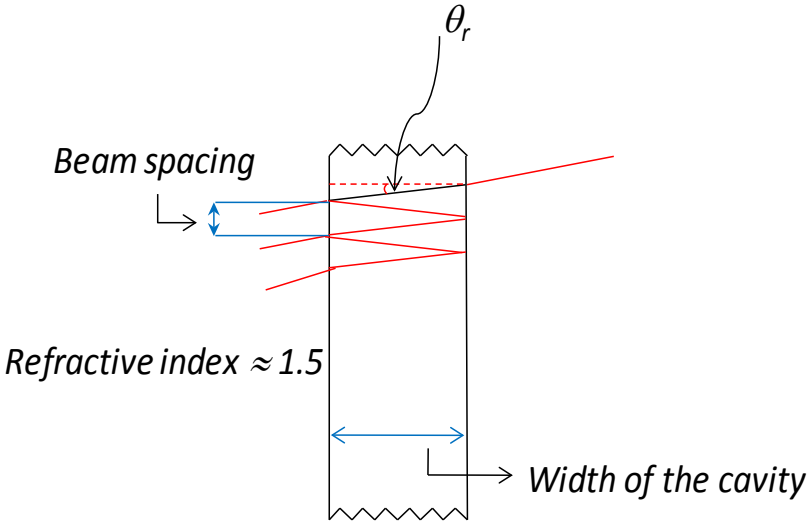

Figure 4.10: Beam spacing for a rectangular cavity.

For the curved optical cavity, the beam spacing increases with increasing the detection range as shown in Figure 4.11; but the beam spacing remains the same after emergence from a rectangular cavity (Figure 4.10), regardless of the detection range.

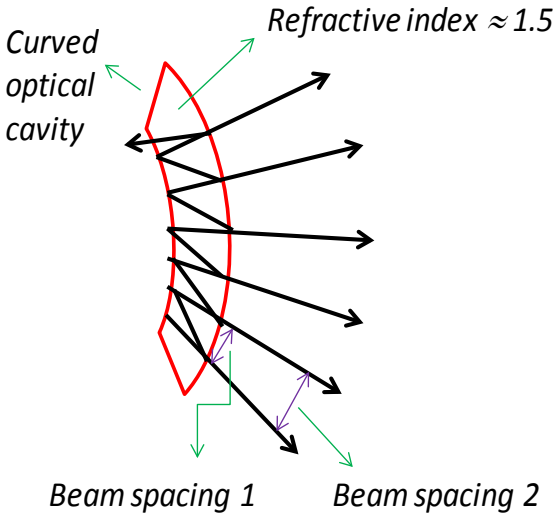

Figure 4.11: Beam spacing in a curved optical cavity. It increases with increasing the detection range.

The major reason for selecting the curved cavity is that the laser beams generated from this structure are spread as a fan-shaped group of beams, which would cover a wide area for security. Optimisation of the incident angle to generate as many beams as possible would considerably reduce the spacing between the beams, and hence there is no much difference in the spacing when the beams propagate at any particular distance.

4.5.2 Gaussian behaviour modelling for laser spot size measurement

The laser beam injected into the optical cavity undergoes internal reflections and refractions, these beams are analysed using the *ABCD* transfer matrix along with the Gaussian complex radius of curvature parameter, *q*, described by (Kogelnik and Li, 1966) and (Saleh and Teich, 1991) as:

$$q = z + iz_R \qquad \text{Eqn. (4.6)}$$

where *z* is the beam propagation distance and z_R is the Rayleigh range, given by

$$z_R = \frac{\pi W_0^{\,2}}{\lambda}. \qquad \text{Eqn. (4.7)}$$

where W_0 is the laser beam radius and λ is the wavelength of the laser source. W_0 can be derived from the divergence angle θ_0 and λ, which is represented as shown in equation (4.8)

$$W_0 = \frac{\lambda}{\pi\theta_0}. \qquad \text{Eqn. (4.8)}$$

The paraxial transfer *ABCD* matrix for free-space propagation and refraction at a spherical boundary is used to derive q_1 at the entrance window and after refraction through it, respectively. After the Gaussian beam propagates through an optical system, a new complex parameter q_2, is calculated through the Kogelnick transformation:

$$q_2 = \frac{A \cdot q_1 + B}{C \cdot q_1 + D}. \qquad \text{Eqn. (4.9)}$$

Calculating the *q* values after *n* reflections is carried out through an iterative two-step process. Initially, the transfer matrix for a beam propagating through a uniform medium is used to evaluate the q value at an interface. Then, the matrix for reflection (or refraction) is used to calculate the *q* values for the transmitted (or reflected) rays.

After the complex radius of curvature has been defined at the laser aperture, the *ABCD* law can be applied to calculate the change in beam parameters. A compound *ABCD* matrix describing the passage of the n^{th} beam propagating from the outer interface of the quasi-cavity can be defined by the optical system matrix as:

$$S_n = F \cdot L \cdot (T \cdot M \cdot T \cdot N)^{n-1} \cdot T \cdot Q \cdot P, \qquad \text{Eqn. (4.10)}$$

where

$$P = \begin{bmatrix} 1 & h \\ 0 & 1 \end{bmatrix}.$$

$$Q = \begin{bmatrix} \dfrac{n_{ac}^2\left(-\sin\theta_{inc}^2\right)^{1/2}}{n_{ac}\cdot\cos\theta_{inc}} & 0 \\ \cos\theta_i - \left(\dfrac{\left(n_{ac}^2-\sin\theta_{inc}^2\right)^{1/2}}{-R_1\cdot\cos\theta_i\cdot\left(n_{ac}^2-\sin\theta_r^2\right)^{1/2}}\right) & \dfrac{\cos\theta_{inc}}{\left(n_{ac}^2-\sin\theta_{inc}^2\right)^{1/2}} \end{bmatrix}.$$

$$T = \begin{bmatrix} 1 & d/n_{glass} \\ 0 & 1 \end{bmatrix}.$$

$$N = \begin{bmatrix} 1 & 0 \\ -2/R_{2\cdot}\cdot\cos\theta_{refr} & 1 \end{bmatrix}.$$

$$M = \begin{bmatrix} 1 & 0 \\ 2/R_{2\cdot}\cdot\cos\theta_{refr} & 1 \end{bmatrix}.$$

$$L = \begin{bmatrix} \dfrac{n_{ca}^2\left(-\sin\theta_{refr}^2\right)^{1/2}}{n_{ac}\cdot\cos\theta_{refr}} & 0 \\ \cos\theta_{refr} - \left(\dfrac{\left(n_{ca}^2-\sin\theta_{refr}^2\right)^{1/2}}{-R_2\cdot\cos\theta_{refr}\cdot\left(n_{ca}^2-\sin\theta_{refr}^2\right)^{1/2}}\right) & \dfrac{\cos\theta_{refr}}{\left(n_{ca}^2-\sin\theta_{refr}^2\right)^{1/2}} \end{bmatrix}.$$

n_{ac} and n_{ca} are refractive index ratios defined as n_{air}/n_{cavity} and n_{cavity}/n_{air}, respectively. θ_{inc} and θ_{refr} are incident and refraction angles, respectively. *h*, *d* and *g* are the distances travelled by the optical beam from the laser aperture to quasi-cavity's entrance window, between the two cavity interfaces and outside the cavity after transmission, respectively. R_1 and R_2 are the inner and outer cavity interfaces, respectively.

To simulate the ray propagation within the quasi-cylindrical cavity, a new optical axis is defined for each ray emerging from the cavity. Hence, the *ABCD* matrices that incorporate coordinate transformation for reflection and refraction of a Gaussian laser beams at an off-axis ellipsoidal surface must be used as reported by Massey and Siegman (Massey and Siegman, 1969).

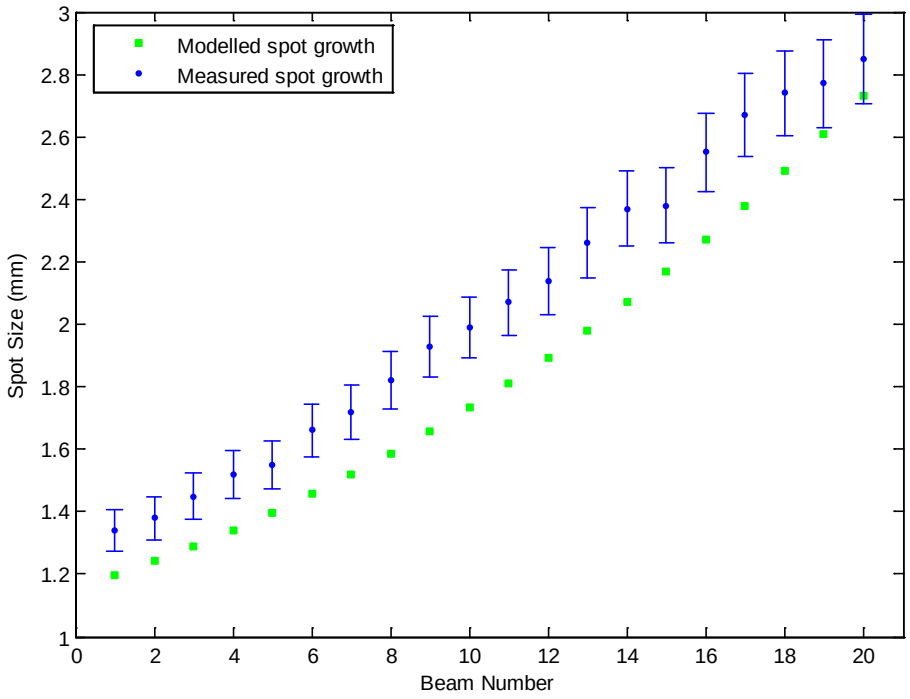

Figure 4.12: Measured and modelled spot size for laser beams projected at 0.5m from the optical cavity. A He-Ne laser of 0.48mm output diameter was used. Incident angle was 25° (Sahba et al., 2007a).

Laser spot size measurements were carried out in laboratory at a distance of 0.5m from the cylindrical cavity. A He-Ne laser of 0.48mm output diameter and 1.7*m*rad divergence was used to produce a beam at an incident angle of 25°. The measured and modelled spot size plots displayed in Figure 4.12 followed the same trend as the results reported by Sahba and et al. (Sahba et al., 2007a, Sahba et al., 2007b). Also shown are the theoretical predictions derived using the above described non-paraxial *ABCD* matrices.

4.6 SUMMARY

This chapter has concisely described the properties, advantages and limitations of a novel curved optical cavity that generates multiple beam spots form a single laser source, through multiple internal beam reflections. The front and rear sides of the

developed optical cavity were coated with specific thin-films so that the front coated surface transmitted a small fraction of the light that falls upon it (~13%), while the rear surface reflected most of the light power (>99%) falling upon it. The entrance and the exit windows in the rear side of the cavity were un-coated. The spacing between the transmitted sensing beams was set by adjusting the incident angle of P_0.

The working principle and the beam propagation inside the optical cavity have also been well explained. We have demonstrated that when a laser beam was injected in the entrance window of the optical cavity, it generated multiple output beams after undergoing multiple internal reflections within the optical cavity.

Additionally, we have shown that by coating front side of the optical cavity with non-uniform coatings, multiple laser beams with equal output intensities can be generated. By using an optimized coating on the front side of the cavity the intensities of the outgoing beams increase, leading to higher SNR levels for all outgoing beams in comparison to the SNR's for a uniformly coated cavity. Various arrangements of optical cavities have been investigated. We have shown that rectangular cavities can be arranged to generate laser beams over a 180° field of view. Moreover, the non- paraxial *ABCD* matrix method to calculate the sizes of the laser beams emerging from the curved optical cavity have been described.

In Chapter 5, a multi-wavelength laser scanner for object identification and discrimination will be discussed. The components and operation principle of the multi-wavelength laser scanner will be described in detail. Object identification and discrimination methodology will be presented and demonstrated experimentally for specific sample objects.

CHAPTER 5

OBJECT IDENTIFICATION AND DISCRIMINATION

5.1 INTRODUCTION

The properties and the concept of generating multiple beams through cylindrical optical cavity were clearly described in Chapter 4. The optimization of the optical cavity along with the principle of laser beam propagation inside the optical cavity was also described in detail. In this chapter, we describe and demonstrate the principle of a multi-wavelength laser scanning system comprising of a multi-wavelength laser module, a curved optical cavity and an image sensor.

Multi-wavelength laser scanning is a natural progression from object detection to object identification and classification, where specific features of objects and materials are discriminated by measuring their reflectance characteristics at specific wavelengths and matching them with their spectral reflectance curves. With the recent advances in the development of high-speed sensors and high-speed data processors, the implementation of multi-wavelength laser scanners for object identification has now become feasible.

While holographic gratings can be used to generate multiple single-wavelength laser spots for intruder detection, the same cannot be implemented for multi-wavelength laser scanning. The reason being laser beams of different wavelengths will be diffracted from a holographic grating at different angles, hence making this technique impractical for maintaining a high-degree of overlapping between the beams of different wavelengths projected at a particular spot. A two-wavelength photonic-based sensor for object discrimination has recently been reported, where an optical cavity was used for generating a laser spot array and maintaining adequate overlapping between tapped

collimated laser beams of different wavelengths over a long optical path (Sahba et al., 2008, Sahba et al., 2007a).

In the first section of this chapter, a multi-wavelength sensor for object identification and discrimination is developed and demonstrated over 2- and 6-metre ranges. Object samples including brick, cement sheet, roof tile, cotton and leather were placed at up to 6m from the sensor and analysed using statistical error analyses.

The sensor architecture is comprised of a laser combination module, a multi-spot beam generator, an area image sensor and a collecting lens. The laser beams are modulated using custom-made electronic drivers integrated on a printed circuit board. This results in laser pulses of different wavelengths illuminating the objects sequentially. Object discrimination and identification is achieved by recording and processing the intensities of the different laser beams reflected from the various spots illuminating the object, for each illuminating wavelength.

In the second section of this chapter, another multi-wavelength sensor architecture is designed and developed, which additionally provides laser beam scanning along the transverse direction. The sample objects used to demonstrate the concept of discrimination over a distance of 6m are leaf, bark, black fabric, PVC, wood and camouflage material. The camouflage material was especially selected to demonstrate the discrimination capability of the sensor through scanning along the transverse direction.

By increasing the number of wavelengths at which the sample objects exhibit different optical characteristics, the number of objects and materials that can be identified and discriminated increases significantly. The reflectance spectra of the sample objects are obtained using two different spectrometers, namely, a visible spectrometer (400-850nm) and an infrared (850-2100nm) spectrometer. The reflectance spectrum of a material can be used as a unique signature that identifies this material from other materials. This is the basis for the multi-wavelength remote object sensing, identification and discrimination.

5.2 MULTI –WAVELENGTH LASER UNIT

The layout of the laser combination module is shown in Figure 5.1. This module comprises five different wavelengths and four free-space beam combiners (or polarised beam splitters). It can generally be divided in two sections named Section 1 and Section 2 in Fig. 5.1.

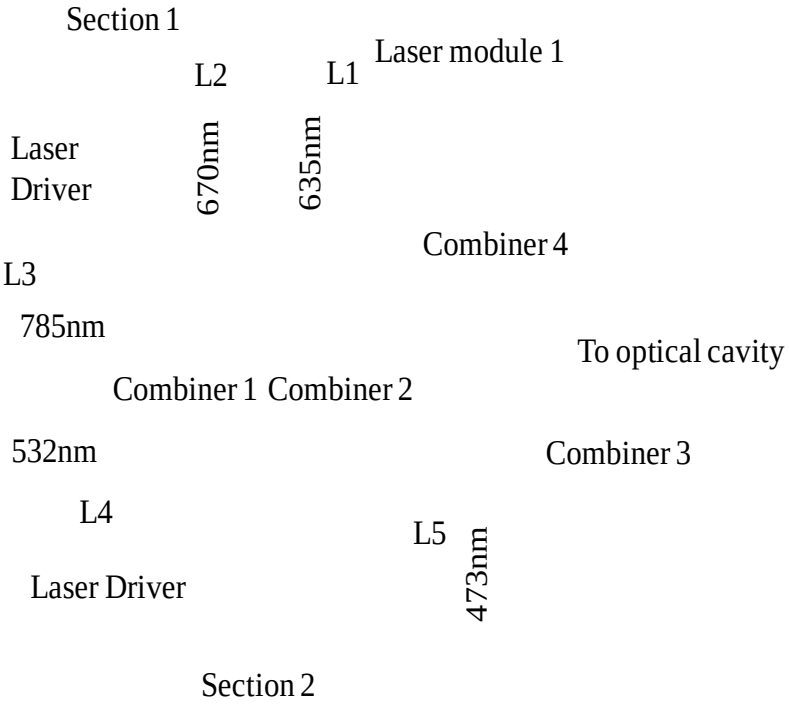

Figure 5.1: Laser combination module employing four free space beam combiners to combine five different wavelengths.

In Section 1 of the module, three different wavelengths namely, 635nm, 670nm and 785nm are combined using two free-space beam combiners. A custom made laser driver circuit is used to control the power levels and pulse widths of the three lasers. The 670nm and 785nm lasers are combined using combiner 1 and combiner 2 is used to combine the output of combiner 1 with the 635nm signal (red laser). In Section 2, the 473nm and 532nm (blue and the green) lasers, which are driven by constant-power drivers, are combined using combiner 3. Finally, the output signals from Section 1 and Section 2 are combined by combiner 4 whose output is launched into a curved optical cavity.

This arrangement of the laser combination module, not only enables the combinations of the various collimated laser beams, but also provides polarisation alignment and

overlapping of five collimated laser beams of different wavelengths. Polarization alignment for all laser beams is performed by rotating each laser source around its optical axis, and this is necessary to minimize the impact of the polarization-dependent scattering loss of the objects under investigation.

5.3 METHODOLOGY FOR OBJECT IDENTIFICATION AND DISCRIMINATION

The object discrimination and identification process is based on determining the slopes of the reflectance spectra at the 635nm, 670nm, 785nm, 473nmand 532nm wavelengths (Sahba et al., 2008, Sahba et al., 2006b, Mynei et al., 1995, Paap.A et al., 2008). The four slope values, S_1, S_2, S_3 and S_4 are defined as in equation (5.1):

$$S_1 = \frac{R_{473} - R_{532}}{\lambda_{532} - \lambda_{473}} \quad , \quad S_2 = \frac{R_{635} - R_{532}}{\lambda_{635} - \lambda_{532}} \qquad \text{Eqn. (5.1)}$$

$$S_3 = \frac{R_{670} - R_{635}}{\lambda_{670} - \lambda_{635}} \quad and \quad S_4 = \frac{R_{785} - R_{670}}{\lambda_{785} - \lambda_{670}}$$

where λ_n is the wavelength of the laser diode in nanometers, $R_\lambda = I_\lambda / P_\lambda$ is the calculated reflectance, I_λ is the peak intensity of a beam spot imaged by the image sensor (usually represented by a 12-bit digital number (DN)) and P_λ is the measured optical power for each spot generated by the optical structure. The peak intensity values, I_λ, were obtained by fitting the intensity profile of each imaged laser spot with a non-normalized Gaussian profile given by.

$$f(x) = a \cdot e^{-\frac{(x-b)^2}{2\sigma^2}} \qquad \text{Eqn. (5.2)}$$

where a, b and σ are the maximum value, maximum position and standard deviation of the fitting Gaussian beam, respectively. Once the imaged laser beam is fitted according to equation (5.2) using a Matlab add-on toolbox, the peak intensity $I_\lambda = a$ is determined for the various laser wavelengths illuminating the samples.

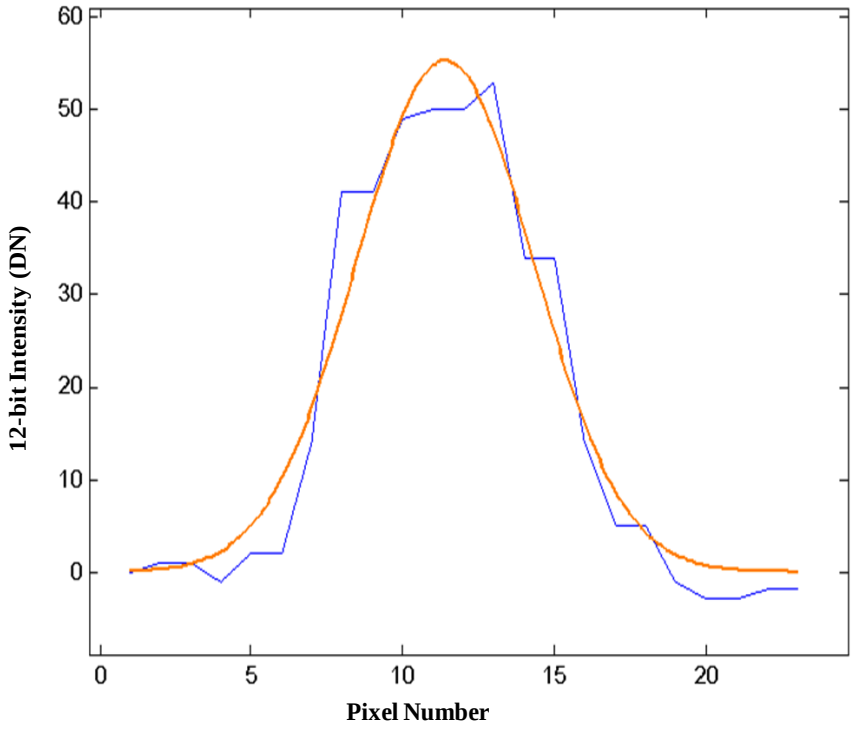

Figure 5.2: Imaged 635nm laser beam reflected off a "Leather" sample fitted with a Gaussian profile.

Note that the beam intensity profile extends over a row of pixels crossing the centre of the laser spot, along the x-axis as illustrated in Figure 5.2, where an imaged 635nm laser beam reflected off a "Leather" sample is fitted with a Gaussian profile according to equation (5.2).

Using equation (5.1), four different slope values can be identified for 5 wavelengths, and to ensure accurate object identification and discrimination, substantial differences in slope values must be exhibited for the reflectance spectra of the various objects.

5.4 OBJECT DISCRIMINATION - EXPERIMENTAL SETUP

5.4.1 Experimental setup for object discrimination using five different wavelengths

The experimental setup for object discrimination is shown in Figure 5.3. The core components of this multi-wavelength sensor demonstrator are the laser combination

module, the custom fabricated curved optical cavity (also called a multi spot beam generator) and the Charged Coupled Device (CCD) imager.

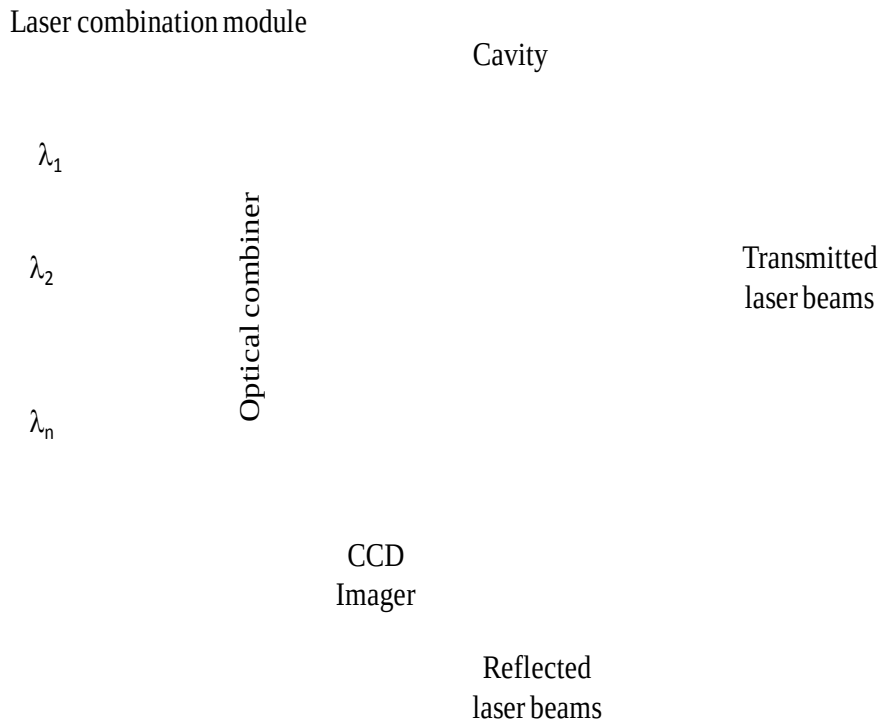

Figure 5.3: Experimental setup of the multi-wavelength sensor for object discrimination.

A. Laser combination module

The laser combination module contains five lasers of different wavelengths appropriately aligned with four free-space beam combiners as explained in Section 5.2. These arrangements of lasers produce five collimated and overlapped laser beams with the same polarisation angle. All laser beams are collimated at a diameter of 4mm. The output optical power for the 473nm and 532nm lasers were set to 8mW and 7mW, respectively, while the other three lasers had equal output power levels of 6mW. The divergence for all output collimated laser beams was less than 1.5 mrad. The experiments were set up in laboratory environments on an optical table, as shown in Figure 5.4, to demonstrate the ability of the multi-wavelength sensor to discriminate between the objects.

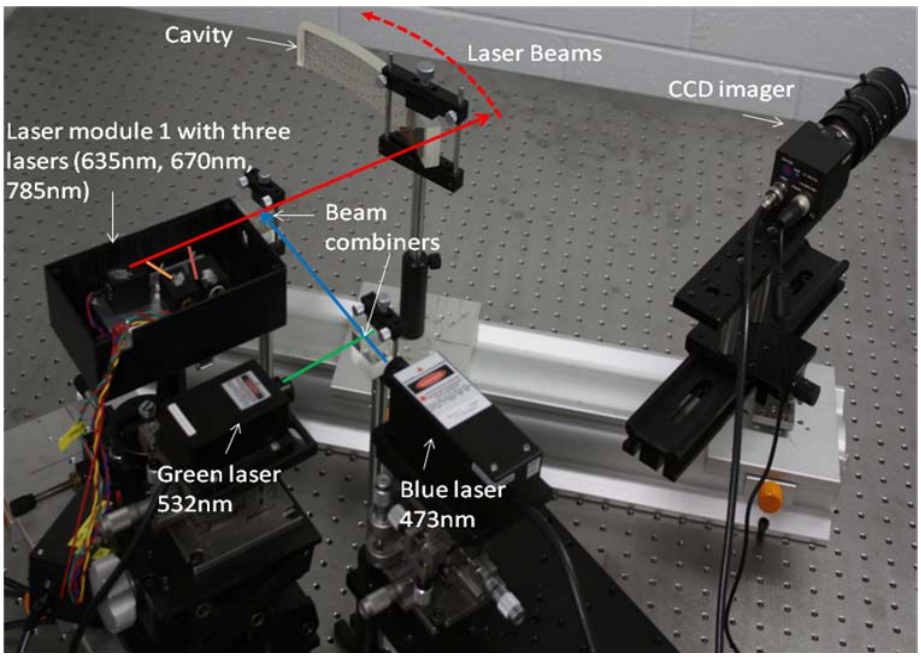

Figure 5.4: Experimental setup for object discrimination. Objects are illuminated with laser beams at various wavelengths overlapped along one optical path at the entrance aperture, thus striking the same spot on the sample object.

The output power of each laser beam emerging from the curved optical cavity was measured using a Newport free-space optical power meter. The diameter of the active area of the photo detector was of 5mm. The optical power meter was mounted onto a linear optical stage, which enabled precise alignment of the laser beams to the centre of the detector's active area and accurate measurements of the laser beam intensities, which are displayed in Figure 5.5.

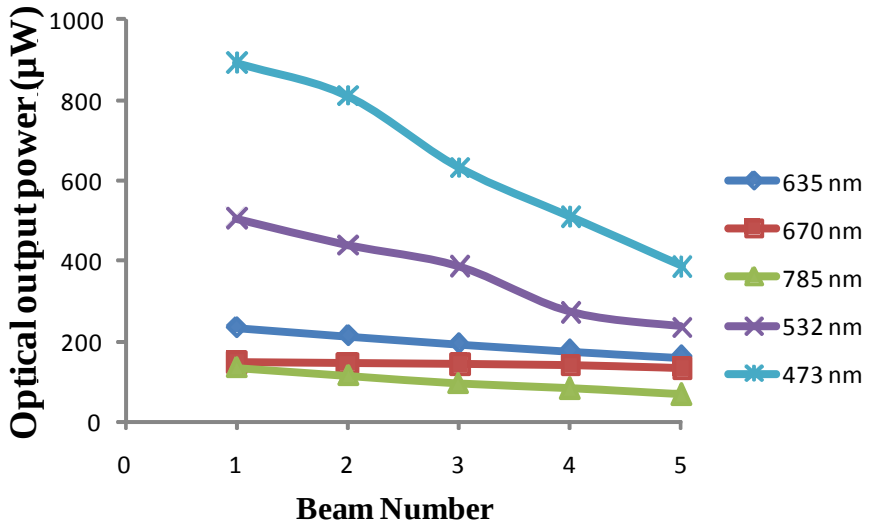

Figure 5.5: Measured output optical power levels for each laser beam after passing through the curved optical cavity.

B. Multi- spot beam generator

The output laser beams from the laser combination module passed through the custom fabricated curved optical cavity to generate multiple laser spots. The optical cavity was made of BK-7 glass with inner and outer interface radii of R_1 and R_2, respectively. The rear side of the glass was coated with a high reflectivity coating (R≥99.5%), while the front side coating had low transmission (T≈13%) thin film as discussed in Chapter 4.

Both entrance and exit non-coated windows at both ends of the rear side of the glass medium were 10mm wide. Hence, an input collimated optical beam underwent multiple reflections within the optical cavity, and every time it hit the front surface, a small fraction (13%) of its optical power was transmitted, thus projecting a laser spot array onto a sample object. This device was able to generate many beams depending upon the incident angle of the laser beams striking the entrance window of the multi-spot beam generator.

C. Charged Coupled Device (CCD) imager

The area scan image sensor captured the reflected intensities of the laser beams sequentially illuminated by the multi spot beam generator. This particular imager exhibited high sensitivity over the wavelength ranging from 470nm to 785nm. The spectral response of the CCD imager used in the experiment is shown in Figure 5.6. An imaging lens was used in conjunction with the imager in order to capture, through imaging, the intensities of the beams scattered from the different laser spots along all directions.

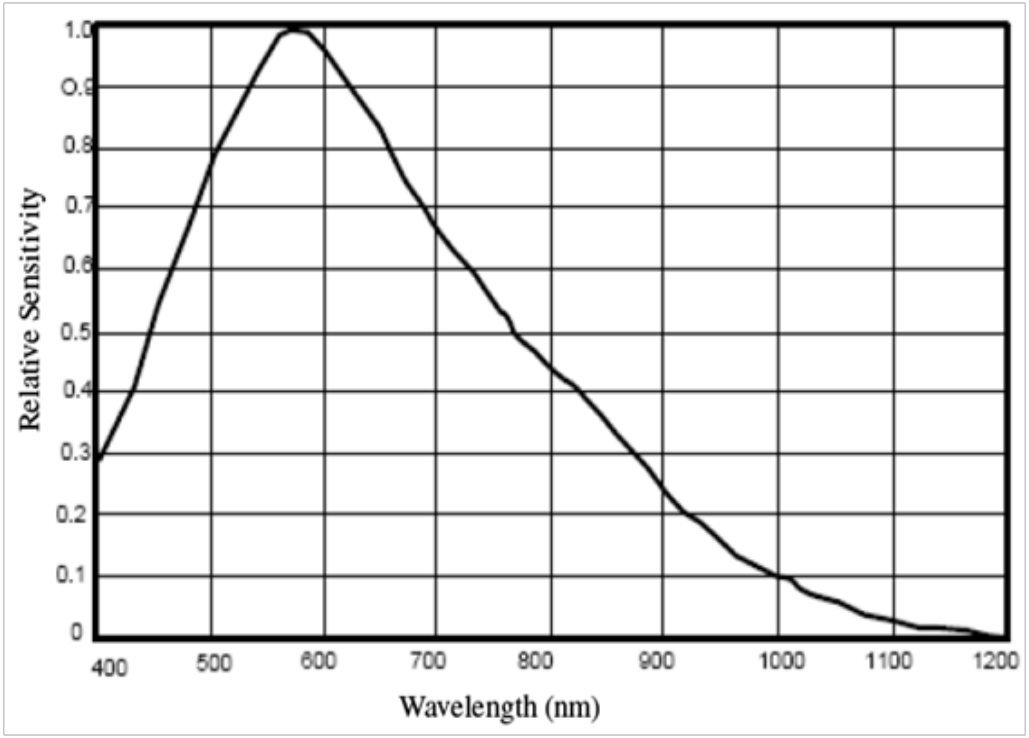

Figure 5.6: Spectral response of the image sensor used for the experiments (manufacturers specifications).

The 0.5-inch interline transfer CCD imager employed to capture the reflected intensities had 768(H) × 494(V) pixels, each of size 8.4μm × 9.8μm. A C-mount TV lens of focal length f = 12.5 mm was used to collect the light scattered from the illuminated laser spots. The estimated CCD acquisition time was 200 µsec and the estimated over all acquisition time was 2 msec. The lens iris was adjusted appropriately to avoid saturation of the imaged laser spot array. The images from the camera were digitized in 12-bit form using a Spiricon frame grabber circuit board.

5.4.2 Experimental results and discussion

The object samples selected for experimentation were brick, cement sheet, roof tile, cotton and leather. The experiments were carried out in the laboratory with a 2m and 6m distance from the multi-wavelength sensor and the objects. The objects were first characterized with two different commercially available (visible and near infrared) spectrometers. The experimental setup for measuring the reflectance spectrum is shown in Figure. 5.7.

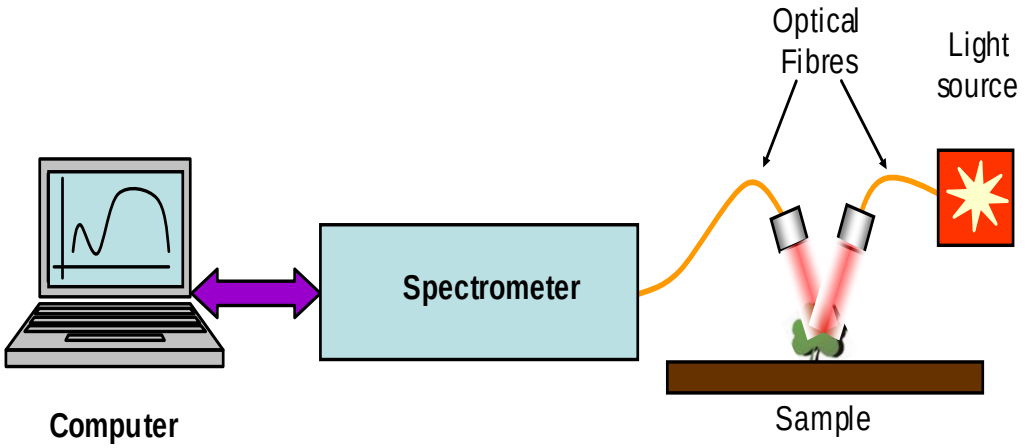

Figure 5.7: Experimental setup for measuring the reflectance spectra of the different sample objects.

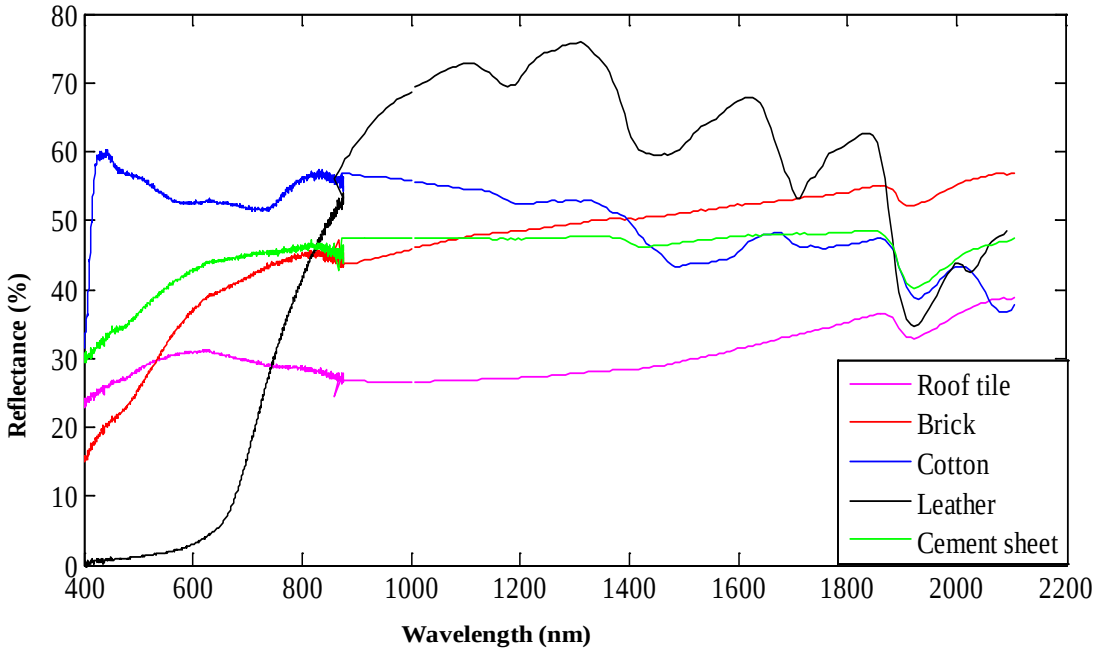

Figure 5.8: Typical measured spectral response of sample objects used for experimentation.

The measured spectral reflectance curves for all objects are shown in Figure 5.8. The reflectance of a roof tile is low (Figure 5.8) but has a peak around 600nm. For a brick, the reflectance spectrum is linear with a higher slope over the visible part of the spectrum. The reflectance of cotton has a peak at 473nm and several deflection points within the visible and near infrared parts of the spectrum. On the other hand, the reflectance of leather is generally low for visible wavelengths and exhibits several peaks over the infrared part of the spectrum. For the cement sheet, the reflectance increases almost monotonically with increasing wavelength. Note that these reflectance spectra

were obtained by using two different spectrometers, namely a visible spectrometer of spectral range 400-850nm and an infrared spectrometer of spectral range 850-2100nm. To identify these objects, specific wavelengths, namely 473nm, 532nm, 635nm, 670nm and 785nm, were selected for two main reasons. Firstly, the spectral reflectance slopes at the different wavelengths are significant and do not overlap simultaneously, and secondly these wavelengths are synthesized using commercially available lasers.

Initially, the object samples were placed at 2m from the optical cavity and then the same samples were placed at 6m from the optical cavity. These objects were illuminated with an array of coplanar laser beams emitted through the multi-wavelength sensor and the reflected intensities from these objects were measured at different times as illustrated in Figure 5.3.

Equation (5.1) was used to calculate the average slopes S_1, S_2, S_3 and S_4 for all objects (Figure 5.9) and their standard deviations. The measured spectral reflectance slopes of the five objects for 2m and 6m ranges are shown in Figure 5.10 and Figure 5.11, respectively. Clearly, there was no simultaneous overlapping between the slope values of the different objects. For example, while the slopes S_2 and S_3 of leather and cement overlap, their S_1 and S_4 slopes do not overlap. Also, the slopes S_4 of the roof tile, leather and brick overlap; however, they can be discriminated through the measurements of their non-overlapping slopes S_1, S_2 and S_3 at a 2m range, and their non-overlapping slopes S_2 and S_3 at a 6m range. The increase in slope variance with an increase in the detection range is attributed to the lower detected signal for a higher range, which results in a lower signal-to-noise ratio. These experimental results validate the capability of the multi-wavelength spectral reflectance sensor to discriminate between the target objects. Note that, by using more wavelengths (of appropriate values that ensure at least two non-overlapping slopes for all objects), more objects can be discriminated.

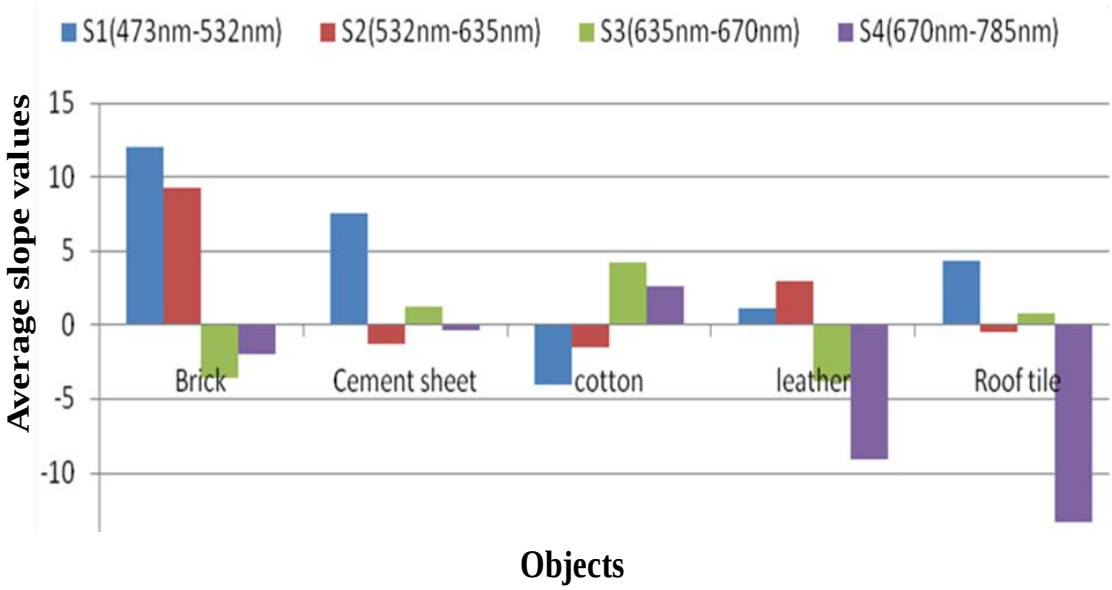

Figure 5.9: Calculated average slope values for five different objects.

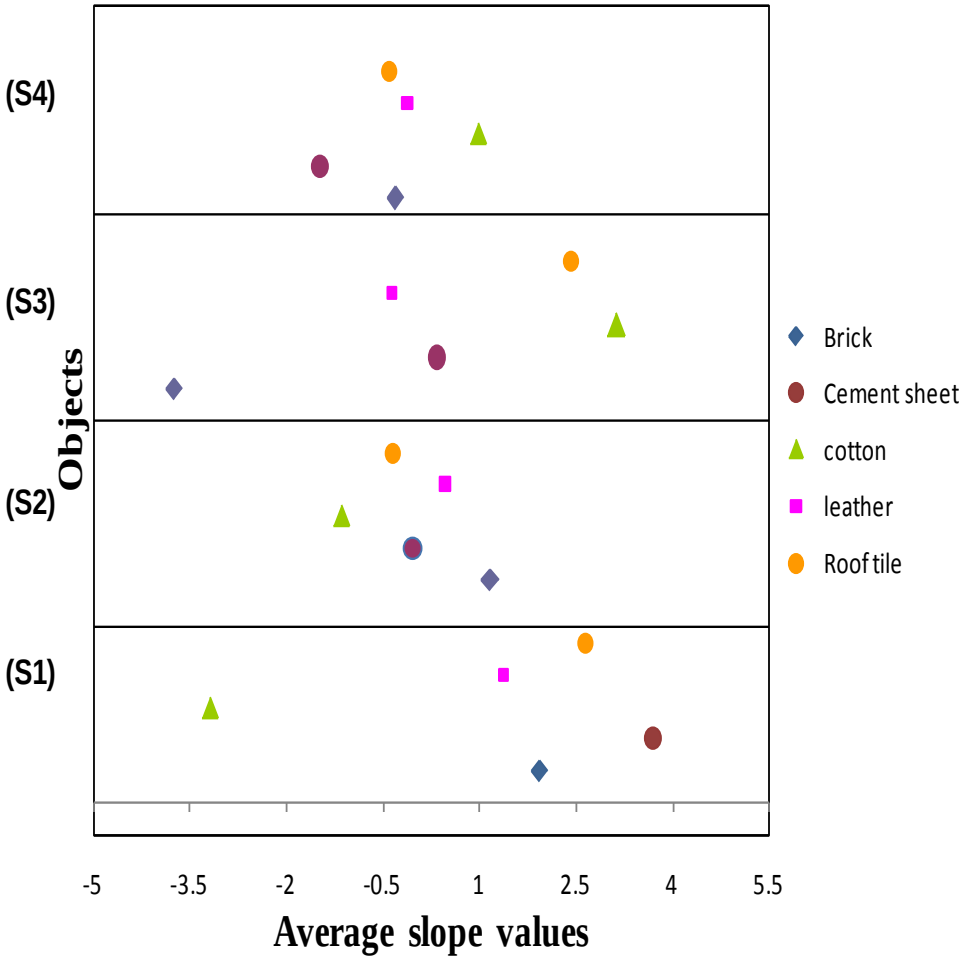

Figure 5.10: Average values with standard deviation for slopes S_1, S_2, S_3 and S_4 for five different objects (2m).

The average values of slopes S_1, S_2, S_3 and S_4 for the sample objects, calculated using Eq. (5.1) are shown in figure 5.9. Each object is distinguishable in at least one slope. The measured standard deviations of the slope values for 2m and 6m are shown in Figure 5.10 and Figure 5.11. Clearly, no simultaneous overlapping between slope values of different objects was present, demonstrating accurate discrimination of the various objects. For example, the average slopes for a cement sheet, shown in Figure 5.10, do not have any overlapping with other objects in slopes S_1, S_3 and S_4, and hence the cement sheet can be discriminated from other objects. For cotton, there is no overlapping in slopes S_1, S_2 and S_4 with the other objects under investigation, while overlapping is seen in slope S_3 with roof tile. For brick, there is no overlapping in slopes S_1, S_2 and S_3, while overlapping is seen in slope S_4 with roof tile and leather. For roof tile, there is no overlapping in slopes S_1, while overlapping is seen in slopes S_2, S_3 and S_4 with other objects. For leather, there is no overlapping in slopes S_1 and S_2 with any other object.

In the Figure 5.11 for cotton there is only one slope S_3 overlaps with other objects. In the case of brick, there are slopes S_2 and S_3 which do not overlap with any sample object. Also, while the slopes S_4 of the roof tile, leather and brick overlap, they can be discriminated through the measurements of their non-overlapping slopes S_1, S_2 and S_3 at a 2m range, and non-overlapping slopes S_2 and S_3 at a 6m range. The increase in slope variance with an increase in the detection range is attributed to the lower detected signal for a higher range, which results in a lower signal-to-noise ratio. These experimental results validate the capability of the novel multi-wavelength sensor to identify and discriminate between the objects frequently encountered in intruder-detection scenarios. Note that, by using more wavelengths (of appropriate values that ensure at least two non-overlapping slopes for all objects), more objects can be discriminated.

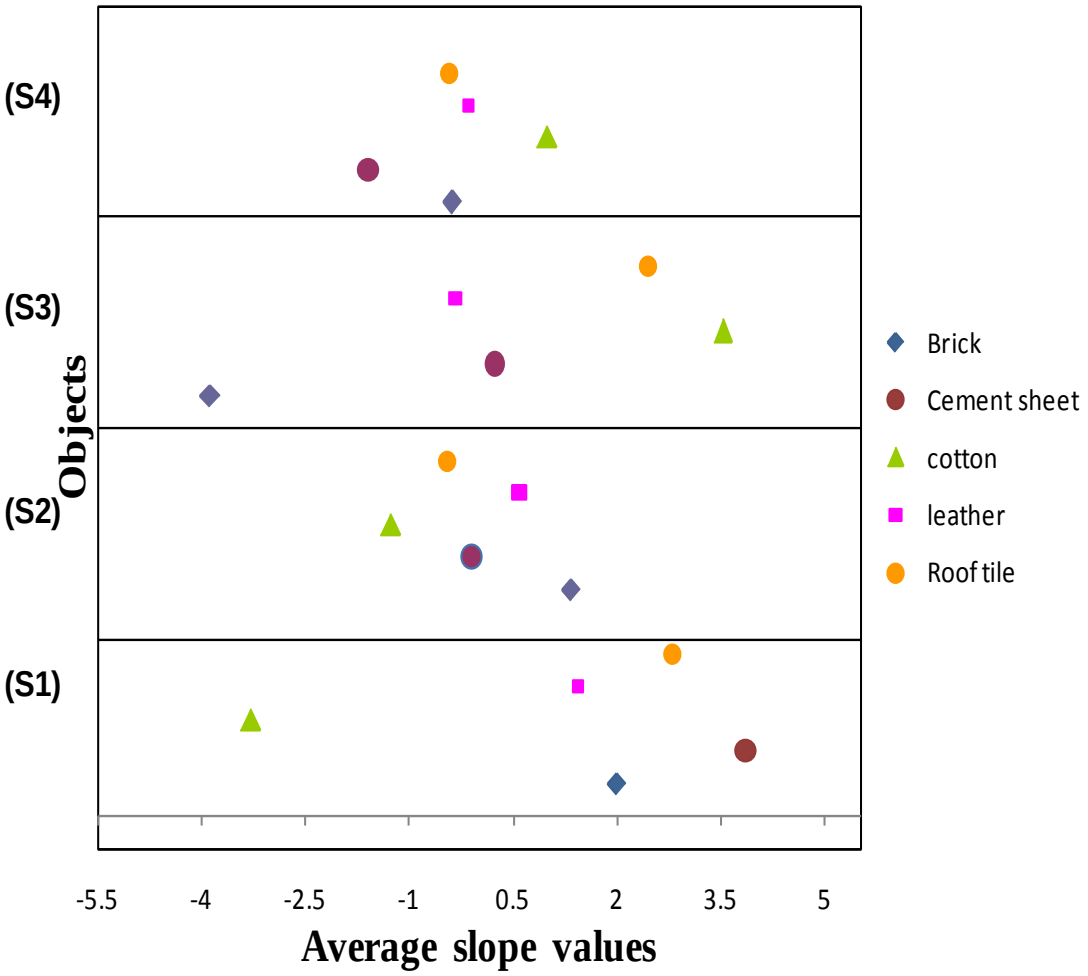

Figure 5.11: Average values with standard deviation for slopes S_1, S_2, S_3 and S_4 for five different objects (6m).

5.4.3 Error Analysis

The measured errors, which occurred while recording the experimental data, were analysed using a statistical algorithm (Shott, 1988), which calculates the standard deviations of the slopes, as shown in Figures 5.11.

The expression for the slope values, defined in Equation (5.1), can be generalized as:

$$s_i = \left| \frac{R_{(\lambda_k)} - R_{(\lambda_j)}}{\lambda_j - \lambda_k} \right| \qquad \text{Eqn. (5.3)}$$

Using Equation (4.3) and $R_\lambda = I_\lambda / P_\lambda$, and after some algebra, the error in slope value measurement is given by

$$|\Delta S_i| = \left|\frac{1}{P_k(\lambda_j - \lambda_k)}\right|\Delta I_k + \left|\frac{I_k}{(\lambda_j - \lambda_k)P_k^2}\right|\Delta P_k + \left|\frac{\left(\frac{I_k}{P_k} - \frac{I_j}{P_j}\right)}{(\lambda_j - \lambda_k)^2}\right|\Delta\lambda_k$$

$$+\left|\frac{1}{P_j(\lambda_j - \lambda_k)}\right|\Delta I_j + \left|\frac{I_j}{(\lambda_j - \lambda_k)P_j^2}\right|\Delta P_j + \left|\frac{\left(\frac{I_k}{P_k} - \frac{I_j}{P_j}\right)}{(\lambda_j - \lambda_k)^2}\right|\Delta\lambda_j \qquad \text{Eqn. (5.4)}$$

For example, the error in slope S_3 measurement is given by

$$|\Delta S_3| = \left|\frac{1}{P_{635}(\lambda_{670} - \lambda_{635})}\right|\Delta I_{635} + \left|\frac{I_{635}}{(\lambda_{670} - \lambda_{635})P_{635}^2}\right|\Delta P_{635} + \left|\frac{\left(\frac{I_{635}}{P_{635}} - \frac{I_{670}}{P_{670}}\right)}{(\lambda_{670} - \lambda_{635})^2}\right|\Delta\lambda_{670}$$

$$+\left|\frac{1}{P_{670}(\lambda_{670} - \lambda_{635})}\right|\Delta I_{670} + \left|\frac{I_{670}}{(\lambda_{670} - \lambda_{635})P_{670}^2}\right|\Delta P_{670} + \left|\frac{\left(\frac{I_{635}}{P_{635}} - \frac{I_{670}}{P_{670}}\right)}{(\lambda_{670} - \lambda_{635})^2}\right|\Delta\lambda_{635} \qquad \text{Eqn. (5.5)}$$

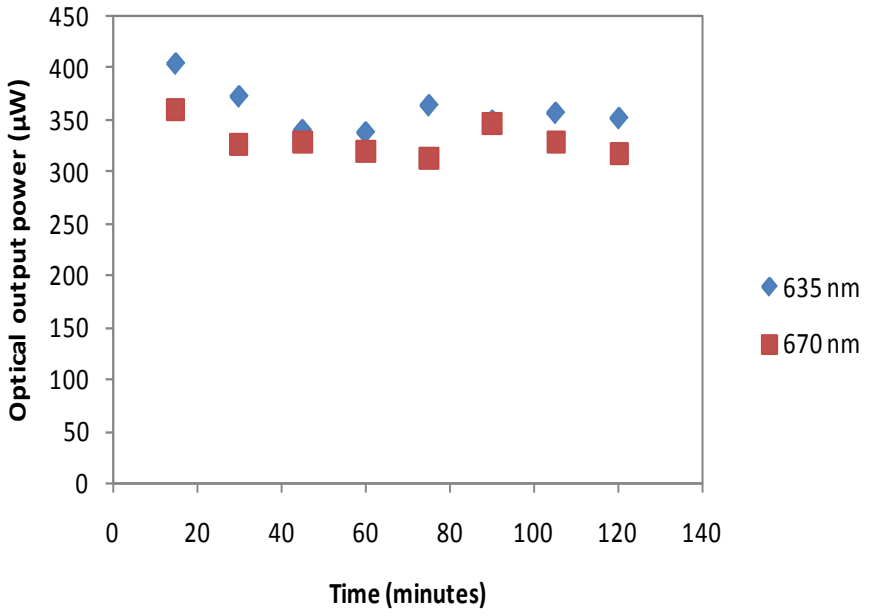

Figure 5.12: The variation of the output optical power for brick illuminated with 635nm and 670nm laser diodes. Power fluctuations were recorded over a time interval of 120 minutes for a 6m range.

where $R_{635} = I_{635} / P_{635}$ and $R_{670} = I_{670} / P_{670}$. To calculate the slope error, ΔS_3 for brick, the 635nm and 670nm lasers were turned on and the transmitted intensities P_{635} and P_{670}, as well as the intensities reflected I_{635} and I_{670} of the imaged object were measured over a long time interval, which enabled ΔI_{635}, ΔI_{670}, ΔP_{635} and ΔP_{670} to be calculated. Note that $\Delta\lambda_{635}$ and $\Delta\lambda_{670}$ were assumed negligible. It was found that the fluctuations in transmitted laser optical power are proportional to the fluctuations in the reflected optical power, which were the major source of error in S_3 calculation. The fluctuations in the imaged optical intensities for 635nm and 670nm over a 120-minute period are shown in Figure 5.12 for brick exhibiting a maximum error in slope S_3 of 13% at a 6 m range.

5.5 OBJECT DISCRIMINATION THROGH TRANSVERSE LASER BEAM SCANNING

5.5.1 Experimental design for object identification through transverse laser beam scanning

This section describes and demonstrates target or object discrimination through the use of a multi-wavelength laser sensor over a distance of 6 meters. The sensor architecture comprises a laser combination module, cylindrical quasi-optical cavity, collecting lens and the charged coupled device (CCD) imager. The most important feature about this particular sensor is the use of a plane mirror arrangement to provide additional transverse laser beam scanning, as shown in Figure 5.13.

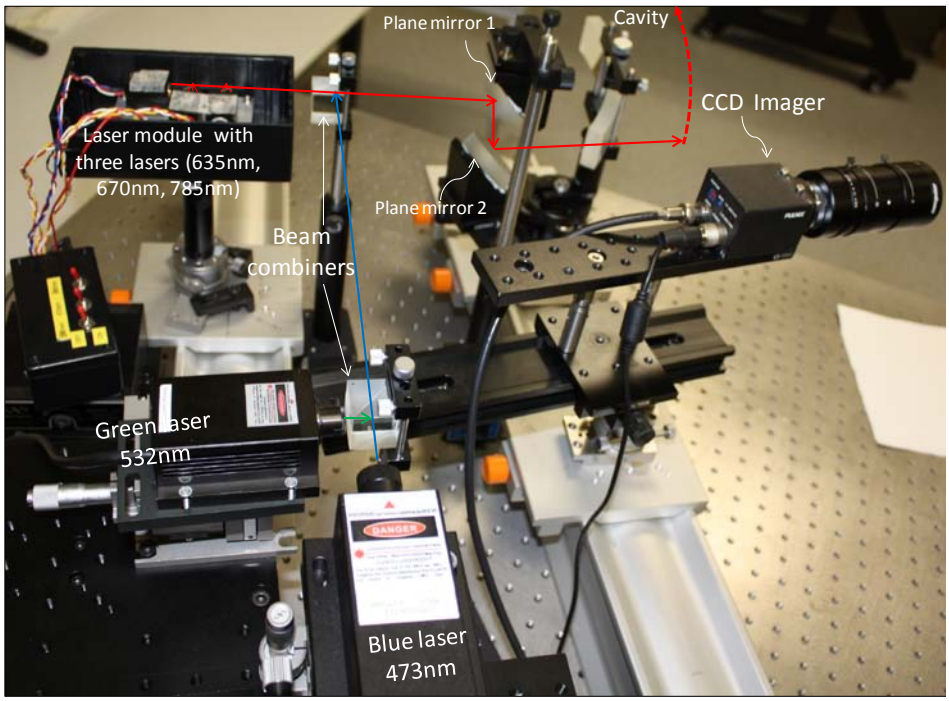

Figure 5.13: Schematic diagram of the multiple-wavelength laser sensor comprising a laser module with five different lasers, a curved optical cavity that generates an array of multiple transverse scanning laser beams and an image sensor.

The sample objects considered to demonstrate the proof-of-concept for detection were leaf, wood, bark, PVC material and black fabric. These objects were easily discriminated by a single laser spot, but a single laser spot was not enough to discriminate the camouflage material from other objects, because it had numerous patterns embedded into its fabric. Hence, it was necessary to strike the camouflage material with several beam spots (each spot sequentially illuminated with various wavelengths) in order to detect it. The ability of the sensor to discriminate the camouflage material was demonstrated over a range of 6m by processing the intensities of the reflected laser beams at different wavelengths.

A. Laser combination module

The above-described laser combination module comprised of five lasers of different wavelengths was used, which produced five collimated and overlapped laser beams of similar polarization. The diameter of each collimated laser beam was 4mm. The 635nm, 670nm and 785nm lasers had 6mW output power each, while both 473nm and 532nm lasers had an output power of 12mW. The optical beams of lasers 635nm, 670nm and 785nm were combined using the beam combiner 1 and 2, respectively. The other two lasers of wavelength 473nm and 532nm were combined with a beam

combiner 3. Finally, the outputs from combiners 2 and 3 were combined with a beam combiner 4.

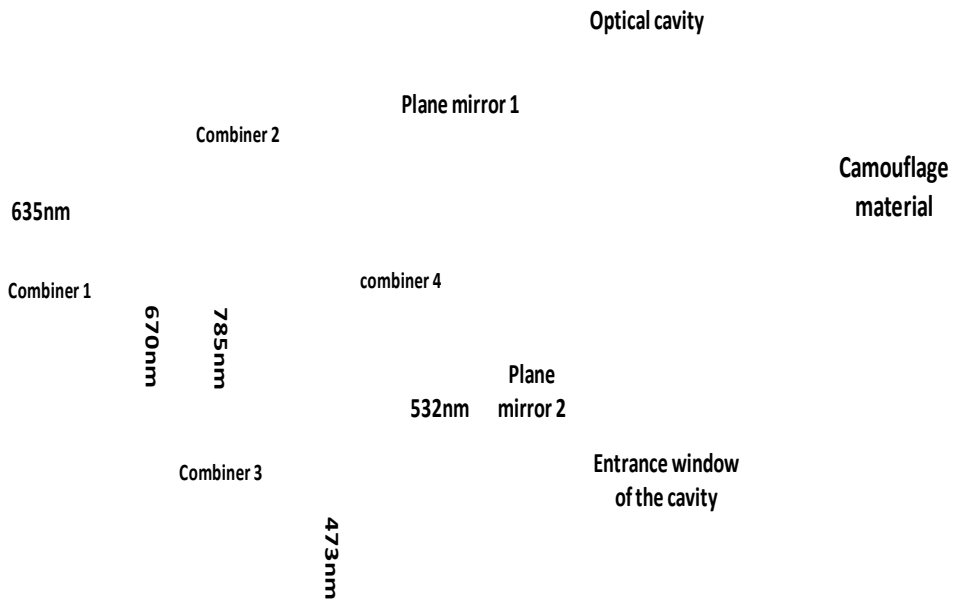

Figure 5.14: Schematic representation of a laser combination module with five lasers and four beam combiners. The vertical output of the combiner 4 was reflected off mirror 1 and 2 and the beam was launched into the entrance window of the optical cavity.

The plane mirror 1 was placed at 45° with respect to the beam combiner 4, while the plane mirror 2 was shifted slightly in such a way that the laser beams stroke the entrance window of the cylindrical quasi optical cavity at different positions. The combined (five) laser pulses were sequentially launched into the entrance window of the optical cavity which produced multiple laser beam spots, and by slightly shifting mirror 2 vertically without changing the angle of the mirror, the laser spots generated at the camouflage material were shifted in the transverse direction, as illustrated in Figure 5.14.

5.5.2 Experimental results and discussion

Six different objects namely leaf, bark, wood, PVC, black fabric and camouflage material were used to demonstrate the concept of spectral object discrimination in the laboratory. The reflectance spectra of leaf, bark, wood, PVC and black fabric are shown in Figure 5.15.

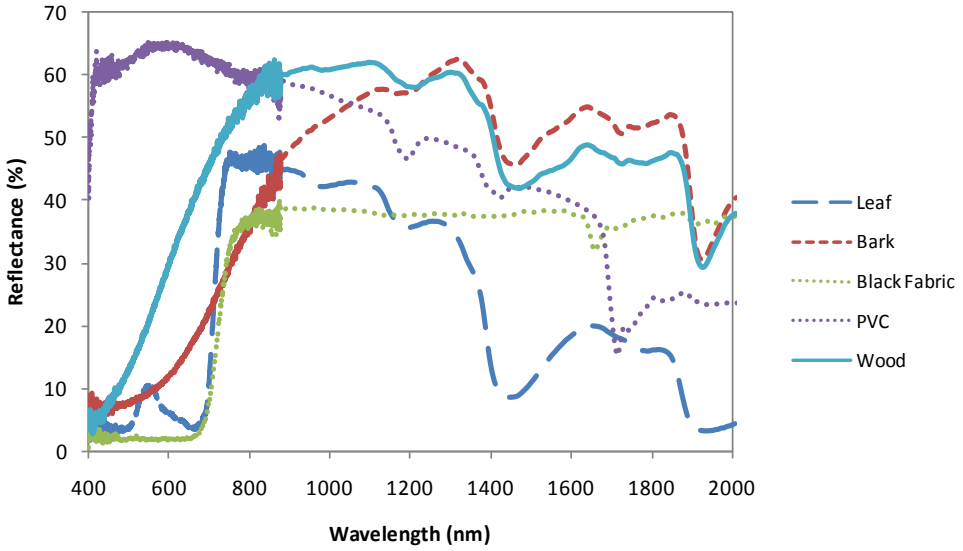

Figure 5.15: Measured spectral response of five different sample objects.

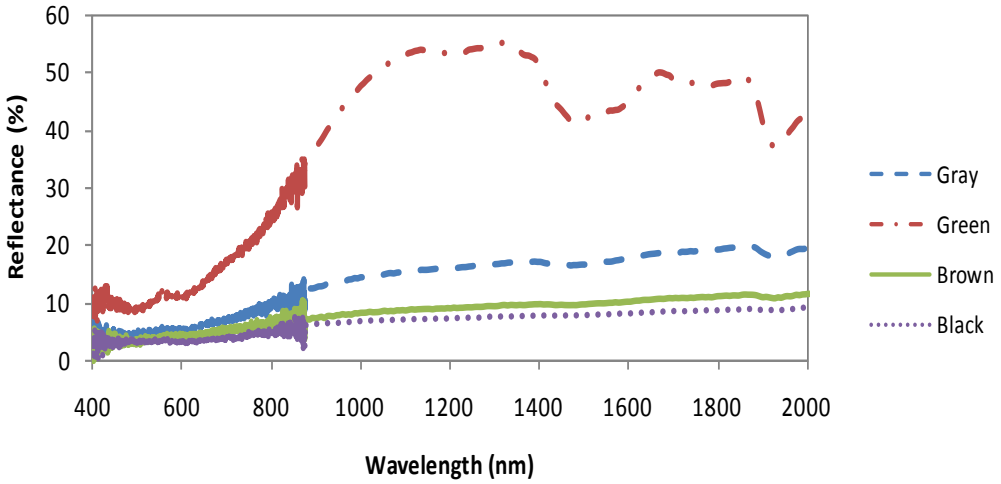

Figure 5.16: Measured spectral responses of the camouflage material components.

The reflectance spectrum of the camouflage material is shown in Figure 5.16. These reflectance spectra were obtained by using two different spectrometers, namely a visible spectrometer of spectral range 400-850nm and an infrared spectrometer of spectral range 850-2100nm. Sample objects were placed at 6m from the multiple-wavelength sensor.

Equation (5.1) was used to calculate the average slopes S_1, S_2, S_3 and S_4 for the various objects, which are shown in Figure 5.17. The results in Figure 5.17 clearly demonstrate that each object differs from others in at least one slope value, making it distinguishable. Note that small errors were encountered during the slope measurements, mainly because of the dark current of the image sensor and, predominantly, the optical power fluctuations of the laser sources.

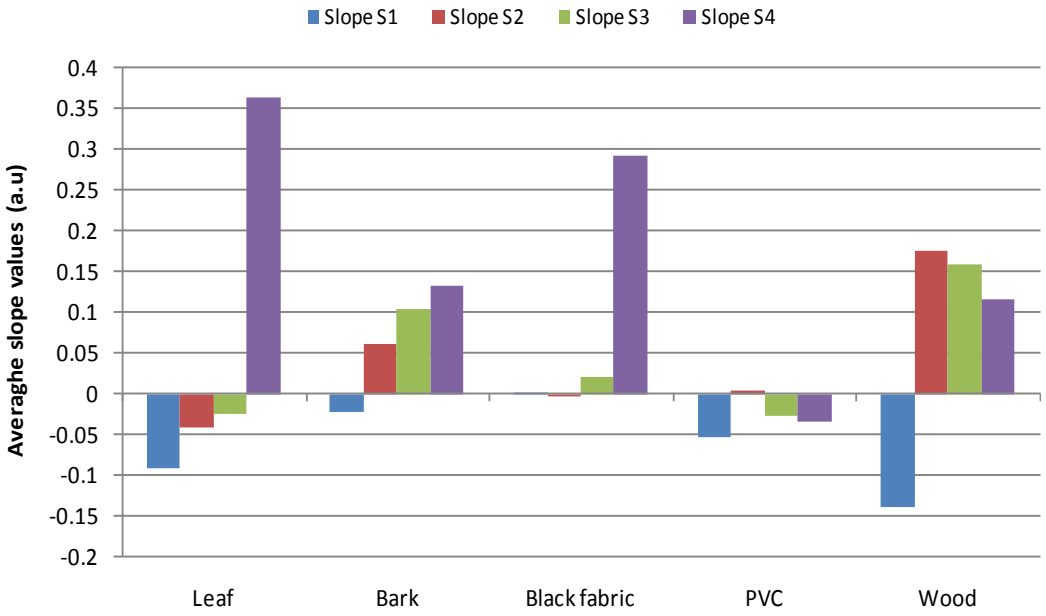

Figure 5.17: Average slope values S_1, S_2, S_3 and S_4 for five different objects calculated from the reflectance spectra.

The objects were placed at 6m from the optical cavity and illuminated with an array of laser beams emitted through the sensor. The reflected intensities from these objects were measured and processed. The average slopes for all objects are shown in Figure 5.18.

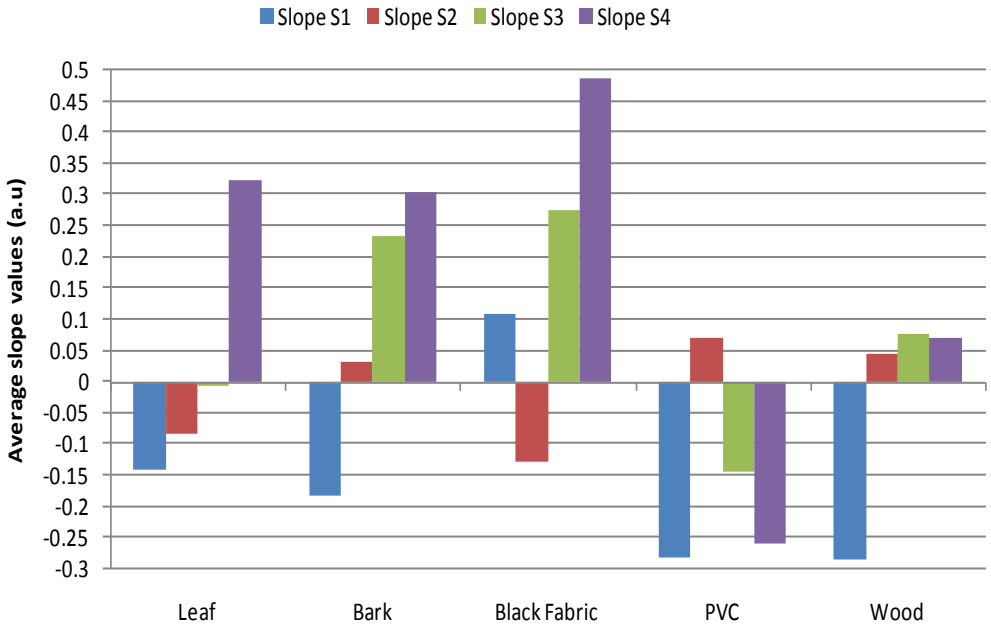

Figure 5.18: Average slope values S_1, S_2, S_3 and S_4 for five different objects measured in the laboratory for the first set of laser spots (without tilting of mirror 2) projected at 6m from the optical cavity.

Slope S_1 in Figure 5.18 shows that all the objects, except the black fabric, have negative non-identical slope values. Note that, the main requirement for object discrimination is that there should be a difference in at least any two slope values, and this criterion was clearly satisfied with all other sample objects. When mirror 2 was tilted the laser spots shifted in the transverse direction resulting in the measured slopes shown in Figure 5.19.

These experimental results shown in Figure 5.18 and Figure 5.19 validate the capability of the multiple wavelength sensor to discriminate between the various objects under investigation.

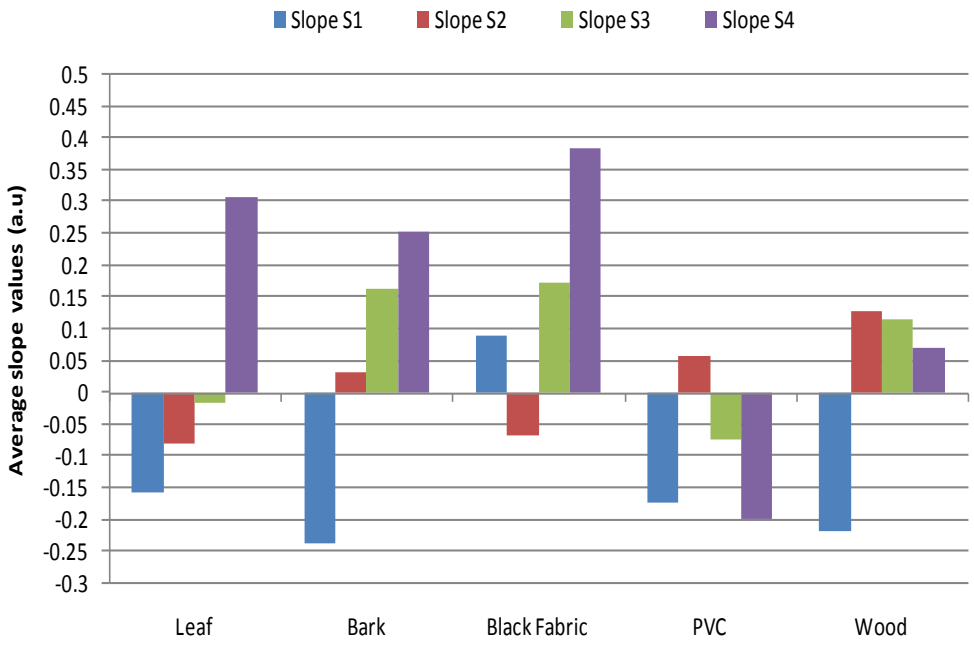

Figure 5.19: Average slope values S_1, S_2, S_3 and S_4 for five different objects measured in the laboratory for the second set of laser spots (with mirror 2 being tilted) projected at 6m from the optical cavity.

The camouflage material however, had complex patterns in comparison with the other objects discriminated in Figures 5.18 and 5.19. These patterns were embedded in a single sample, and when the laser beams were projected onto that material, the intensities of reflected laser beams were dependent upon the pattern whereon the beam was projected. Scanning of the beam spots was required in order to identify that material. The multiple wavelength sensor (Figure 5.13) had five different wavelengths, however, the improved optical design shown in Figure 5.14 had the capability to emit

multiple sets of parallel laser beams and this was a key characteristic necessary to discriminate materials of complex patterns within a single sample.

Figure 5.20 shows the average slope values S_1, S_2, S_3 and S_4 for the camouflage material patterns measured from the reflectance spectra captured by a spectrometer.

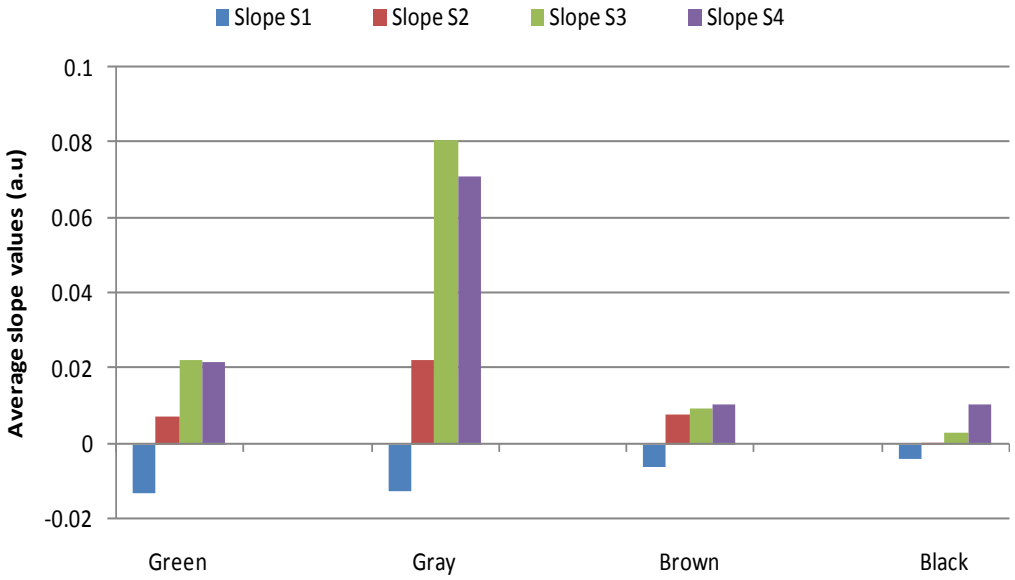

Figure 5.20: Calculated average slope values S_1, S_2, S_3 and S_4 for camouflage material measured in laboratory.

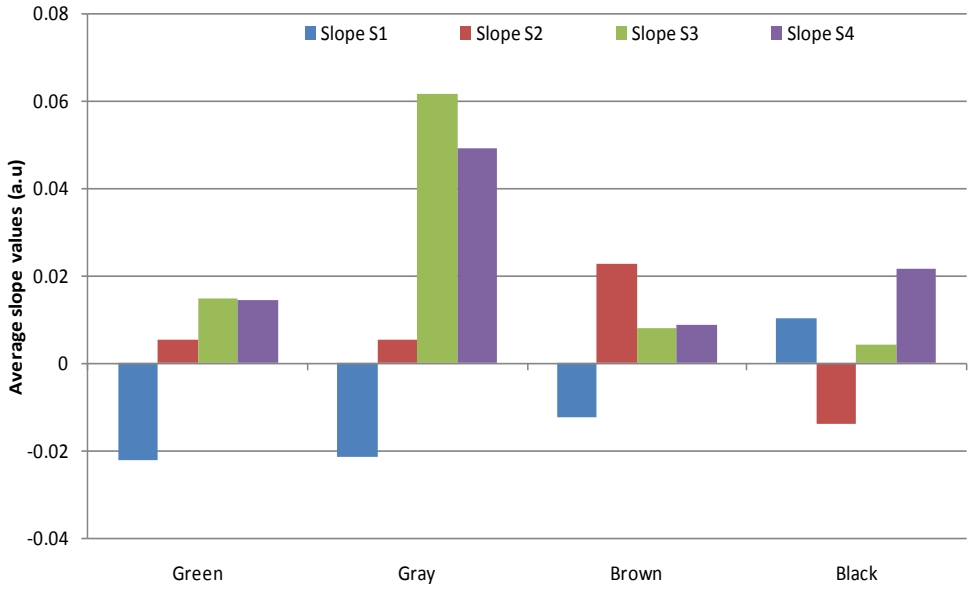

Figure 5.21: Average slope values S_1, S_2, S_3 and S_4 for camouflage material measured in laboratory.

The Figure 5.21 shows the average slope values S_1, S_2, S_3 and S_4 for the camouflage material patterns measured by the multiple wavelength sensor at 6m in the laboratory. The measured slope values in Figure 5.21 were in excellent agreement with the slope values calculated from the measured reflectance spectra of the camouflage material patterns shown in the Figure 5.20. This clearly demonstrates that camouflage materials can be identified through transverse laser beam scanning.

5.6 SUMMARY

In this chapter, we have described and demonstrated the concept of a multi-wavelength sensor capable of performing object identification and discrimination. The optical reflectance properties of various natural objects commonly encountered in the military perimeter have been measured, and the optimum wavelengths necessary for object identification and discrimination have been determined. Analyses of the spectral characteristics for the selected objects have shown that the laser wavelengths 473nm, 532nm, 635nm, 670nm and 785nm are the most appropriate for the identification and discrimination of the selected objects.

Object discrimination has successfully been demonstrated over a 6m range by determining four spectral reflectance slopes at the employed wavelengths. Statistical investigations and calculated standard deviations have confirmed no simultaneous overlapping between the slope values of the sample objects, making the identification of the selected objects accurate.

Object samples have been illuminated with an array of collimated laser beams emitted through a multi-spot beam generator integrating lasers, free-space beam combiners and an image sensor, and the reflectance properties of the objects under investigation have been measured. These measurements were carried out in the laboratory with ambient fluorescent light. Since our initial goal has been to demonstrate the concept of the multiwavelength sensor, the experiments were carried out in laboratory conditions only. The optimization of the performance of the multi-wavelength laser scanning system in the field would be an excellent scope for future R&D activities.

The multi-wavelength sensor with additional optical design provides transverse laser beam scanning for intruder detection, and discrimination has been developed and demonstrated over a 6m range. Sample objects namely leaf, bark black fabric, PVC, wood and camouflage material have been used to demonstrate the concept of the

multiwavelength sensor. Camouflage material of complex patterns have been identified by shifting the laser spots along the transverse direction thus enabling various camouflage patterns to be individually identified. The results have confirmed the agreement between the calculated and measured values.

The next chapter will investigate and demonstrate object position detection using the triangulation method with three different laser beams.

CHAPTER 6

LASER TRIANGULATION METHOD FOR OBJECT POSITIONING

6.1 INTRODUCTION

The concept of object identification and discrimination through multi-wavelength laser sensor was described in the previous chapter. An additional optical design used for transverse laser beam scanning was also discussed in detail to identify and discriminate camouflage materials. This chapter deals with position-finding of objects in a secured perimeter through laser triangulation. To determine the positions of various objects along a secured area, only a single laser wavelength from the multiple wavelength laser combination module, described in Chapter 5 - Section 5.2, is needed. The laser of wavelength 635nm is selected to demonstrate the position-finding experiment.

Position-finding is achieved by launching an optical beam into the custom fabricated curved optical cavity, thereby generating multiple laser beams through partial internal beam reflections within the cavity, as illustrated in Figure 6.1. The three main parameters that are needed to determine the position of the object in the triangulation geometry are: (i) the baseline distance, i.e. the distance between the outgoing laser beam and the lens axis, (ii) the outgoing angle of the laser beam and (iii) the peak-intensity positions of the imaged laser spots onto the imager's pixels. The object position, P is determined by calculating its coordinates (X, Z) (Hartrumpf and Munser, 1997). A system of linear algebra formulas is derived to simulate the position of X and Z coordinates. A CCD imager is used to capture the projected laser spot images and Spiricon software is used to locate the centre of each projected laser beam. Position

finding experiment is demonstrated in controlled indoor environments over a distance of 6m. The experimental results are in excellent agreement with the simulation results.

6.2 LASER TRIANGULATION METHODOLOGY FOR POSITION FINDING

The schematic diagram illustrating the principle of active laser triangulation is shown in Figure 6.1. The target object point P, the lens centre positioned in line with the Z-axis and the outgoing laser beam from the cavity determine the triangle required to measure the coordinates of P (Hartrumpf and Munser, 1997). The X-axis is positioned in the centre of the lens L, b is the baseline distance between the outgoing laser beam and the lens axis, f is the focal length of the lens used to image the laser spots and θ is the tilting angle of the laser source with respect to the lens axis. Each transmitted laser beam has a unique outgoing angle, θ_i, and is at a determined baseline distance, b_i, from the axis of the imager's lens.

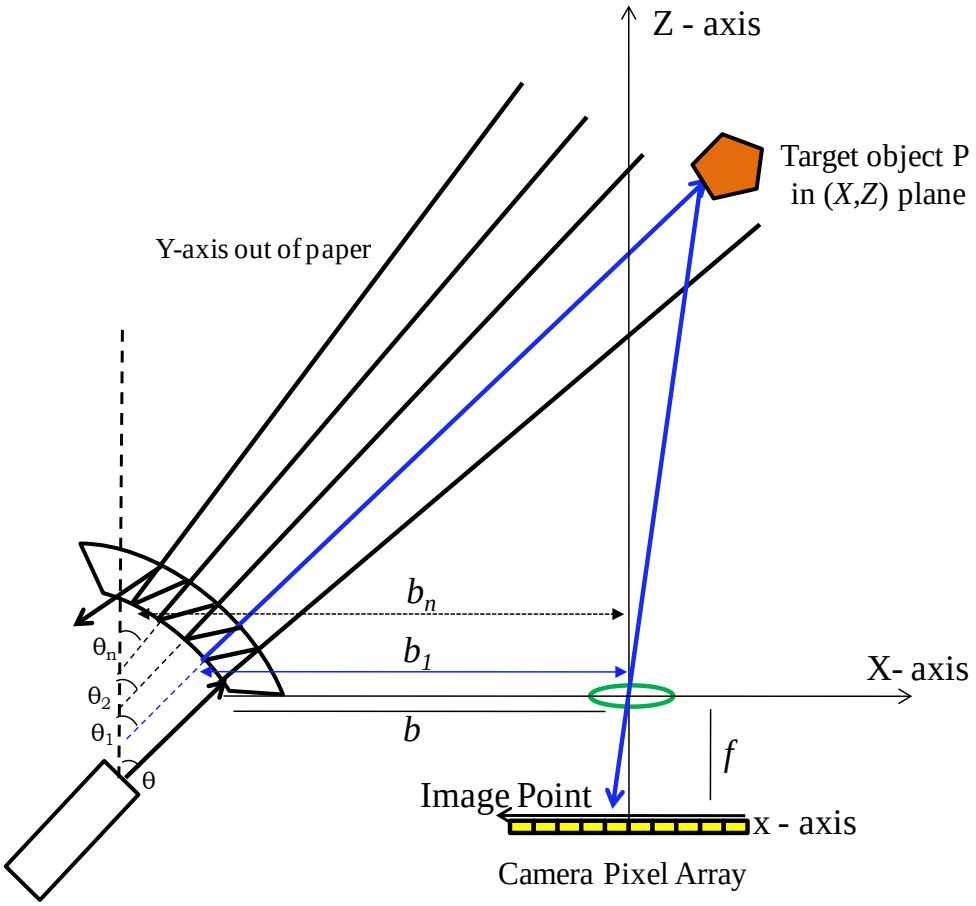

Figure 6.1: Schematic diagram illustrating the principle of laser triangulation.

The baseline distance, *b*, can be calculated as follows:

$$b = \sqrt{\left(\left(\frac{L_b - P_b}{P_m + L_m}\right) - L(x)\right)^2 + \left(\left(\frac{(P_m.L_b) - (L_m.P_b)}{P_m.L_m}\right) - L(z)\right)^2} \qquad \text{Eqn. (6.1)}$$

where, *b(x)* and *b(z)* are given by:

$$b(x) = \frac{L_b - P_b}{P_m + L_m} \quad \text{and} \quad b(z) = \frac{(P_m.L_b) - (L_m.P_b)}{P_m.L_m} \qquad \text{Eqn. (6.2)}$$

The angle of the outgoing beam is given by:

$$\tan\theta = \left(\frac{\alpha - L_m}{1 + (L_m.\alpha)}\right) \qquad \text{Eqn. (6.3)}$$

L_m and L_b are the slope and the Z-intercept of the lens line. P_m and P_b are the slope and the Z-intercept of the projected ray, respectively (Sahba et al., 2008).

The basic equation for deriving X and Z, from image formation (Hartrumpf and Munser, 1997) and hence the parameters needed for locating the object in the (*X, Z*) plane are given by:

$$X = \frac{xZ}{f} - x \quad \text{and} \quad Z = \frac{X + b}{\tan(\theta)}$$

$$Xf\tan(\theta) - xX = xb - xf\tan(\theta)$$

$$\tan\theta = \left(\frac{\alpha - L_m}{1 + (L_m.\alpha)}\right)$$

$$X(x - f\tan(\theta)) = x(f\tan(\theta) - b)$$

$$X = x\left(\frac{f\tan(\theta) - b}{x - f\tan(\theta)}\right) \qquad \text{Eqn. (6.4)}$$

Similarly,

$$Z\tan(\theta) - b = \frac{xZ}{f} - x$$

$$fZ\tan(\theta) = xZ + fb - xf$$

$$Z(x - f\tan(\theta)) = f(x - b)$$

$$Z = f\left(\frac{x-b}{x - f\tan(\theta)}\right) \qquad \text{Eqn. (6.5)}$$

where f is the focal length of the lens, x is the image point in the camera pixel array, b is the baseline distance from the laser beam to the lens centre and θ is the outgoing angle of the laser beam.

The X coordinate represents the distance from the optical axis to the laser spot image and the Z coordinate represents the distance from the imagers centre to the projected laser spot. The images captured in the CCD imager enable, through the use of the beam profiling software Spiricon, the calculation of x. Note that a small change in the parameter x changes the X and Z values and those in turn affect the position P of the object. If the object is moving but struck by the same laser spot, then the outgoing angle θ and the baseline distance b will remain the same. On the other hand, if an object is moving across the projected laser beams, then the values of b and θ, as well as the X and Z coordinates will change.

6.3 EXPERIMENTAL RESULTS FOR OBJECT POSITION DETECTION

The object position detection experimental design is shown in Figure 6.2. The 6mW 635nm laser, described in chapter 4, was selected to obtain the coordinates of the sample objects using the triangulation method.

The optical cavity and the imager were mounted on the same stage with a separation distance of 17.7cm, which defined the baseline distance b (Figure 6.1). The optical cavity produced multiple beams depending upon the angle of the incident beam. Object position finding was demonstrated using a laser tilting angle of 40̊ , which resulted in 20 laser spots after the laser beam underwent multiple reflections within the curved optical cavity.

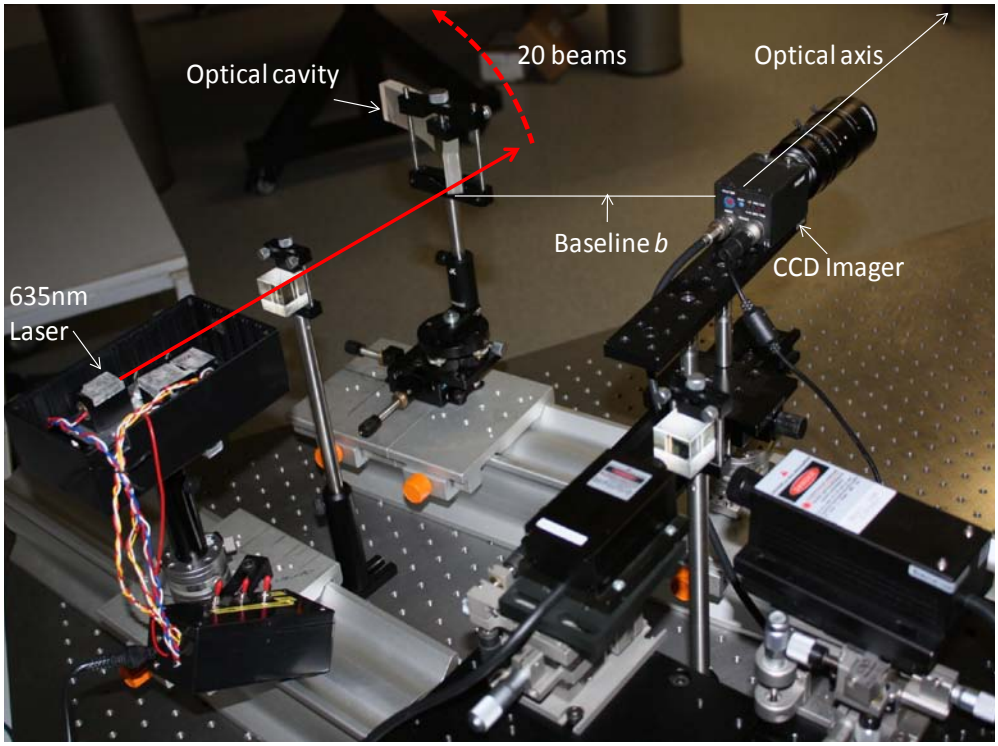

Figure 6.2: Experimental setup for demonstrating the principle of object position detection using triangulation method.

The objects were placed within the imager's field of view at a particular distance from the optical cavity and the triangulation method was used to calculate the position of objects, which were illuminated by the laser beams. The collected data was then processed via projecting the measured values of θ and b into the actual (X, Z) plane and hence determining the object coordinates as shown in Figure 6.1.

In general, several beams might illuminate a single object and reflect off it, where each beam corresponds to a set of θ and b values. In this case, it is possible to get a sense of the object's shape by simply measuring $\Delta\theta_{\{i,i+1\}} = \theta_i - \theta_{i+1}$ and $\Delta b_{\{i,i+1\}} = b_i - b_{i+1}$, where i is the number of the beam reflected off the same object. Threshold methods can be used to determine, using $\Delta\theta$ and Δb, the degree of uniformity of the object's surface.

Alignment errors were experienced during the experiments. These errors can be attributed to (i) the inaccuracy in the measurement of the baseline distances, b_i, from the image sensor's lens centre to the laser beam spot and (ii) the slight misalignment of the optical axis and the centre of the lens. By accurately measuring the position of the

object's image on the image sensor (Figure 6.1) the errors in calculating the object's position were significantly reduced.

In order to demonstrate the capability of the triangulation method and to determine the position of the object, a sample object was placed within the imager's field of view. The coordinates of the sample objects illuminated by laser spots 2, 3, and 4 were measured using the triangulation method described in Section 6.2.

Laser spot 2, 3 and 4 had baseline distances 19cm, 21cm and 23cm, respectively and outgoing angles 41°, 42° and 43, respectively. The object was slightly moved along the laser spots, and several measurements taken repeatedly for each beam spot and analysed to calculate the object's coordinates using an especially developed statistical error algorithm. The measured and simulated values for the *X* and *Z* coordinates versus the pixel number, *x*, for the three laser spots are shown in Figure 6.3(a-f).

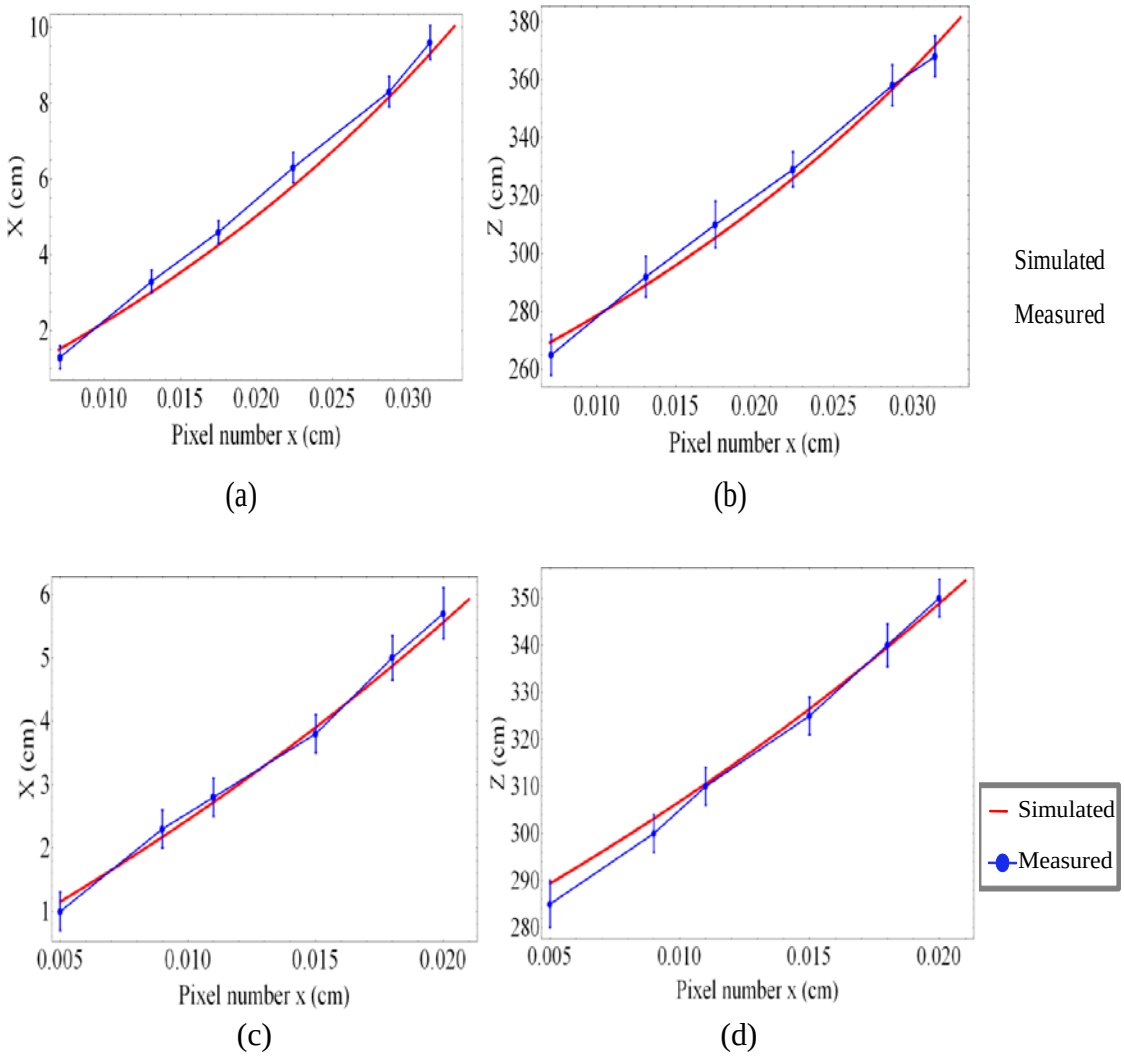

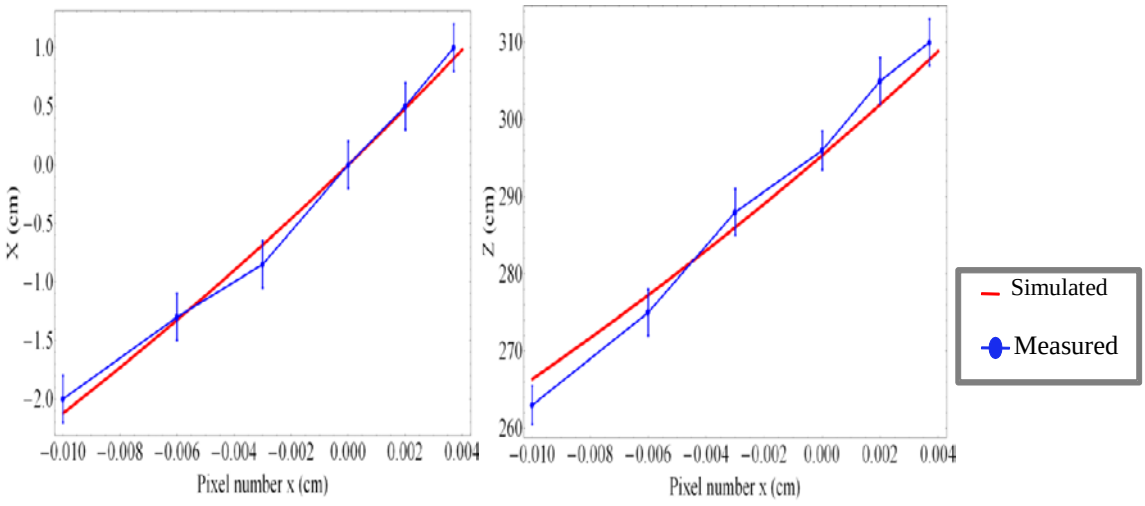

(e) (f)

Figure 6.3: Measured and simulated coordinates X and Z of the object illuminated by (a) and (b) the 2nd laser spot, (c) and (d) the 3rd laser spot and (e) and (f) the 4nd laser spot.

The measured and simulated values for the *X* and *Z* coordinates versus the pixel number *x* demonstrate excellent agreement between simulation and experimental results. The maximum object position finding error in the *X* and *Z* directions was 8% when analysed with the statistical error algorithm. All these measurements were carried out in the laboratory with fluorescent ambient lighting.

6.4 SUMMARY

The capability of the developed multiwavelength sensor to accurately predict the coordinates of objects, in addition to object identification and discrimination, has been demonstrated over a 6m range, using the triangulation method. A system of linear equations has been used to simulate the X and Z coordinates of target objects. The 635nm laser was used to inject the laser light from the laser combination module into the curved cavity and project multiple beam spots onto the target object. Experiments have been carried out using three different laser spots to validate the system performance. Each laser spot had unique baseline distance *b* and outgoing angle θ. The X and Z coordinates have been measured at various distances from the optical axis of the sensors imager and the image point on the image plane has been determined to calculate the target object position. A statistical algorithm, especially developed to

analyze the measurement errors, has shown that the triangulation method resulted in a maximum error of 8% in target object position finding.

CHAPTER 7

CONCLUSION AND FUTURE WORK

7.1 OVERVIEW OF THE STUDY

This thesis has presented a comprehensive investigation on a multi-wavelength laser scanner for an intruder detection sensor capable of material discrimination and position location over a distance of 6m. Theoretical frame works such as optical reflectance properties of various natural materials commonly encountered in perimeter security and object position finding algorithms have been discussed. A comprehensive literature review has been conducted, providing an overview of laser scanning fundamentals which includes introduction to LASER RADAR, problems associated with LASER RADAR, optical distance measurement methods, surface reflectance and laser scanning for security systems.

This thesis has described and demonstrated the concepts of material discrimination and object positioning through a novel photonic based multi-wavelength intruder detection sensor. The combination of multi-wavelength lasers using beam splitters has been explained in detail. Discrimination and identification of various materials have been demonstrated experimentally over a distance of 6m form the optical cavity. Sample materials namely brick, cement sheet, roof tile, cotton and leather have been used to validate the discrimination capability of the sensor. Spectral analyses have shown that the laser wavelengths 473nm, 532nm, 635nm, 670nm and 785nm are the most appropriate for material discrimination. Sample materials have been illuminated with an array of collimated laser beams emitted through a multi-spot beam generator integrating lasers, free space beam combiners and an image sensor, and the reflectance

properties of the materials under investigation have been measured. These measurements were carried out in the laboratory with fluorescent ambient light. Discrimination between materials has been demonstrated by determining four spectral slopes at the selected wavelengths. Statistical investigations and calculated slope standard deviations have confirmed no simultaneous overlapping between the slope values of the various sample objects, making the identification of the selected objects accurate even in the presence of laser power fluctuations.

In addition to material discrimination, the capability of the sensor to accurately determine the coordinates of target objects has been demonstrated over a 6m range and has resulted in an accuracy exceeding 92% using the triangulation method.

Discrimination with an improved optical design has demonstrated over a 6m range. The sample materials, namely, leaf, bark black fabric, PVC, wood and camouflage material have been used to demonstrate the concept of the developed multiwavelength sensor demonstrator. Camouflage material has been chosen because it has complex patterns embedded within a single sample. The experimental results have demonstrated the excellent discrimination capability of the sensor due to its improved optical design in addition to the use of five different wavelengths. It is important to notice that the addition of too many lasers increases the cost, bulkiness and slows the operating speed of the sensor.

7.2 OUTCOME OF THE RESEARCH

The significance of this research is the design and development of a motionless photonic-based multi-wavelength intruder detection sensor demonstrator capable of discriminating materials and to locate them in the secured perimeter. The major drawbacks of mechanical laser scanning systems include wobble, jitter, windage and synchronization errors. These drawbacks can be overcome through our static photonic-based intruder detection sensor. Also, beam deflection inside a laser scanning unit is typically accomplished through the use of electro-mechanically steered polygonal mirrors, oscillating mirrors or stepper motors, thus generating mechanical noise (errors) that cannot be filtered out. Additional mechanical-steering-related errors can result from the random wobble produced by ball bearings, motor cogging and torque variations.

Also, the developed photonic-based multi-wavelength intruder detection sensor is unique for its multiple wavelength laser module, which had proven the ability to

discriminate and locate the material over a distance of 6m. An intruder detection sensor with two different lasers had already been developed, but the discrimination capability has been limited with few materials. The multiple wavelength sensor developed through this PhD project has the capacity to discriminate various natural materials through transverse laser scanning, including complex materials such as camouflage materials of different patterns embedded into them.

7.3 COMPLETION OF OBJECTIVES

The major objectives sated in Section 1.3 have been successfully achieved through (i) a detailed literature investigation; (ii) the development of the algorithm and (iii) conducting experiments demonstrating the concept of the proposed sensor architecture. Table 7.1 summarizes the achieved research objectives of the thesis.

Table 7.1 Summary of the research objectives achieved throughout the PhD project.

Table 7.1 summary of the work accomplished.

Tasks	Chapter	Description
Literature Reviews	2,3	▪ The basic principles of LASER RADAR and problem associated with them have been discussed. ▪ Several laser ranging method have been described and discussed. ▪ Fundamentals of laser scanning and core of laser scanning for perimeter security have been discussed. ▪ Applications of laser scanning and its limitations have also been summarised.
Optical Cavity	4	▪ The operation principle of the optical cavity has been discussed in detail. ▪ Beam propagation through the curved

		optical cavity has been discussed. The percentage of front transmittance have been optimized and explained through examples. ▪ Advantages and limitations of the curved optical cavity over conventional rectangular cavity have been discussed.
Experimental demonstrations and results	5	▪ Five lasers of different wavelength have been combined using four beam splitters to develop the laser module of the intruder detection sensor. ▪ Object identification and discrimination experiment have been carried out over 2m and 6m ranges. ▪ Statistical algorithm has been developed to analyse the slope errors in 6m result. ▪ Experiments to discriminate complex materials have been carried out, employing transverse laser scanning.
Experimental demonstrations and results	6	▪ Object position finding experiments have been described and demonstrated over a 6m range. ▪ Laser triangulation method has been used to determine object coordinates for various scenarios, demonstrating accuracy in object position finding exceeding 92%.

7.4 RECOMANDATION FOR FUTURE RESEARCH AND DEVELOPMENT

The research outcomes of this PhD project can be further improved through the investigation of various approaches, namely:

- The optical cavity is made up of a BK-7 glass medium with entrance and exit windows. Light transmission is achieved by depositing a nano-layered thin film coating on front side of the cavity as shown in Figure 7.1. The same optical cavity can be deposited with multiple transmission coating for uniform distribution of the laser power across the beam spots illuminating the target objects. For the four different coatings shown in Fig. 7.1 the simulated output optical power levels for the various beams emerging from the cavity are shown in Figure 7.2. This approach leads to improved SNR performance and hence more accurate object discrimination and position finding.

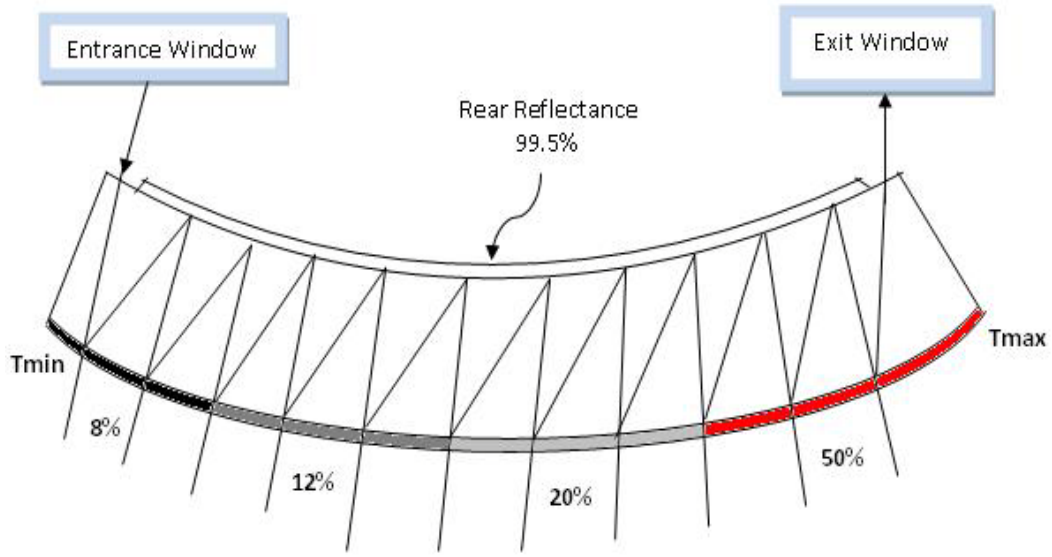

Figure 7.1: Curved optical cavity with multiple transmission coating.

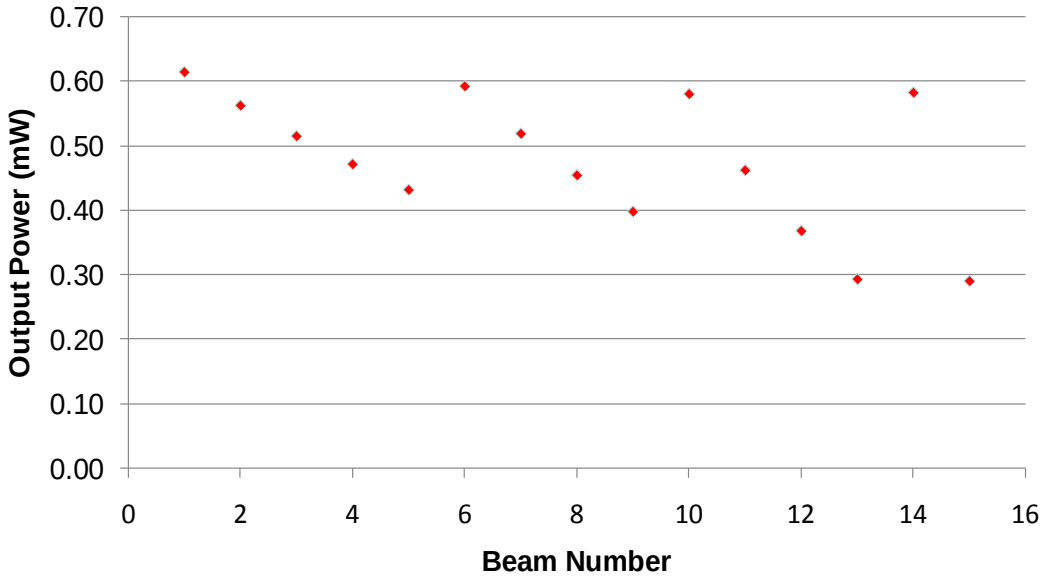

Figure 7.2: Calculated output optical power for each spot projected from the optical cavity with multiple transmission coating.

- The maximum range of the sensor can be extended from 6m to more that 10m through an improved imager lens relay design, and also, a look-up table can be created, which stores the spectral signatures of potential materials, thus providing a path for easy identification of intruding object materials. Spectral signatures for various materials can be measured and a look-up table could be built to store the spectrum. When there is any intrusion in the secured area, depending upon the reflected light captured by the imager, the system would calculate the slope values of the received intensity and the pre-developed algorithm would process the data to match the received information with the stored spectrum and identify the material. By adopting this approach, the discrimination range can also be extended to more than 10m.

- Implementing dual-view triangulation, which significantly improves the object position finding accuracy. The problem due to occlusion discussed in Section (2.5) can be eliminated by implementing the dual-view triangulation method, where two cameras are symmetrically placed with respect to the optical cavity leading to an increased field of view (FOV) and creating redundancy when the FOVs of the imagers overlap. However, this method would increase the cost of the system as well as the power consumption due to additional image processing

- Expand the application of the developed sensor beyond perimeter security, e.g. agriculture (weed-from-crop discrimination), food (moisture level in food samples change their optical reflectance properties), environmental monitoring (Lidar-based atmospheric remote sensing), etc.

REFERENCES:

AILISTO, H., HEIKKINEN, V., MITIKKA, R., MYLLYLA, R., KOSTAMOVAARA, J., MANTYNIEMI, A. & KOSKINEN, M. (2002) Scannerless imaging pulsed-laser range finding. *Journal of Optics a-Pure and Applied Optics,* 4**,** S337-S346.

AULL, B. (2005) 3D Imaging with Geiger-mode Avalanche Photodiodes. *OSA Optics and Photonics News.*

BARIBEAU, R. & RIOUX, M. (1991) Influence of speckle on laser range finders. *Applied Optics,* 30**,** 2873-2878.

BARNARD, L. R. (1988) *Intrusion Detection Systems,* Butterworth - Heinemann.

BERALDIN, J. A. (2004) Integration of Laser Scanning and Close-Range Photogrammetry - The Last Decade and Beyond. IN ALTAN, O. (Ed.) *Geo-Imagery Bridging Continents - XXth ISPRS Congress.* Istanbul, Turkey, ISPRS.

BERALDIN, J. A., BLAIS, F., COURNOYER, L., GODIN, G., RIOUX, M. & TAYLOR, J. (2003) Active 3D Sensing. *The e-Way into the Four Dimensions of Cultural Heritage Congress.* Vienna, Austria.

BESL, J. (1988) Active, Optical Range Imaging Sensors. *Machine Vision and Applications,* 1**,** 127-152.

BLAIS, F. (2004) Review of 20 Years of Range Sensor Development. *Electronic Imaging,* 13**,** 231-240.

BLAIS, F. (2006) Terrestrial Laser Scanning. *International Summer School "Digital Recording and 3D Modeling".* Aghios Nikolaos, Crete, Greece.

BOEHLER, W., HEINZ,G, MARBS,A. (1999) The potential of non-contact close range laser scanners for cultural heritage recording. *XVII CIPA Symposium.* Recife, Brazil.

BOSCH, T. & LECURE, M. (1995) Selected Papers on Laser Distance Measurements. *SPIE Milestone Series,* 115**,** 206-208.

BRADSHAW, G. (1999) Non-Contact Surface Geometry Measurement Techniques. Dublin, Ireland, Image Synthesis Group, Trinity College.

CAMPBELL, J. B. (1996) *Introduction to Remote Sensing,* New York, The Guilford Press.

DANDRIDGE, A. & GOLDBERG, L. (1982) Current-induced frequency modulation in diode lasers. *IEEE Electronics Letters,* 18**,** 302-304.

DOSSETOR, K. (2011) Cost-benefit analysis and its application to crime prevention and criminal justice research. Australian Institute of Criminology, Canberra.

EINSTEIN, D. A. S. (2011) The Integrated Physical Security Handbook. Homeland Defense Publishing and Training.

ELKHALILI, O., SCHREY, O. M., MENGEL, P., PETERMANN, M., BROCKHERDE, W. & HOSTICKA, B. J. (2004) A 4 X 64 pixel CMOS image sensor for 3-D measurement applications. *Ieee Journal of Solid-State Circuits,* 39**,** 1208-1212.

EPA (2011) Security Product Guides IN AGENCY, U. S. E. P. (Ed.).

GAGNON, A. (2006) New Developments in Millimeter Wave Packaging Brings Down The Cost Of Ground Based Perimeter Surveillance RADARs. *40th Annual 2006 International Carnahan Conference on Security Technology.* Kentucky, IEEE.

GARCIA, M. L. (2001) *The Design and Evaluation of Physical Protection Systems,* Boston, Butterworth-Heineman.

GARCIA, M. L. (2006) *Vulnerability Assessment of Physical Protection Systems,* Oxford, Elsevier Butterworth-Heineman.

GARCIA, M. L. (2008) *The design and evaluation of physical protection system,* Elsevier Butterworth-Heineman.

GONÇALVES, J. G. M., SEQUEIRA, V. & WHICHELLO, J. (2001) Laser technologies for on-site surveillance. *IAEA Symposium on International Safegaurds.* Vienna, Austria.

HANCOCK, J. (1999) Laser Intensity-Based Obstacle Detection and Tracking. *The Robotics Institute.* Pittsburgh, Pennsylvania.

HANCOCK, J., LANGER, D., HEBERT, M., SULLIVAN, R., INGIMARSON, D., HOFFMAN, E., METTENLEITER, M. & FRÖLICH, C. (1998) Active Laser Radar For High-Performance Measurements. *IEEE International Conference on Robotics & Automation.* Leuven, Belgium, IEEE.

HARTRUMPF, M. & MUNSER, R. (1997) Optical three-dimensional measurements by radially symmetric structured light projection. *Applied Optics,* 36**,** 2923-2928.

HAUGE, R. (2003) LADAR Puts the Puzzle Together. *SPIE's OE magazing.*

HEBERT, M. (2000) Active and Passive Range Sensing for Robotics. *IEEE International Conference on Robotics and Automation.* San Francisco, IEEE.

HEBERT, M. & KROTKOV, E. (1991) 3-D Measurements From Imaging Laser Radars: How Good Are They? *IEEE/RJS International Workshop on Intelligent Robots and Systems IROS.* Osaka, IEEE.

HOSMER, P. (2004) Use of laser scanning technology for perimeter protection. *Ieee Aerospace and Electronic Systems Magazine,* 19**,** 13-17.

JAMIESON, J. & RAY, M. (2006) Laser perimeter awareness system. U.S.A, Rosemount Aerospace Inc.

JARVIS, R. A. (1983) A Perspective on Range Finding Techniques for Computer Vision. *IEEE Transactions on Pattern Analysis and Machine Intelligence,* PAMI-5**,** 505-512.

KLANČNIK S, B. J., PLANINŠIČ P (2007) Obstacle detection with active laser triangulation. *APEM journal,* 2**,** 79-90.

KOGELNIK, H. & LI, T. (1966) Laser Beams and Resonators. *Applied Optics,* 10**,** 1550-1567.

KURTTI, S. & KOSTAMOVAARA, J. (2010) An Integrated Laser Radar Receiver Channel Utilizing a Time-Domain Walk Error Compensation Scheme. *Ieee Transactions on Instrumentation and Measurement,* 60**,** 146-157.

LASEROPTRONIX (n.d) Laser Optronix Security Systems.

LEOT (2001) Laser Electro-Optics Technology (LEOT) - Module 5: Laser Information Systems. IN CENTER FOR OCCUPATIONAL RESEARCH AND DEVELOPMENT, T. (Ed.).

LI, Y. & KATZ, J. (1995) Laser beam scanningby rotary mirrors. *Applied Optics,* 34.

LICHTI, D. D., CHOW, J. & LAHAMY, H. (2011) Parameter de-correlation and model-identification in hybrid-style terrestrial laser scanner self-calibration. *Isprs Journal of Photogrammetry and Remote Sensing,* 66**,** 317-326.

LICHTI, D. D. & GORDON, S. J. (2004) Error Propagation in Directly Georeferenced Terrestrial Laser Scanner Point Clouds for Cultural Heritage Recordings. *FIG Working Week, International Federation of Surveyors.* Athens, Greece.

MADSEN, C. K., BAE, T. & SNIDER, T. (2007) Intruder signature analysis from a phase-sensitive distributed fiber-optic perimeter sensor - art. no. 6770OK. IN UDD, E. (Ed.) *Fiber Optic Sensors and Applications V.* Bellingham, Spie-Int Soc Optical Engineering.

MARBS, W. B. A. A. (2007) Investigating Laser Scanner Accuracy. Mainz, Germany

MASSEY, G. A. & SIEGMAN, A. E. (1969) Reflection and Refraction of Gaussian Light Beams at Tilted Ellipsoidal Surfaces. *Applied Optics,* 8**,** 975-978.

MORING, I., HEIKKINEN, T., MYLLYLÄ, R. & KILPELÄ, A. (1989) Acquisition of three-timensional range data by a scanning laser range finder. *Opt. Eng.,* 28**,** 897-902.

MYNEI, B. R., HALL, F. G., SELLERS, J. P. & MARSHAK, A. L. (1995) The interpretation of spectral vegetation indexes. *IEEE Transactions on Geoscience and Remote Sensing,* 33.

NISE (1997) Perimeter Security Sensor Technologies Handbook. NISE East Electronic Security Systems Engineering Division.

NISHINO, K., NAKAMURA, M., MATSUMOTO, M., TANNO, O. & NAKAUCHI, S. (2011) Optical filter for highlighting spectral features Part I: design and development of the filter for discrimination of human skin with and without an application of cosmetic foundation. *Optics Express,* 19**,** 6020-6030.

NITZAN, D., BRAIN, A. E. & DUDA, R. O. (1977) The Measurement and Use of Registered Reflectance and Range Data in Scene Analysis. *Proceedings of the IEEE,* 65**,** 206-220.

OFFICE OF HOMELAND SECURITY (2002) National strategy for homeland security Washington DC. .

PAAP.A, ASKRABA.S, ALAMEH, K. E. & ROWE.J (2008) Photonic-based spectral reflectance sensor for ground-based plant detection and weed discrimination. *Optics Express,* 16**,** 1051-1055

PALOJARVI, P., MAATTA, K. & KOSTAMOVAARA, J. (2002) Pulsed time-of-flight laser radar module with millimeter-level accuracy using full custom

receiver and TDC ASICs. *Ieee Transactions on Instrumentation and Measurement,* 51**,** 1102-1108.

PEARS, N. P., P.; (1992) Active Triangulation Rangefinder Design For Mobile Robots. *International Conference on Intelligent Robots and Systems,* .

POPPINGA, J., BIRK, A. & PATHAK, K. (2010) A Characterization of 3D Sensors for Response Robots Robocup 2009:. *Robot Soccer World Cup Xiii*, 5949**,** 264-275.

RAY, M., EVANS, O. & JAMIESON, J. (2005) Three dimensional laser radar for perimeter security. *Electro-Optical Remote Sensing, Proc. of SPIE,* 5988.

RIOUX, M. (1984) Laser range finder based synchronized scanners. *Applied Optics,* 23**,** 3837-3844.

RIZA, N. A. & MUZAMMIL, A. A. (2003) Code-multiplexed optical scanner. *Applied Optics,* 42**,** 1493-1501.

RODRIGUEZ, J. R., DRY, B. & MATTER, J. C. (1991) Interior intrusion detection systems. Albuquerque, Sandia National Labs.

ROWE, D. M. (1997) Developments in holographic-based scanner designs. IN BEISER, L. & SAGAN, S. F. (Eds.) *SPIE Conference on Optical Scanning Systems.* San Diego, SPIE.

SAHBA, K., ALAMEH, K. E. & SMITH, C. L. (2006a) A proposed motionless laser scanning architecture for perimeter security. *40th Annual IEEE International Carnahan Conferences Security Technology, Proceedings***,** 9-16.

SAHBA, K., ALAMEH, K. E. & SMITH, C. L. (2008) Obstacle detection and spectral discrimination using multi-wavelength motionless wide angle laser scanning. *Optics Express,* 16**,** 5822-5831.

SAHBA, K., ALAMEH, K. E., SMITH, C. L. & PAAP, A. (2007a) Cylindrical quasi-cavity waveguide for static wide angle pattern projection. *Optics Express,* 15**,** 3023-3030.

SAHBA, K., ALAMEH, K. E., SMITH, C. L. & PAAP, A. (2007b) A Novel Beam Deflection Method for Wide Angle Lasser Scanning. *6TH International Conference on the Optical Internet (COIN) held jointly with the 32nd Australian Conference on Optical Fibre Technology (ACOFT).* Melbourne, Australia.

SAHBA, K., ASKRABA, S. & ALAMEH, K. E. (2006b) Non-contact laser spectroscopy for plant discrimination in terrestrial crop spraying. *Optics Express,* 14**,** 12485-12493.

SALEH, B. E. A. & TEICH, M. C. (1991) *Fundamentals of Photonics,* U.S.A., Wiley-Interscience.

SCHNADT, K. & KATZENBEIßER, R. (2004) Unique Airborne Fiber Scanner Technique for Application-Oriented LIDAR Products. IN THIES, M., KOCH, B., SPIECKER, H. & WEINACKER, H. (Eds.) *Proceedings of the International Society of Photogrammetry and Remote Sensing (ISPRS) Working Group VIII/2.* Freidburg, Germany, Institute for Remote Sensing and Landscape Information Systems.

SCHULZ, T. & INGENSAND, H. (2004) Terrestrial Laser Scanning - Investigations and Applications for High Precision Scanning. *TS26 Positioning and Measurement Technologies and Practices II - Laser Scanning and Photogrammetry, FIG Working Week.* Athens, Greece.

SHOTT, M. P. M. (1988) *Handling Experimental Data,* Open University Press.

SICK (2006) LMS 200/LMS 211/LMS 220/ LMS 221/ LMS 291 Laser Measurement Systems Technical Description. AG, Division Auto Ident.

SICK (2011) Building Automation.

SMARTSECSYSTEMS (n.d) Applications of LFS.

SOO HOO, M. S. & CHAPEK, J. F. (1996) Physical protection design and analysis training for the former Soviet Union. *37th annual meeting of the Institute of Nuclear Materials Management.* Naples.

STUTZ, G. (2005) Guiding Light. *SPIE's oemagazine,* 5**,** 25-27.

TAYLOR, C., BARLETT, D., CHASON, E. & FLORO, J. (1998) A Laser-Based Thin-Film Growth Monitor. *The Industrial Physicist,* 4**,** 26-30.

THIEL, K.-H. & WEHR, A. (2004) Performance Capabilities of Laser Scanners - An Overview and Measurement Principle Analysis. IN "THIEL, K. H. W. A., PERFORMANCE CAPABILITIES OF LASER-SCANNERS - AN, OVERVIEW AND MEASUREMENT PRINCIPLE ANALYSIS, I. P. O. T. I., WORKING GROUP VIII/2, L.-S. F. F. A. L. A. & FREIBURG, G.-O., PP 14-18." (Eds.) *Laser-Scanners for Forest and Landscape Assessment.* Freidburg, Germany.

TULEY, J., VANDAPEL, N. & HEBERT, M. (2005) Analysis and Removal of Artifacts in 3-D LADAR Data. *IEEE International Conference on Robotics and Automation.* Barcelona, IEEE.

VAN LEEUWEN, M., HILKER, T., COOPS, N. C., FRAZER, G., WULDER, M. A., NEWNHAM, G. J. & CULVENOR, D. S. (2011) Assessment of standing wood and fiber quality using ground and airborne laser scanning: A review. *Forest Ecology and Management,* 261**,** 1467-1478.

WAGNER, W., ULLRICH, A., MELZER, T., BRIESE, C. & KRAUS, K. (2004) From Single-Pulse to Full-Waveform Airborne Laser Scanners: Potential and Practical Challenges. IN ALTAN, O. (Ed.) *Geo-Imagery Bridging Continents.* Istanbul, International Society for Photogrammetry and Remote Sensing.

WEHR, A. & LOHR, U. (1999) Airborne laser scanning - an introduction and overview. *ISPRS Journal of Photogrammetry & Remote Sensing,* 54**,** 68-82.

WESTIN, S. H., HONGSONG, L. & TORRANCE, K. E. (2004) A Field Guide to BRDF Models. New York, Program of Computer Graphics, Cornell University.

WU, J.-H., HORNG, K.-Y. & CHANG, R.-S. (2006) Triangulation-based laser range finder using a complementary metal-oxide semiconductor image sensor for application to automotive systems. *Opt. Eng.,* 45**,** 044302-1:7.

WULF, O. & WAGNER, B. (2003) Fast 3D Scanning Methods For Laser Measurement Systems. Hannover, University of Hannover.

ZENG.L, YUAN.F, SONG.D & ZHANG.R (1999) A two-beam laser triangulation for measuring the position of a moving object. *Optics ans Lasers in Engineering***,** 445-453.